



**HAL**  
open science

# Contractility-induced morphological transitions in smooth muscle cells

Xiuyu Wang

► **To cite this version:**

Xiuyu Wang. Contractility-induced morphological transitions in smooth muscle cells. Cellular Biology. Université Paris-Saclay, 2021. English. NNT : 2021UPAST031 . tel-03187003

**HAL Id: tel-03187003**

**<https://theses.hal.science/tel-03187003>**

Submitted on 31 Mar 2021

**HAL** is a multi-disciplinary open access archive for the deposit and dissemination of scientific research documents, whether they are published or not. The documents may come from teaching and research institutions in France or abroad, or from public or private research centers.

L'archive ouverte pluridisciplinaire **HAL**, est destinée au dépôt et à la diffusion de documents scientifiques de niveau recherche, publiés ou non, émanant des établissements d'enseignement et de recherche français ou étrangers, des laboratoires publics ou privés.

Transitions morphologiques induites par la  
contractilité dans les cellules musculaires lisses  
*Contractility-induced morphological transitions in  
smooth muscle cells*

**Thèse de doctorat de l'université Paris-Saclay**

École doctorale n°573, Interfaces: Matériaux, systèmes, usages  
Spécialité de doctorat: Biologie  
Unité de recherche: LadHyX, Ecole polytechnique, CNRS, , 91128 Palaiseau, France  
Réfèrent : CentraleSupélec

**Thèse présentée et soutenue à Paris-Saclay,  
le 16/03/2021, par**

**Xiuyu WANG**

**Composition du Jury**

<b>Pascal SILBERZAN</b> Directeur de recherche, Institut Curie	Président
<b>Chantal BOULANGER</b> Directrice de recherche, Paris Cardiovascular Centre	Rapportrice & examinatrice
<b>Frank SCHNORRER</b> Directeur de recherche, Institut de Biologie du Développement de Marseille	Rapporteur & examinateur
<b>Cécile PERRAULT</b> Co-fondatrice, Eden Tech	Examinatrice
<b>David GONZALEZ-RODRIGUEZ</b> Maitre de conférences, Université de Lorraine	Examinateur
<b>Elsa VENNAT</b> Maitre de conférences, Central-Supelec	Examinatrice

**Direction de la thèse**

<b>Abdul BARAKAT</b> Directeur de recherche, Ecole Polytechnique	Directeur de thèse
---	--------------------

## ***Acknowledgements***

March 2021 :

It has been almost 9 years that I lived in France. During the first half of the time, I obtained my mechanical engineering diploma and worked in car industry. But there is a voice inside of me which kept telling me that I should work in bio-related project. So, I took a brave step in my life: I quitted my job and went back to the campus. After one year of studying in bio-mechanical engineering at Ecole Polytechnique, I decided to stay in Abdul Barakat's team to do a Ph.D. I am grateful for my supervisor's support, Abdul. Thanks for his qualitative listening and his constant encouragement, as well as the precious freedom he offered during my Ph.D.

I also want to thank the Barakat-team for having formed a united team that helps each other and allows everyone to feel happy at work. Beside Avin, Alessia, Claire L. Clara and Sara, Silvia, as well as some previous member, Olga, Alexandra, Anna, Carlo, and Elizabeth, I want to express my thanks to my Ph.D.-mate: Thévy and Claire D. I also want to thank Julien, who accompanied and guided me during my Ph.D. We shared so much happiness as well as sadness during these years. When I feel confused, you are always there to listen, to support and to encourage me. Our friendship will last forever.

Thanks also to LadHyX of its nice atmosphere for not only research but also a relax daily life. I want to thank Christophe and Emmanuel for having welcomed me to the lab. I want to mention Sébastien, Caroline, Gabriel, Francesco and Chuhan for their kind support. Then to mention the administrative and technical support from Sandrine, Toai, Daniel, Thérèse and Delphine, Magdalena and Patricia. Without your work, our lab won't be such an organized place for research. And I also want to thank the representative for Ph.D. student and post-doc, Claire D., who seriously take her responsibility and try to speak for the non-permanent members. It is a pleasure to have my three years and a half journey in this lovely lab.

Finally, I want to thank the whole school, l'Ecole Polytechnique, where is, definitely, a wonderful place to learn. I enjoyed attending different workshop and seminar held by the school or different labs. And the collaboration within the school is a great advantage. I want to thank a Ph.D. student, Yanan, from Gautreau's lab, who warmly accompanied my in their lab for western blot experiments. Beside academic collaboration, one of the best things on the campus is the opportunity of different kind of sports. I enjoyed the sport time (before the Covid confinement) on the campus, including swimming and air rifle. Moreover, I also want to thank Sandrine O. and Isabelle who helped me with the document for my maternity leave and the prolongation of my contract.

Thank to my great collaborators, who helped me improve my project and made it a complete story. I want to express my great appreciation for David. His decisive help at all

key moments, efficient and super helpful discussions, and more generally for having opened the doors of the biophysical world. I take to opportunity to thank the collaborators from the Silberzan's lab at Institute Curie, Thomas, Nastassia and Mathilde for productive exchanges of data analysis and experimental expertise.

I passed 3 months' exchanges in Beihang University, in the bio-medical engineering department. I would like to thank the whole team for their sense of welcome. I think of Hongyan, Anqiang and Xiao for their academic exchanges, administrative help. And also the students in their teams, especially, Jiali, Chenglin, Haoran. It was such a magic exchange journey in the country where I came from. I learned precious spirit of overcoming difficulties driven by the enthusiasm for research.

I finally thank my thesis committee. Thanks to my two rapporteurs, Chantal Boulanger and Frank Schnorrer for their careful reading and insightful comments. Thanks to the rest of my committee, Cecile M. Perrault, David Gonzalez-Rodriguez, Pascal Silberzan, Elsa Vennat for attending my defense and asking many valuable scientific questions.

A PhD journey go beyond the professional framework, this journey would be certainly different without support from life outside the lab.

First of all, I would like to express my most sincere gratitude to my parents, who support me and trust me as they always do. I want to thank my mum for her endless love and unconditional understanding. Without her support in life, the last year of the doctorate will be 100 times harder than what I have experienced.

I would also like to thank Tianyu, who accompanied me for the whole time during my Ph.D. Sharing of life burden together and understanding the value of my work allow me to move forward in my work without being distracted by the minutiae of life. There is another family member I want to mention, Nougat, who makes me quickly forget about unhappy things and helps to reduce stress.

Then, I would like to thank all my friends, thanks for your listening and giving advice. Thank you for making me realize that one should not only look at science, especially when there were some difficulties, I should embrace the wonderful life!

Last but not the least, thanks to my baby girl, Shuman, who come and join in my life. You make me brave and make me responsible. Thank you for the fresh energy you have injected into my life.

- 宝剑风从磨砺出，梅花香自苦寒来。
- The precious sword wind comes from sharpening, the fragrance of plum blossoms comes from the bitter cold.

*To Shuman*

# Contents

0.1	Abstract . . . . .	4
0.2	Abbreviation . . . . .	6
<b>1</b>	<b>Introduction</b>	<b>7</b>
1.1	Atherosclerosis . . . . .	8
1.1.1	Development of atherosclerosis . . . . .	8
1.1.2	Therapy . . . . .	12
1.2	Biophysical approaches to collective cell behavior . . . . .	17
1.2.1	Collective migration . . . . .	17
1.2.2	Physical models to describe cell collective behavior and organization	19
1.3	Specific focus: smooth muscle cells . . . . .	24
1.3.1	Additional characteristics . . . . .	24
1.3.2	SMC dysfunction and associated diseases . . . . .	25
1.3.3	SMC phenotypes . . . . .	26
1.3.4	SMC Lineage . . . . .	29
<b>2</b>	<b>Balloon angioplasty-induced endothelial damage</b>	<b>32</b>
2.1	Introduction . . . . .	32
2.1.1	Methods . . . . .	33
2.1.2	Results . . . . .	34
2.1.3	Discussion . . . . .	40
2.1.4	Conclusions . . . . .	41
<b>3</b>	<b>Contractility-induced self-organization of smooth muscle cells</b>	<b>42</b>
3.1	Introduction . . . . .	42
3.2	Article submitted . . . . .	43
3.2.1	Abstract . . . . .	43
3.2.2	Introduction . . . . .	44
3.2.3	Results . . . . .	45
3.2.4	Discussions and conclusions . . . . .	54
3.2.5	Materials and methods . . . . .	54
3.3	Supplementary documents . . . . .	58
3.3.1	Supplementary Figures . . . . .	58
3.3.2	Supplementary Notes . . . . .	65

<b>4</b>	<b>SMC organization within clusters</b>	<b>69</b>
4.1	Introduction . . . . .	69
4.2	Methods . . . . .	70
4.3	Results . . . . .	75
4.3.1	Protein quantification . . . . .	75
4.3.2	TFM results . . . . .	76
4.3.3	Spatial distribution of protein expression within SMC clusters . . . . .	77
4.3.4	Micro-injection . . . . .	80
4.4	Discussion and conclusions . . . . .	85
<b>5</b>	<b>Conclusions</b>	<b>86</b>
<b>6</b>	<b>Appendix</b>	<b>101</b>
6.1	Experimental protocols . . . . .	101
6.2	Matlab Codes . . . . .	114

## 0.1 Abstract

L'athérosclérose est une maladie artérielle dont les complications pathologiques, à savoir les crises cardiaques et les accidents vasculaires cérébraux, sont la première cause de mortalité dans le monde. Ces événements pathologiques sont dus à l'obstruction des artères et à l'obstruction du flux sanguin vers le cœur ou le cerveau. Le traitement le plus courant de l'athérosclérose est le déploiement d'un stent endovasculaire, un dispositif à mailles métalliques qui rouvre l'artère obstruée et rétablit ainsi la circulation sanguine. Les stents apportent également une stabilité structurelle à la paroi artérielle malade. Des millions de stents sont déployés chez les patients chaque année dans le monde entier. Cependant, malgré leur utilisation répandue, environ 1 procédure de pose de stent sur 10 entraîne des complications, dont les deux plus courantes sont la resténose et la thrombose. Ces deux complications trouvent leur origine dans le fait que le déploiement de stents provoque une lésion massive de l'endothélium artériel, la monocouche cellulaire qui tapisse la surface intérieure des vaisseaux sanguins. Au-delà de la lésion endothéliale, la resténose vasculaire implique une prolifération et une migration incontrôlées des cellules musculaires lisses ainsi que des changements importants dans l'organisation des cellules musculaires lisses artérielles. Le présent travail se concentre sur l'utilisation d'une combinaison d'expériences *in vitro* dans une imitation artérielle endothélialisée, l'analyse quantitative d'images et la modélisation physique pour aborder deux questions importantes : 1) comprendre comment se produisent les dommages endothéliaux induits par les stents et 2) étudier le remodelage et la réorganisation spontanés des cellules musculaires lisses. Les résultats de l'étude des lésions endothéliales montrent que l'étendue des lésions induites par les dispositifs endovasculaires est significativement plus élevée pour une paroi artérielle rigide (imitation artérielle PDMS) que pour une paroi souple (imitation artérielle en hydrogel de collagène). En outre, alors que les dommages endothéliaux dans le cas des parois souples se produisent principalement par des forces de cisaillement, les contraintes orthogonales induisent des dommages beaucoup plus importants dans le cas des artères plus rigides. Les études sur les cellules des muscles lisses montrent que lorsqu'elles atteignent une densité critique, ces cellules peuvent spontanément passer de feuilles cellulaires plates à des amas tridimensionnels de type sphéroïde. Ces amas s'initient lorsque les forces de contraction cellulaire induisent un trou dans la feuille cellulaire plate, un processus qui peut être modélisé comme la fracture fragile d'un matériau viscoélastique. L'évolution ultérieure de l'amas naissant peut être modélisée comme un processus de démouillage active avec une évolution de la forme de l'amas, entraînée par un équilibre entre la tension superficielle de l'amas, résultant à la fois de la contractilité et de l'adhérence des cellules, et la dissipation visqueuse de l'amas. La description des mécanismes physiques régissant l'émergence spontanée de ces intrigants amas tridimensionnels offre un aperçu des troubles liés aux cellules des muscles lisses.

**Mot clés:** athérosclérose, dommages endothéliaux, cellules musculaires lisses, sphéroïde/-cluster, transition morphologique

Atherosclerosis is an arterial disease whose pathological complications, namely heart attacks and strokes, are the leading cause of mortality worldwide. These pathological events arise from blockage of arteries and obstruction of blood flow to the heart or the brain. The most common treatment for atherosclerosis is the deployment of an endovascular stent, a wire-mesh device that re-opens the obstructed artery and thus restores blood flow. Stents also provide structural stability to the diseased arterial wall. Millions of stents are deployed in patients annually around the world. Despite their widespread use, however,  $\sim 1$  in every 10 stenting procedures develops complications, the two most common of which are restenosis and thrombosis. Both of these complications have their root in the fact that stent deployment induces massive injury to the arterial endothelium, the cellular monolayer that lines the inner surfaces of blood vessels. Beyond the endothelial damage, vascular restenosis involves uncontrolled smooth muscle cell proliferation and migration as well as extensive changes in the organization of the arterial smooth muscle cells. The present work focuses on using a combination of *in vitro* experiments in an endothelialized arterial mimics, quantitative image analysis, and physical modeling to addressing two important issues: 1) understanding how endothelial damage induced by stents occurs and 2) investigating spontaneous remodeling and re-organization of smooth muscle cells. The results of the endothelial damage study show that the extent of damage induced by endovascular devices is significantly higher for a rigid arterial wall (PDMS arterial mimic) than for a soft wall (collagen hydrogel arterial mimic). Furthermore, while endothelial damage in the case of soft walls occurs primarily through shear forces, orthogonal stresses induce much more extensive damage in the case of more rigid arteries. The smooth muscle cell investigations demonstrate that upon reaching a critical density, these cells can spontaneously transition from flat cell sheets to three-dimensional spheroid-like clusters. These clusters initiate when cellular contractile forces induce a hole in the flat cell sheet, a process that can be modeled as the brittle fracture of a viscoelastic material. The subsequent evolution of the nascent cluster can be modeled as an active dewetting process with cluster shape evolution driven by a balance between cluster surface tension, arising from both cell contractility and adhesion, and cluster viscous dissipation. The description of the physical mechanisms governing the spontaneous emergence of these intriguing three-dimensional clusters offers insight into smooth muscle cell-related disorders.

**Keywords:** atherosclerosis, endothelial damage, smooth muscle cells, spheroid, cluster, morphological transition

## 0.2 Abbreviation

<b>EC</b>	Endothelial cell
<b>ECM</b>	Extracellular matrix
<b>HV</b>	Hill-Valley
<b>LDL</b>	Low density lipoprotein
<b>MSC</b>	Mesenchymol stromal Cells
<b>PCI</b>	Percutaneous coronary intervention
<b>PIV</b>	Particle image velocimetry
<b>SMC</b>	Smooth muscle cell
<b>UF</b>	Uterine fibroid

# Chapter 1

## Introduction

*In chapter 1, I introduce background information on atherosclerosis, collective cell behavior and smooth muscle cell structure, function, and morphological organization. This chapter will provide a description of the general framework of this project and introduce the aims of this thesis.*

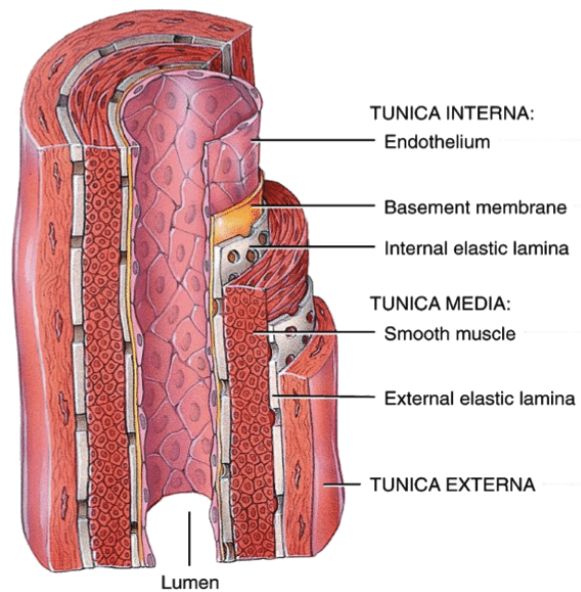


Figure 1.1: **Structure of an artery.** Adapted from [https://www.researchgate.net/figure/Structure-of-a-medium-size-elastic-artery-Adapted-from-27\\_fig1\\_263466531](https://www.researchgate.net/figure/Structure-of-a-medium-size-elastic-artery-Adapted-from-27_fig1_263466531).

## 1.1 Atherosclerosis

Atherosclerosis, the disease that leads to heart attacks and strokes, is the leading cause of mortality and morbidity worldwide [1]. Atherosclerosis is a chronic inflammatory disease that involves the progressive buildup of lipids, lipoproteins and immune cells (plaques) within the arterial wall, which can restrict blood flow. Some plaques are vulnerable to rupture, a catastrophic event that leads to rapid thrombosis and is often life-threatening. Other plaques, on the other hand, are more stable structurally and pose lower risk. Identification of the composition and structure of vulnerable plaques is an active field of research.

Patients typically do not develop atherosclerosis symptoms until an artery is so narrowed or clogged that it is unable to supply adequate blood to the organs and tissues. Sometimes a blood clot completely blocks blood flow, or even breaks apart and can trigger a heart attack or stroke.

Symptoms of moderate to severe atherosclerosis depend on which arteries are affected. For example:

Atherosclerosis in the heart's coronary arteries may lead to symptoms such as chest pain or pressure (angina). Atherosclerosis in cerebral arteries may lead to symptoms that include sudden numbness or weakness in the arms or legs, difficulty speaking or slurred speech, or temporary loss of vision in one eye. These symptoms can be transient; however, if left untreated, they may ultimately trigger a stroke. Atherosclerosis in arm or leg arteries may lead to symptoms of peripheral artery disease, such as leg pain when walking. Atherosclerosis in the renal arteries that supply blood to the kidneys may lead to high blood pressure or even kidney failure.

### 1.1.1 Development of atherosclerosis

Atherosclerosis is a chronic disease that affects virtually everyone to some degree by the age of 65. It generally starts at a very early age and progresses throughout lifetime. Signs and symptoms of atherosclerosis only appear after severe narrowing or closure impedes blood flow to different organs. Most of the time, patients realize that they have the disease only when they experience other cardiovascular disorders such as stroke or heart attack. These symptoms, however, still vary depending on which artery or organ is affected.

## 1.1. ATHEROSCLEROSIS

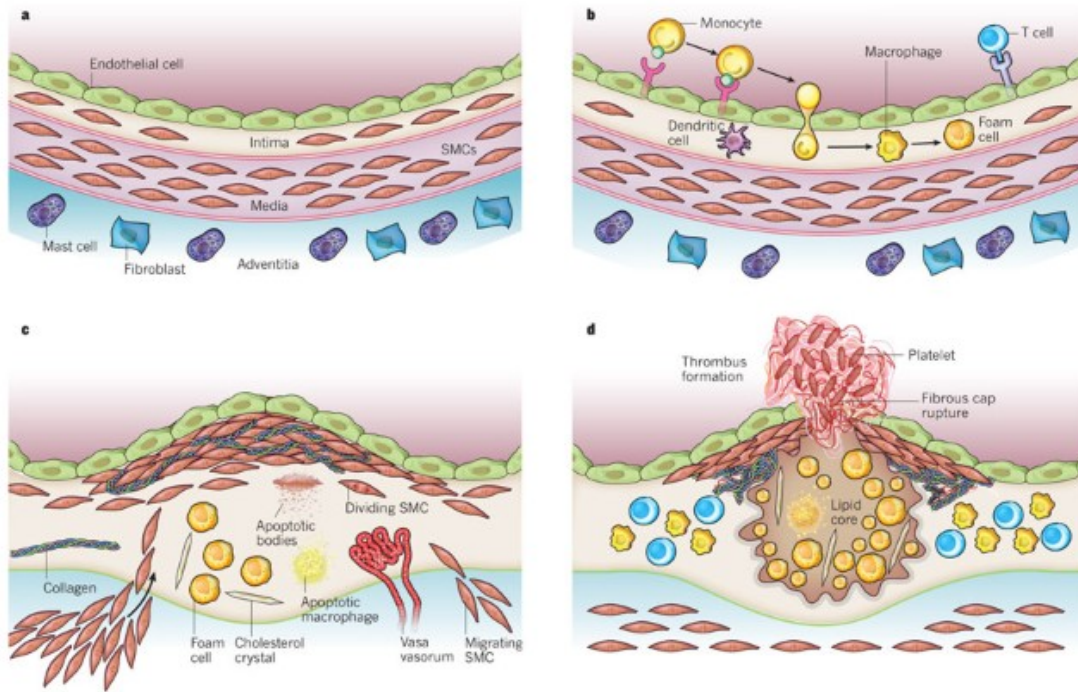


Figure 1.2: **Stages in the development of atherosclerotic lesions.** The pathological progression and the cell changes from normal muscular artery towards thrombosis are shown. a: The healthy artery with three layers. b: The activated (inflamed) endothelial layer initiates the recruitment of immune cell (monocyte). c: The migration of SMCs from the media into the intima aggravate the lesion thickening. d: Thrombosis, the ultimate complication of atherosclerosis, sometimes follows physical disruption (rupture) of the atherosclerotic plaque. Adapted from [1].

### Initiation of atherosclerotic lesions

Atherosclerotic plaques have been described to begin as fatty streaks with accumulation of lipid-laden foamy macrophages and smooth muscle cells (SMCs) [1,3], although this lesion is known to regress [2] under the appropriate physico-chemical conditions. The fatty streak phase of atherosclerosis begins with dysfunctional endothelial cells (ECs) and the retention of apoB-containing lipoproteins (LDL, VLDL, and apoE remnants) in the sub-endothelial space. Retained lipoproteins are modified (oxidation, glycation, enzymatic), which, along with other atherogenic factors, promotes activation of ECs.

Endothelial dysfunction and activation is thus the first step of atherosclerotic lesion formation and is more likely to occur at arterial curves and branches where arterial blood flow is "disturbed". Although the type of blood flow disturbance that best correlates with the localization of atherosclerotic lesions remains a subject of intense study, many

investigations have implicated low and oscillating wall shear stress. Research over the past two decades has clearly established that ECs exhibit hormonal, metabolic, and structural responses to the mechanical forces associated with blood flow and that these responses are crucial for regulating vascular tone as well as the cells' inflammation (EC activation) state. Activated ECs express leukocyte adhesion molecules that recruit monocytes from the bloodstream into the intima. Mature monocytes in the intima can then differentiate into macrophages whose excessive uptake of lipids yields foam cells, one of the hallmark features of atherosclerotic lesions [1]. EC activation is also accompanied with the recruitment of SMCs from the media into the intima[3].

The combination of arterial inflammation, foam cell accumulation, and recruitment of SMCs leads to intimal thickening that increases progressively as SMCs proliferate and secrete additional extracellular matrix proteins. Thus, the proliferation of resident intimal SMCs and media-derived SMCs and the associated extracellular matrix secretion leads to progressive thickening of the arterial wall.

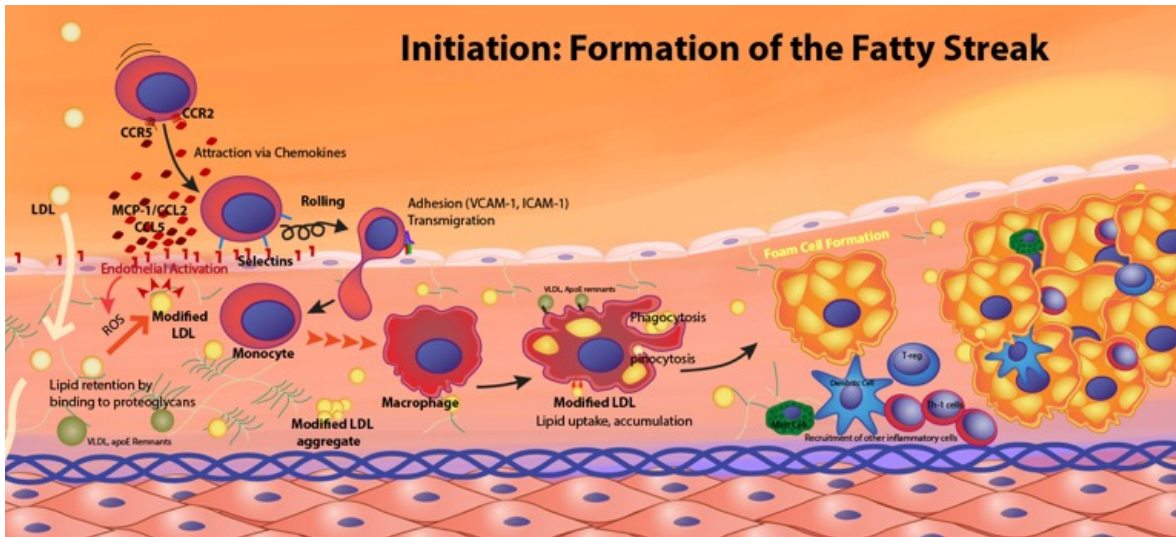


Figure 1.3: **Initiation and fatty streak formation of atherosclerosis.** The fatty streak phase of atherosclerosis begins with dysfunctional endothelial cells. Retained lipoproteins are modified (oxidation, glycation, enzymatic). These factors, in conjunction with other atherogenic factors, facilitate endothelial activation. Adapted from [3].

### Advanced atherosclerotic lesions

The more advanced stage of atherosclerotic lesion is classified as fibroatheroma [4][5], which is characterized by the presence of a lipid-rich necrotic core encapsulated by fibrous tissue. In all types of atherosclerotic lesions, once the necrotic lipid-rich core is

formed, the lesion is considered as advanced. Between the lipid core and the endothelial surface, the intima contains SMCs with or without lipid droplet inclusions. Frequently, macrophages, macrophage-derived foam cells, and lymphocytes are more densely concentrated in the lesion periphery. The identification of different cell types are based on morphological features and expressed biomarkers. During lesion development, intimal SMCs undergo phenotypic switching and thus become phenotypically distinct from their medial counterparts. More specifically, intimal SMCs switch from a contractile phenotype to a more synthetic phenotype characterized by increased synthesis and secretion of extracellular matrix proteins [6].

The concept of SMC phenotypic switching is widely accepted. SMCs possess remarkable phenotypic plasticity which allows rapid responses to environmental cues. Responding to certain mechanical or biological factors, SMCs undergo phenotypic transition and can even turn into macrophage-like cells both *in vitro* [7] and *in vivo* [8]. This notion introduces additional ambiguity regarding definitive identification of the cells present within atherosclerotic lesions.

In the past decades, studies applying fate-mapping and lineage-tracing techniques have revealed the limitations of relying on ‘SMC-specific’, function-associated markers to infer SMC identity [9][10][11]. These studies revealed a much more substantial role for SMCs in atherosclerosis than previously thought, contributing to macrophage-like cells, foam cells, osteochondrogenic cells, and MSC-like cells. Therefore, although it is widely accepted that SMCs play a key role in atherosclerosis development, their full involvement remains far from fully understood.

### **Stable vs. vulnerable plaques**

In stable plaques, intimal SMCs form a fibrous cap covering the lipid core. This type of plaque poses smaller risk of an acute clinical event. SMC recruitment to and proliferation within fatty lesions is a landmark step in the transition from a fatty streak to a fibrous lesion. SMCs are recruited to the luminal side of the lesion where they proliferate and generate an extracellular matrix network that forms a barrier between lesional pro-thrombotic factors and blood platelets as well as pro-coagulant factors.

Vulnerable plaques, which have a higher risk of rupture, are thought to arise from chronic inflammation of the arterial wall. The vulnerable plaque is characterized by two fundamental morphological changes: 1) formation of a necrotic core and 2) thinning of the fibrous cap. Macrophage and EC inflammatory signaling continues to promote the recruitment of monocytes and immune cells into the plaque. Macrophage-derived foam cells and other inflammatory cells produce a number of chemoattractants [3], including transforming growth factor- $\beta$  (TGF- $\beta$ ), platelet-derived growth factor (PDGF) isoforms, matrix metalloproteinases, fibroblast growth factors (FGF),

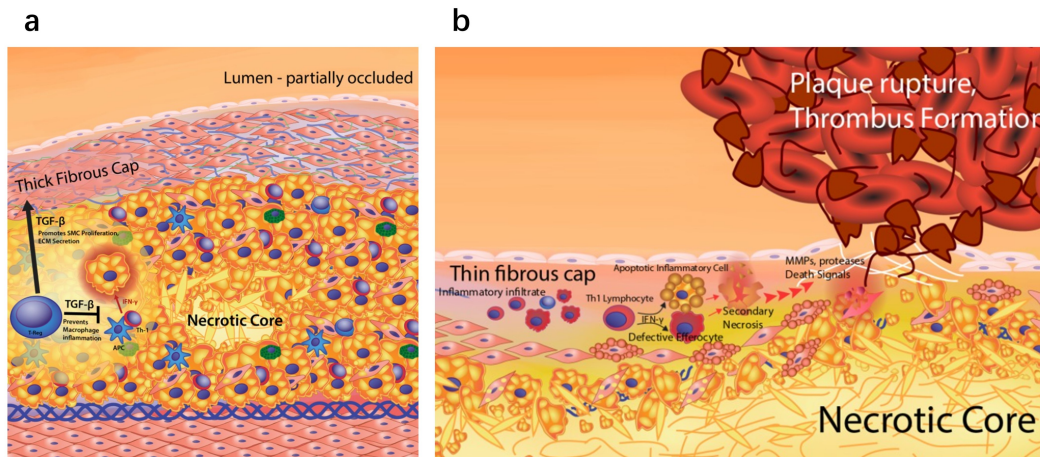


Figure 1.4: **Stable vs. vulnerable atherosclerotic plaques.** a: Formation of a stable plaque. If the cell volume of the intima increases, vascular remodeling begins such that the lumen is only partly occluded. The dense fibrous cap of the stable plaque provides an important barrier to the avoidance of plaque rupture and to the release of prothrombotic lesion factors to the blood. The release of  $TGF-\beta$  by T-reg cells and macrophages preserves the stability of the fibrous cap by being a potent stimulator for the production of collagen in smooth muscle cells. b: Formation of vulnerable plaque. The vulnerable plaque arises from the elevated, unsolved inflammatory state of the foam cell nucleus of the lesion. Thin fibrous cap areas are vulnerable to breakup by exposing prothrombotic components to platelets and pro-coagulation factors, contributing to thrombus development and clinical incidents. Adapted from [3]

and heparin-binding epidermal growth factor (HB-EGF). In addition, pro-inflammatory macrophages have impaired atheroprotective functions including cholesterol efflux and efferocytosis. The defective efferocytosis of inflammatory apoptotic macrophages results in secondary necrosis leading to an enlarged necrotic core composed of leaked oxidative and inflammatory components. This unresolved inflammation causes thinning of the fibrous cap resulting from increased SMC death, enhanced extracellular matrix degradation and decreased extracellular matrix production. Areas of thin fibrous cap are prone to rupture exposing pro-thrombotic components to platelets and pro-coagulation factors leading to thrombus formation and clinical events.

### 1.1.2 Therapy

Atherosclerosis may be preventable to some extent, and there are some treatment options that appear to improve patient outcome. Treatment of established atherosclerotic disease may include medications to control blood pressure and cholesterol level, or medications that decrease risk of clotting, such as aspirin[12]. When medication alone is

insufficient to control the process of vascular obstruction, a number of interventional procedures of varying degrees of invasiveness may also be carried out including percutaneous coronary intervention (PCI) and surgery[13].

### Drugs to Reduce High Blood Pressure

Lowering blood pressure decreases the risk of atherosclerosis and its complications[14]. The long-term regimes, such as diet and regular exercise, are sometime insufficient when advanced atherosclerotic disease has already developed[15].

– **Thiazide diuretics:**

Thiazide diuretics are often the first[], but not the only, choice in high blood pressure medications[16][17]. Thiazide diuretics include chlorthalidone, hydrochlorothiazide (Microzide) and others. Diuretics, sometimes called water pills, are medications that act on the kidneys to help the body eliminate sodium and water, reducing blood volume.

– **Angiotensin-converting enzyme (ACE) inhibitors:**

The role of ACE in thickening of arterial wall has been well established in animal models. ACE activation contribute to the neointima restenosis and myocardial structure changes after vascular injury[18][19]. ACE inhibitor prevent ACE activation, which prohibit the cardiac remodeling and extend survival time after myocardial infraction[20][21]. ACE inhibitors includes lisinopril (Zestril), benazepril (Lotensin), captopril (Capoten) and others, help relax blood vessels by blocking the production of vasoconstricting agents that narrow blood vessels[22].

– **Angiotensin II(Ang II) receptor blockers (ARBs):**

Historically, neurohormonal regulation of blood pressure is the major function of Ang II[23]. Local production of Ang II within the arterial wall can regulate the arterial tone in the normal artery, as well as can potentially lead to atherosclerosis and form pathological artery. ARBs help relax blood vessels by blocking the Ang II action of angiotensin II[24]. ARBs include candesartan (Atacand), losartan (Cozaar) and others. Individuals with chronic kidney disease may benefit especially from having an ARB as one of their medications.

– **Calcium channel blockers(CCBs):** The concept CCBs have the anti-atherosclerotic effect originated from Fleckenstein’s pioneering work[25]. The related potential cellular mechanisms includes interactions with vascular smooth muscle cells: migration, inhibition of proliferation, or both[26][27] These medications, including

amlodipine (Norvasc), diltiazem (Cardizem, Tiazac, others) and others, induce SMC relaxation. Some have been shown to reduce heart rate.

### **Lower LDL Cholesterol**

Low density lipoprotein (LDL) is the primary carrier of cholesterol in the bloodstream[28]. LDL level has been considered as one of the most direct indices of atherosclerosis risk, although this issue has recently been the subject of renewed debate[29][3].

– **Statins:**

Statins are the the most effective medications for lowering LDL cholesterol levels in most individuals[30]. Thus, they are also the most widely used cholesterol-lowering drugs. Statins have been reported to cause LDL levels to fall by up to 50%[31]. They also raise the levels of high density lipoprotein (HDL), which is often referred to as the "good" cholesterol. Statins can also help lower the level of triglycerides in the bloodstream.

One effect of statins is to reduce vascular inflammation, which has a stabilizing effect on the plaque. For this reason, statins are now widely used for treating atherosclerosis.

– **Fibrates:**

Fibrates are drugs that reduce triglyceride levels. Triglycerides are not cholesterol, but they are lipids that have been reported to contribute significantly to the development of atherosclerosis. Combination therapy with statin and fibrate provides a major clinical benefit in the treatment of severe hyperlipidemia. [32]

– **Niacin:**

Niacin is a vitamin that appears to reduce both triglycerides and LDL. It also has been reported to increase HDL[33]. The used of Niacin is not the most widely used because its side-effect. Niacin may cause skin flushing in many patient[34]. In addition, this medication can increase blood sugar levels, which is a problem especially for diabetic patients.

### **Percutaneous coronary intervention (PCI)**

Percutaneous coronary intervention, previously termed angioplasty, is a minimally invasive endovascular interventional procedure using either a balloon catheter alone or a balloon catheter plus a stent to open up narrowed vessels.

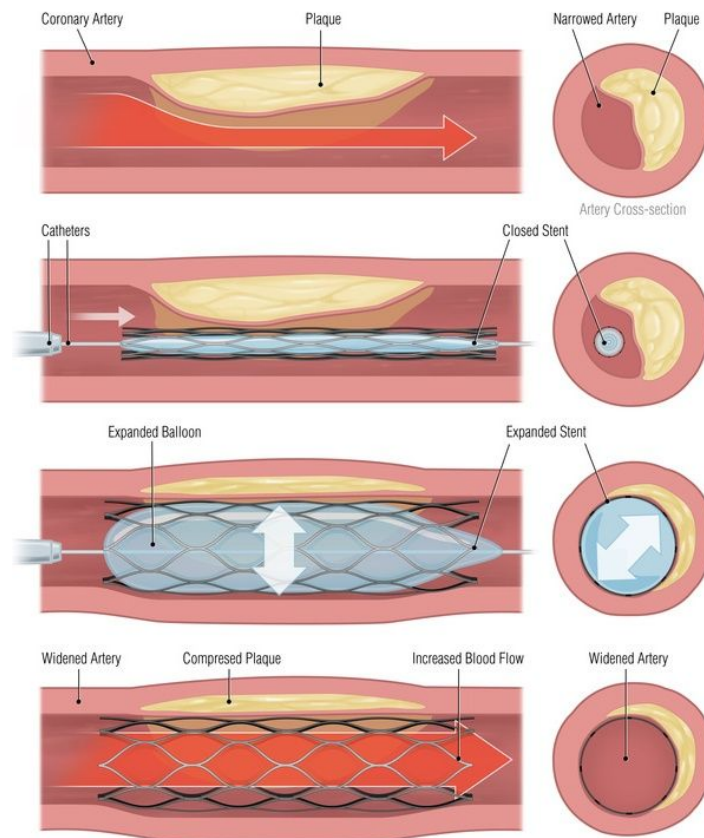


Figure 1.5: **Process of PCI.** Adapted from <https://www.pinterest.ch/pin/54043264255726049/>.

### – Balloon angioplasty

Balloon angioplasty, or percutaneous transluminal coronary angioplasty (PTCA) in the specific case of coronary arteries, consists of the inflation of a balloon catheter at the blockage site in the artery in order to compress the plaque against the arterial wall. In addition to coronary arteries, balloon angioplasty can also be performed on different narrowed vessels including carotid arteries, the aorta, iliac arteries, femoral arteries, popliteal arteries and the tibial and peroneal arteries in the lower leg.

Balloon angioplasty alone is associated with high rates of restenosis[35] within several months within months post-angioplasty due to uncontrolled SMC proliferation and migration leading to intimal hyperplasia. The elevated incidence of restenosis in the case of balloon angioplasty led to the development of endovascular stents.

### – Endovascular stents:

Stents are thin, mesh-like devices, that are most commonly metallic (but can also be polymeric). Stents are deployed into a narrowed artery in a collapsed state and are expanded at the stenosis site. Stent expansion is most commonly accomplished using a balloon catheter on the back of which the unexpanded stent is loaded [36].

The objective of leaving a stent in artery is to maintain the vessel open (and hence re-establish blood flow) as well as to provide a scaffold that lends structural stability to the diseased arterial wall. The rate of restenosis decreased compare with balloon angioplasty. However, thrombosis and restenosis are still two major complication of stent implantation[37].

## Surgery

The PCI treatment have led to severe complication. It occur fast, typically within months to years, compared with the decades that it generally takes for disease initiation. Moreover, if the blockage is too severe to implant a stent, doctors will choose surgical treatment.

- **Coronary artery bypass grafting(CABG):**

Bypass surgery in coronary artery is a surgical operation to transplant a normal artery to substitute a blocked artery and transport natural blood flow to the obstructed coronary artery. The rates of severe complications at 12 months were significantly lower in patients with the CABG treatment compare to the patients with the PCI[38].

- **Carotid endarterectomy**

Carotid endarterectomy is a procedure that extracts the buildup of the plaque from the inside of the carotid artery in your neck[39]. If a diagnostic test such as carotid ultrasound imaging reveals a severe blockage, carotid endarterectomy may be carried out. Removing plaque that causes your artery to widen can increase blood flow in your carotid artery and reduce your risk of stroke. Patient will get a local or general anesthetic in carotid endarterectomy. Your surgeon makes an incision in the front of your spine, exposes the carotid artery, and removes the plaques that obstruct the artery. Then, the surgeon can restore your artery with stitches or a patch made of a vein or artificial material.

In atherosclerotic lesions and stent-related complications, there is extensive reorganization of SMCs as well as accumulation of immune cells. SMC recruitment and mobilization from the media into the thickening intima can be thought of as a form of collective cell migration and aberrant proliferation; therefore, it is useful to review some of the concepts associated with collective cell behavior.

## 1.2 Biophysical approaches to collective cell behavior

The application of physics-based approaches to biological phenomena has received considerable attention in the past decade. In the specific case of collective cell behavior, considerable insight has been gleaned by using the principles of soft matter physics, nematic liquid crystals, and active fluids. The most significant aspect of my PhD work has focused on describing the sequence of specific events that lead to the spontaneous emergence of three-dimensional SMC clusters from multi-layer cell sheets. In this work, the experimental characterization of each of these events is accompanied with some physical modeling that provides insight into the underlying processes. This work is described in detail in Chapter 3. Here, I wish to provide more general information about some of the relevant phenomena and frameworks.

### 1.2.1 Collective migration

Collective migration is one of the most commonly studied phenomena in collective behavior. Collective migration can be viewed at different scales: from the microscopic cellular level to the macroscopic organisms level. At the macroscopic level, insects [40], birds [41], fish [42], and humans [43] can collectively organize themselves as highly dynamic flocks in order to maximize the individuals' chances to survive against a predator, to find food more efficiently [44], and to minimize energy consumption [45]. In animal models, there are generally three dynamically-stable states of organization: the swarm (S) state, the polarized (P) state and the milling (M) group state (Fig. 1.7).



Figure 1.6: Examples of collective behavior in different animal groups. a: Bird flock <https://earthsky.org/earth/how-do-flocking-birds-move-in-unison> b: School of fish <https://allthatsinteresting.com/schooling-fish> c: Crowds of human marchers <https://www.istockphoto.com/de/foto/antenne-die-menschen-dr%C3%A4ngen-sich-im-hintergrund-ansicht-von-oben-gm1170710326-324055832>.

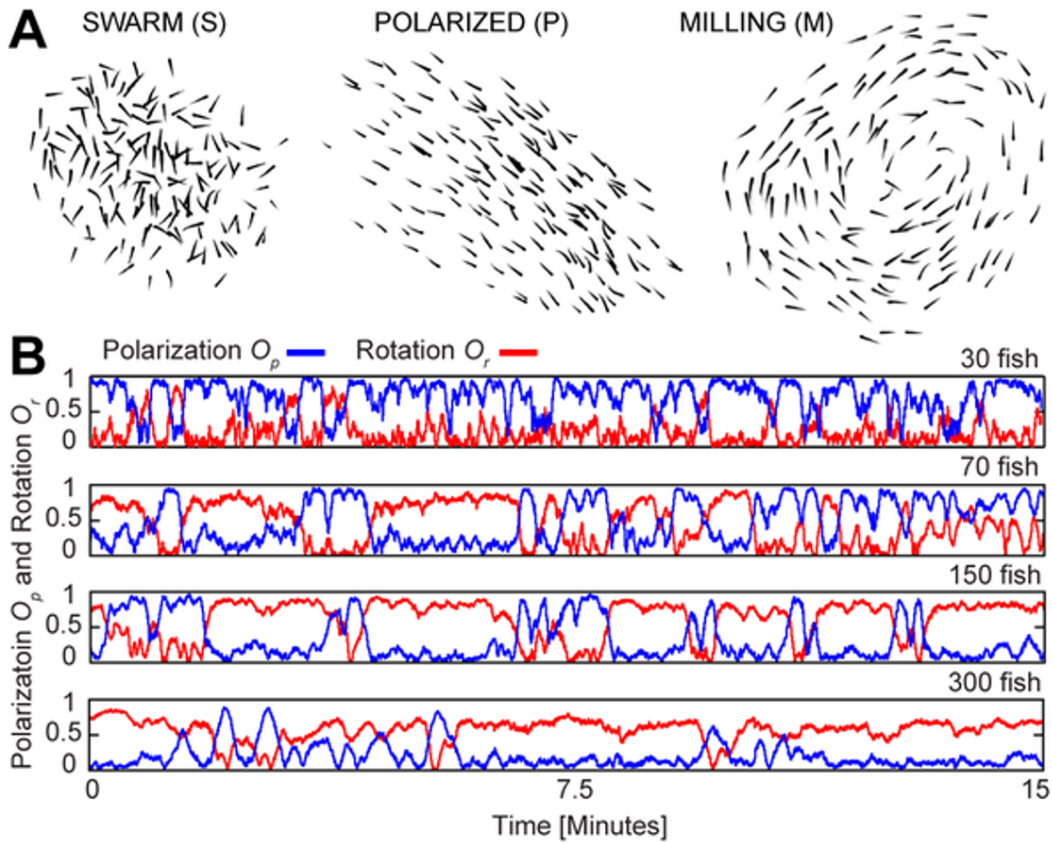


Figure 1.7: **A: Dynamical state of schooling fish.** Illustration of the configurations that displayed by the fish schools: swarm state (S), polarized state (P) and milling state (M). **B:** Extracts of time series of order parameters for classes of 30, 70, 150, and 300 golden shiners. The rotation  $O_r$  in red tests the rotation grade near the center of mass of the fish school. The rotation  $O_r$  measures the rotation grades in blue. [42].

At the cell and tissue levels, collective cell migration has been extensively studied during the past decade. Single cell migration and collective migration are the two principal modes of migration at the cellular scale. Understanding collective cell migration is important in many areas including tissue morphogenesis, embryonic development, tissue remodeling and tumor growth [46]. In an area more closely related to my PhD research, collective migration of medial SMCs into the intima is at the heart of intimal hyperplasia and atherosclerotic plaque initiation.

There are three key aspects that characterize collective cell migration: 1) cells are physically and functionally connected during the motion, 2) cytoskeleton-mediated traction forces and protrusion forces are generated to allow cells to migrate while maintaining their cell-cell contacts, and 3) structural modifications of the tissue during migration [47]. The cytoskeleton and associated molecular motors play a central role in regulating cellular migration; therefore, it is important to discuss the different cytoskeletal

elements and their roles in force generation and migration.

The cellular cytoskeleton is principally composed of three families of filamentous proteins: actin filaments(F-actin), microtubules and intermediate filaments [48]. F-actin are formed from double-helix polar polymers. The ratio of the polymerization rate to the depolymerization rate can trigger various dynamics, including "tread-milling" where the length of the filament remains constant. Microtubules are long and rigid hollow polymers of tubulin that form part of the cytoskeleton and support the shape of a cell. Similarly to F-actin, They will dynamically change their length by polymerization and depolymerization at both ends. It play a vital role in chromosome separation during cell division. Intermediate filaments are the third major type of cytoskeleton filaments appeared in eukaryotic cells. The assembly of intermediate filaments does not require ATP or GTP hydrolysis. Moreover, it is not considered to be involved in the cell migration or the force generation.

In living cells, the F-actin cytoskeleton encompasses a number of different mechanisms that are central to many different aspects of cell physiology[49]. For each phase, the F-actin cytoskeleton has a distinct molecular composition and structure which indicates that the mechanical properties of these networks can be aligned to a particular aspect of cell physiology, such as cell protrusion (lamellipodia and filopodia)[50][51], adhesion (lamella[52] and stress fiber[53]) and shape change (cortex[54]).

### 1.2.2 Physical models to describe cell collective behavior and organization

#### Nematic liquid crystals

In both passive and active nematics, the local orientation of "matter in liquid crystals" can oscillate, but in general, the block point towards a "leading direction". The dynamics of these systems is represented by the spatio-temporal related directional evolution. These systems can be further defined as 'active' if their components absorb energy and generate forces, producing a wealth of complex behavior. Through the contractile forces that they generate, cells certainly fall in this category.

Recently, the structure of active nematics has been shown to be informative in the interpretation of different phenomena in a number of biophysical systems [56][57], including *in vitro* cytoskeletal networks [58], cell monolayers [59][60], bacterial cultures [61] and *in vivo* cell culture [62].

The transition from randomly-orientated cells to aligned cells can be perfectly explained by a physical concept, the isotropic-to-nematic transition. Thus, many spindle-shaped cells alignment is described by nematic matters. So far, most of the active systems

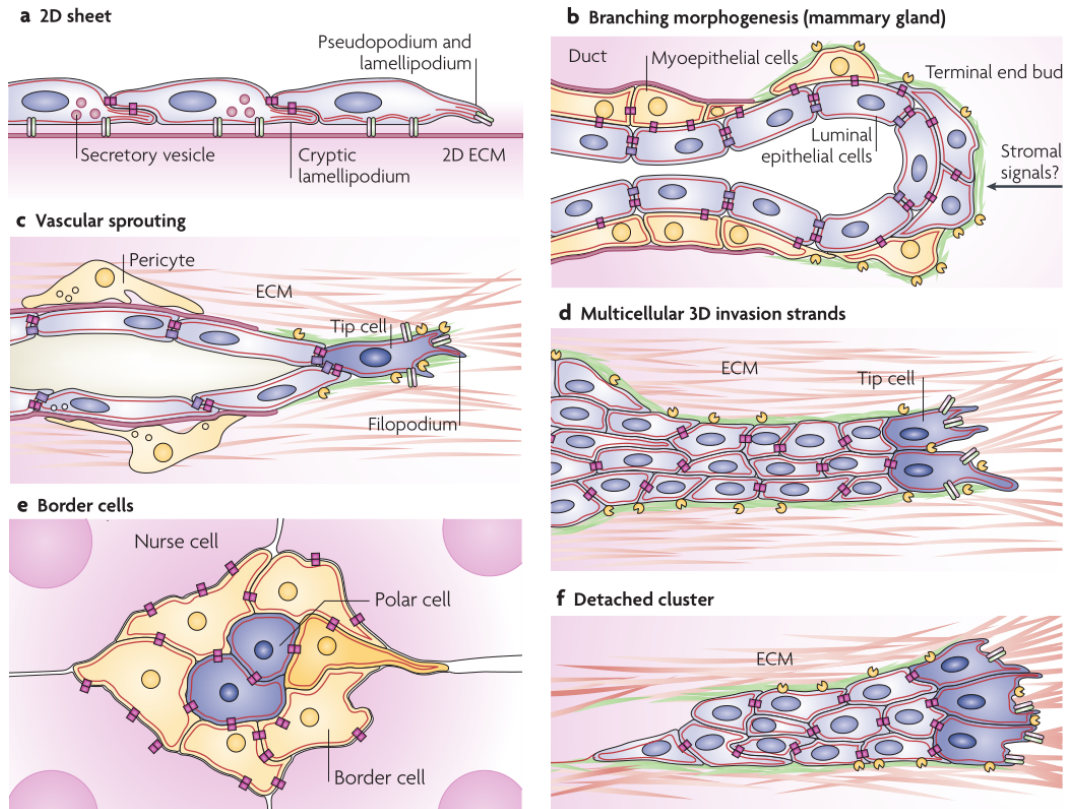


Figure 1.8: **Types and variants of collective cell migration.** In various modes of collective migration, cell morphology and cell-cell and cell extracellular matrix (ECM) adhesion. a: A coherent monolayer of the epidermal that travels across a two-dimensional substrate. b: The terminal bud sprouts during morphogenesis. c: Sprouting of vessels during angiogenesis. d: Invasion of cancer by poorly distinguished multi-cellular masses and elongated strands. e: A border cell cluster of mobile outer cells and two less mobile polar cells that move around nurse cell junctions. f: Collective invasion as a cluster. Adapted from [47]

found exist under a regime where operation is high and viscous damping is dominant in cell-substrate friction. However, live cells are known to build cell-substrate adhesion, which results in significant friction.

Topological defects are fairly ubiquitous, from fingerprints [63] to micro-level bacterial organization. To classify topological defects, the term "charge" is commonly used. Topological charge is a transition in the direction of the molecules along the singular points with a complete  $360^\circ$  rotation: for  $+1$ ,  $+1/2$ ,  $-1/2$  and  $-1$  faults. The molecules spin through  $+360^\circ$ ,  $+180^\circ$ ,  $-180^\circ$  and  $-360^\circ$ , respectively 1.10. Topological defects can shift and interact with each other on the basis of their charge, unlike electrical systems. In active systems, topological defects can appear randomly, occur in pairs of oppositely

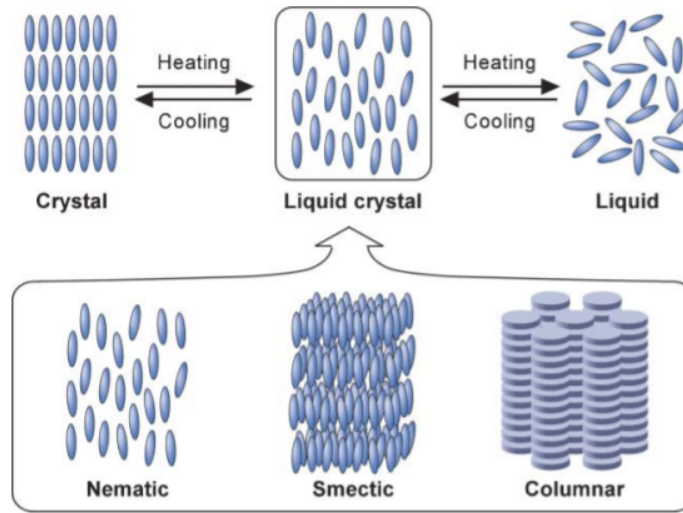


Figure 1.9: **Schematic graph of a solid crystal, a nematic liquid crystal and an isotropic liquid for a suspension of anisotropic particles.** The isotropic process has both the positional and orientational order of the short term. Low positional order and long-range orientational order are present in the nematic stage. Liquid crystals also occur in partial positional order, as in a smectic process in which the particles form a liquid-like monolayer that is two-dimensional one rod long. Adapted from: [55]

charged ones, and can be reformed by the energy input [64].

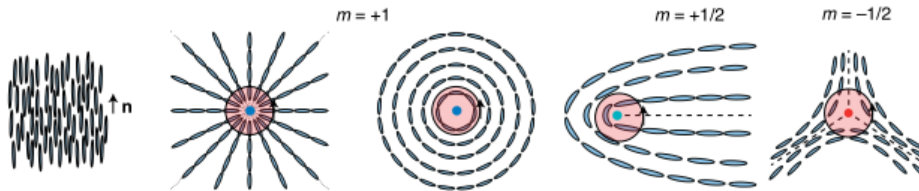


Figure 1.10: **Defect and charge.** Five typical pattern of a nematic liquid crystal. Typical director fields in a two-dimensional nematic liquid crystal in the topological defect area can be categorized by the value of the director's integral field along an imaginary circle enclosing the defect:  $m = +1$ ,  $m = +1/2$  and  $m = -1/2$ . Adapted from:[64]

Topological defects spontaneously form in different cellular systems including SMCs and cancer cells [65]. It has been shown that when plated on a surface at a sufficiently high density, these cells become self-aligned in a bi-dimensional nematic process [66][67]. With time, cell proliferation initially creates nematic ordering until a sufficiently elevated density is attained whereby cellular "jamming" occurs and the cell movement is arrested [68][69][70], resulting in the juxtaposition of broad, well-ordered domains

whose directors are not aligned. These domains are isolated by topological defects locked within the structure. From the theoretical standpoint, some previous research has addressed the behavior of defects in active nematics by incorporating active terms in the hydrodynamic equations of liquid crystals. Though there are variations among the methods [71], they nevertheless demonstrate that active structures differ from passive nematics by the random motion of  $+1/2$  topological defects acting as self-propelled particles [72][73], the formation or annihilation of pairs of opposite signs, or the related velocity correlations in mass. Most of the active structures found so far work under a zone where operation is high and viscous damping is prevalent over cell-substrate friction [58]. Live cells are known to establish adhesion to their substrate, resulting in significant friction.

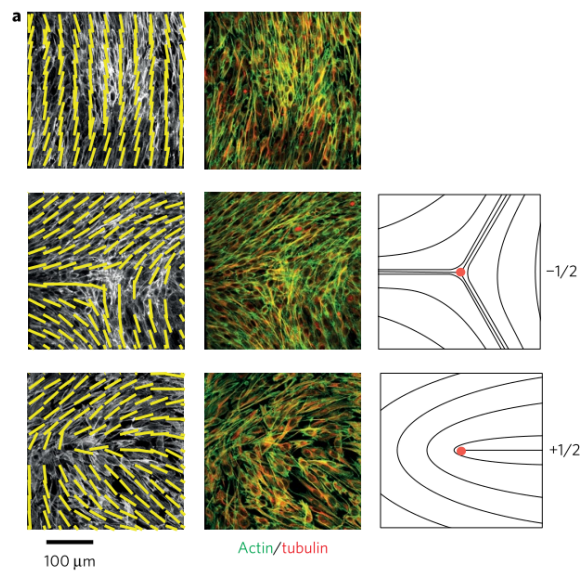


Figure 1.11: **Topological effect observed in spindle cell layer.** Identification of the two types of defects:  $m= +1/2$  and  $m=-1/2$  defects. Left: orientation field array superimposed on fluorescence images. Center: same area where actin and tubulin have been labeled. Right: Schematic figures. Adapted from: [65]

## Cellular aggregates

Cellular aggregates represent a commonly seen collective organization. Cellular aggregates are typically spheroidal structures, with a diameter of a few hundred microns, containing a few thousand cells. Aggregates have been used as a practical experimental tool to study the multi-cellular structural and tissue biophysical properties. Physically, spreading and protrusion of cellular aggregates are analogous to wetting [74][75] and

## 1.2. BIOPHYSICAL APPROACHES TO COLLECTIVE CELL BEHAVIOR

dewetting of droplets [76](Fig. 1.12 a). Biologically, 3D aggregates have been used as an *in vitro* model for research of the mechanisms of cancer invasion [77], migration [78][78] and metastasis. Moreover, aggregates are regarded as viscoelastic materials in that they exhibit a short-time elastic behavior (Elastic modulus  $E_t$ ) and a long-time viscous behavior (dynamic viscosity  $\eta_t$ ).

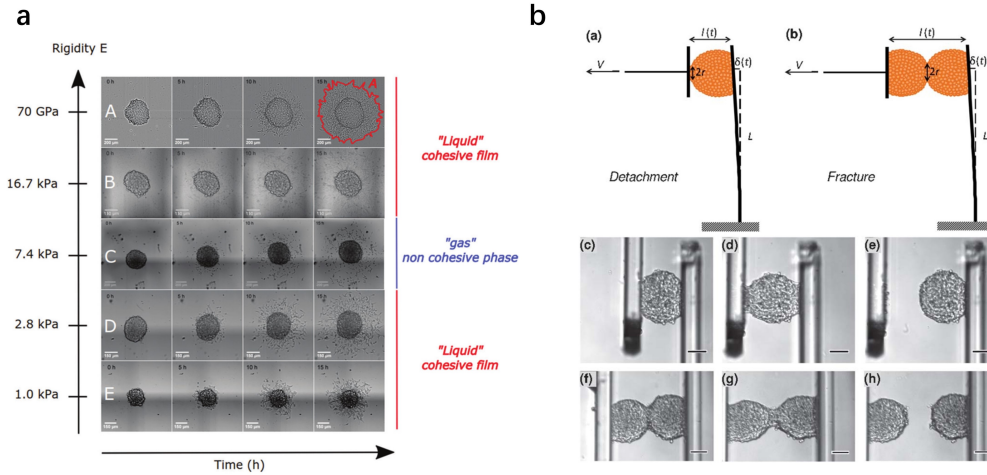


Figure 1.12: Aggregate experiments. a: Spreading of a cellular aggregate on a fibronectin coated surface which has a rigidity spectrum from rigid to soft substrates. Contact area A is defined by the red color. b: Viscoelastic fracture of cellular aggregate (a) Detachment experiment. The left plate is pulled at a velocity  $v$  until the detachment. The deflection of the cantilever on the right side reveals the applied force. (b) Fracture experiment. Two partially fused aggregates are pulled apart by pulling the left plate at a velocity  $v$ . (c) No force at the beginning of the experiment. (d) Stretched aggregate before detachment. (e) Aggregate detached. (f–h) Sequences of the fracture experiment of two aggregates,  $v=0.05 \mu\text{m}\cdot\text{s}^{-1}$ . The scale bar corresponds to  $100 \mu\text{m}$ . Adapted from [79]

Different cell types have been shown to be capable of forming aggregates. These include different types of cancer cells as well as normal tissues, such as VSMCs, and epithelial cells. The principal project during my PhD involves the observation and characterization of SMC cluster formation (see Chapter 3).

## 1.3 Specific focus: smooth muscle cells

SMCs are mural cells present in many tissues. SMCs' most vital function is contraction. SMCs are found in the walls of the digestive tract from the middle portion of the esophagus to the internal sphincter of the anus, in the walls of the ducts in the glands associated with the alimentary tract, in the walls of the respiratory passages from the trachea to the alveolar ducts, in the urinary and genital ducts, and in the walls of arteries, veins, and large lymphatic vessels.

Smooth muscle constitutes one type of muscle tissue, along with skeletal muscle and cardiac muscle. SMCs are commonly found in connective tissues. In blood vessels, along with endothelial cells, SMCs are recognized as connective tissue and can divide and provide a source of new fibroblasts, especially following tissue injury. SMCs are sometimes categorized as myoepithelial, where single SMCs localize along ducts or blood vessels lying inside the basement membrane, i.e. they are part of the epithelial layer. (Adapted from: [https://www.histology.leeds.ac.uk/tissue\\_types/epithelia/epi\\_cell\\_junctions.php](https://www.histology.leeds.ac.uk/tissue_types/epithelia/epi_cell_junctions.php))

### 1.3.1 Additional characteristics

Smooth muscle specializes in slow and long-lasting lower intensity contractions. In a smooth muscle tissue, cells contract together instead of having motor units. The smooth muscle has intrinsic contractility, and its contracting can be impaired by the autonomous nervous system, hormones and local metabolites. Since it is not controlled by subjective awareness, smooth muscle is an involuntary muscle type.

Spindle-shaped SMCs constitute of smooth muscle fibers. SMCs are generally much shorter than skeletal muscle cells. The myosin and actin filaments are dispersed throughout the sarcoplasm and are bound to adhesion spot on the cell membrane. As a fact that the contractile proteins of these cells are not organized in myofibrils, such as those of the skeletal and cardiac muscles, the striated-like pattern are not shown in smooth muscle fibers. (Adapted from: [http://medcell.med.yale.edu/histology/muscle\\_lab.php](http://medcell.med.yale.edu/histology/muscle_lab.php))

SMCs have two principal roles: contraction and secretion of extracellular matrix proteins. External mechanical and biochemical stimuli such as blood pressure and inflammatory factors modulate SMC phenotype. Further leading to the change in protein expression and thus cause pathological changes. (Adapted from: [http://medcell.med.yale.edu/histology/muscle\\_lab.php](http://medcell.med.yale.edu/histology/muscle_lab.php))

### 1.3. SPECIFIC FOCUS: SMOOTH MUSCLE CELLS

---

<b>Tissue</b>	<b>Histology</b>	<b>Function</b>	<b>Location</b>
Skeletal	Long cylindrical fiber, striated, many peripherally located nuclei	Voluntary movement, produces heat, protects organs	Attached to bones and around entrance points to body (e.g., mouth, anus)
Cardiac	Short, branched, striated, single central nucleus	Contracts to pump blood	Heart
Smooth	Short, spindle-shaped, no evident striation, single nucleus in each fiber	Involuntary movement, moves food, involuntary control of respiration, moves secretions, regulates flow of blood in arteries by contraction	Walls of major organs and passageways

Table 1.1: Comparison of Structure and Properties of Muscle Tissue Types. Adapted from: <https://open.oregonstate.education/aandp/chapter/4-4-muscle-tissue/>

#### 1.3.2 SMC dysfunction and associated diseases

Abnormalities in SMC proliferation and contraction play a central role in the development and progression of several chronic diseases such as atherosclerosis and asthma. Interestingly, despite the central involvement of SMC dysfunction in these diseases, they are rarely studied together because of the diversity of tissues in which they develop.

The role of SMC in different stages of atherosclerosis development was presented, as we have introduced in introduction 1.1. The majority of the experimental work of my PhD was using aortic smooth muscle cell. The pathological manifestations of SMC in atherosclerosis is the inspiration for my most important work (See Chapter3).

Table 1.2: SMC aberrant proliferation related diseases

Disease	Anatomical location	Abnormal tissue	Ref.
Atherosclerosis	Artery anywhere in the body: coronary artery, abdominal artery...	Thickening of intima	[80],[81]
Asthma	Trachea Bronchus	Thickening of the epithelial reticular basement membrane	[82],[83]
Uterine fibroid	Uterine	Round, well circumscribed, solid nodules	[84],[85]

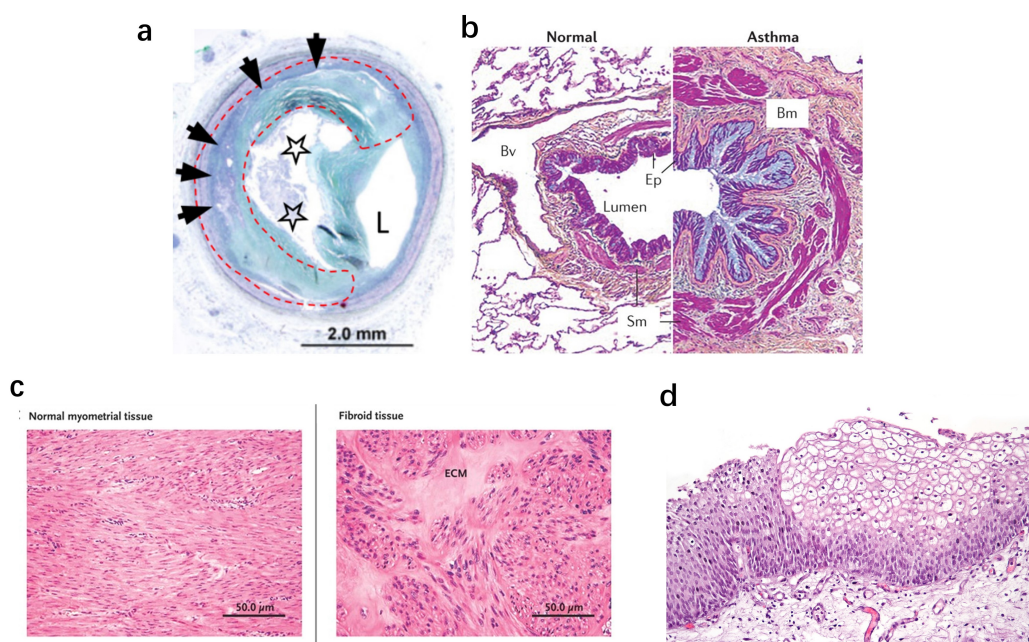


Figure 1.13: Different representations of SMC proliferation and hyperplasia in diseases. a: Atherosclerotic plaque [86], b: Bronchial asthma [87] c: Uterine fibroid[88] d: Urothelial hyperplasia[89]

### 1.3.3 SMC phenotypes

In healthy arteries, SMCs have a fusiform shape, express contractile proteins (including *alpha*-smooth muscle actin (SMA, also called ATCA2) and smooth muscle myosin heavy chain (SMMHC; also known as myosin 11 (MYH11)), which are organized into myofil-

### 1.3. SPECIFIC FOCUS: SMOOTH MUSCLE CELLS

aments) and secrete extracellular matrix macromolecules including elastins, collagens and proteoglycans.

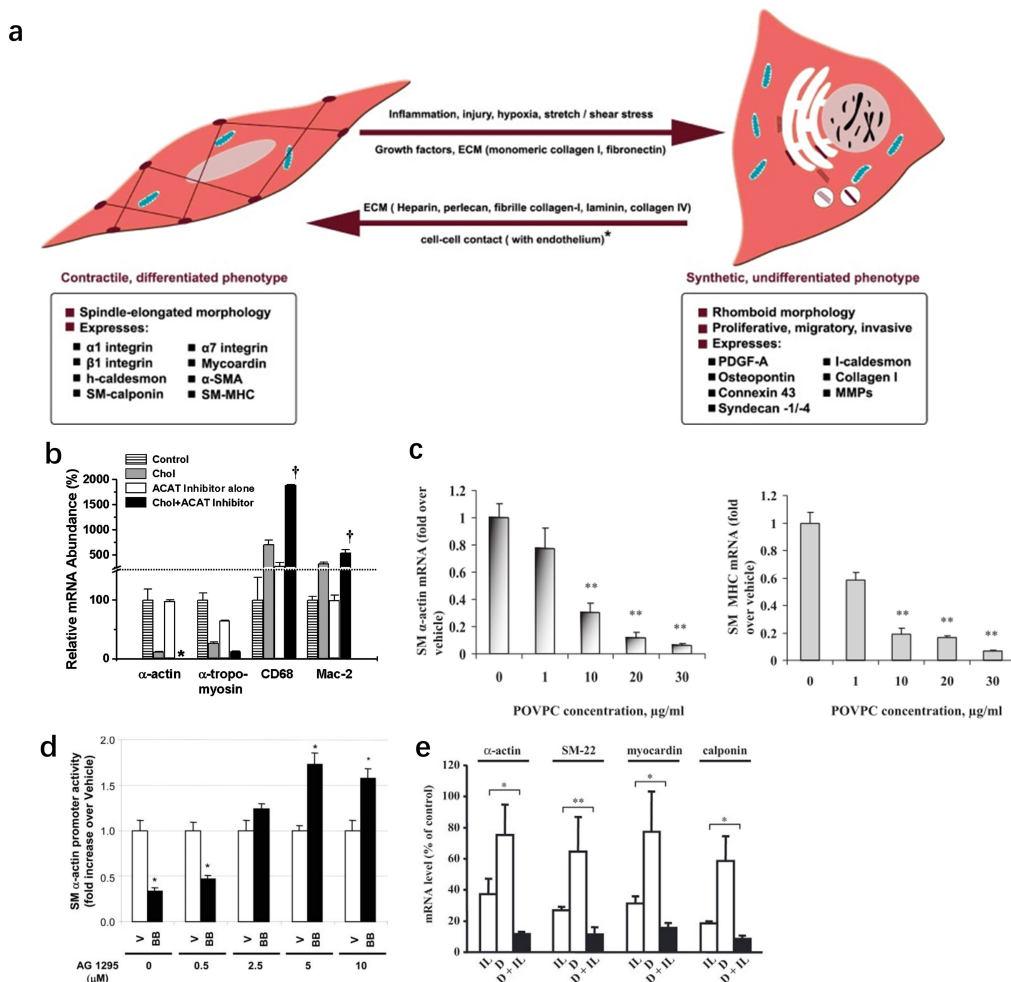


Figure 1.14: Phenotypic switching of SMC with specific marker expression. a: Schematic graph of SMC phenotypic change [90] b: The effects of free cholesterol on SMC- and macrophage-related gene expression [7]. c: POVPC decreased expression of SMC marker genes in cultured SMCs [91]. d: PDGF- $\beta$  receptor tyrosine kinase inhibition blocked PDGF-BB-induced repression of SM alpha-actin promoter activity [92]. e: The effect of IL-1 $\beta$  on the SMC markers:  $\alpha$ -Actin, SM-22, myocardin and calponin [93].

The study of SMC phenotypic identification based on specific markers [96][97] or on gene expression profiles [98] both *in vivo* and *in vitro* dates back to 1970. Due to the differential nature of a mature SMC, phenotypic switching of SMC with specific protein expression are intensively used as a classical methods of understanding the role of SMC during the development of disease. In the field of atherosclerosis, numerous reports

### 1.3. SPECIFIC FOCUS: SMOOTH MUSCLE CELLS

Gene	Function	Nor M	Normal I	Athero M	Athero I	Reference
SMA	Contraction	++++	-	+++*	+ <sup>FC</sup>	[94]
MHC	Contraction	++++	-	?	?	
Osteoglycin	Matrix	+++	+	+	+ <sup>FC</sup>	[95]
MGP	Matrix	++	++	++	++	[94]
OP	Matrix	-	-	-	+/-	[94]

Table 1.3: Marker expression in atherosclerosis. Normal vessel indicates with dense media (M) and diffuse intimal thickening (I) composed of matrix and SMCs; atherosclerotic vessel with lesions ranging from fatty streak to eccentric lipid, calcium and macrophages containing plaque. Levels of gene expression are described as -, undetectable; +/-, barely detectable; or + to +++, detectable to high. \* indicates that the marker gene has not been expressed by all cells. +<sup>FC</sup> indicates that the most common region of expression in the intima was the fibrous cap.

showing that SMCs down-regulate the expression of SMC differentiation marker gene when triggered with environmental cues present in atherosclerotic lesions, including cholesterol[7], POVPC[91], PDGF-BB[92], and interleukin (IL)-1 $\beta$ [93].

Identification of cell types by specific markers to distinguish cell types from different cell types in atherosclerotic plaque[96][99][97][98] has been taken as a "golden role" since 1970. Thus, combined with the immunostaining of the histological results, it's widely accepted till today that, atherosclerotic plaque or thickening intima consist of smooth muscle cell, macrophage, T cells, foam cells and osteocytes. Dating back to 1980, people have naturally arrived at the impression of a far-reaching dogmatic conjecture that immune cells, such as, macrophage, T cells and foam cells are differentiated from monocyte and osteocytes are differentiated from Mesenchymol Stromal Cells (MSC). In the majority of advanced atherosclerotic plaque, SMA positive cells only appear at cap and plaque shoulder of a plaque. In the rest places of a plaque, immune cells are distributed. The role of immune cells in atherosclerosis development has thus become a widely discussed subject[100][101].

However, the role that SMCs play in atherosclerosis development has been underestimated because of inaccurate cell identification in atherosclerotic lesion. Studies about the phenotypic switching of cells in plaque led to the previous dogma. Researchers gradually discovered that many cell types found in atherosclerotic lesions originated from vascular SMCs. Since the 1960s, it has been known that SMCs can give rise to foam cells[102][103]. In the late 1990s, it was discovered that osteochondrogenic cells can be differentiated from SMCs [104][105], which leads to calcification in plaques. Later, the mechanisms governing SMC switching to macrophages both *in vitro* [8] and *in vivo*[10] were elucidated. Due to the plasticity of SMCs, they can apparently differentiate into most cell types present in atherosclerotic plaques, which implies that the markers rou-

### 1.3. SPECIFIC FOCUS: SMOOTH MUSCLE CELLS

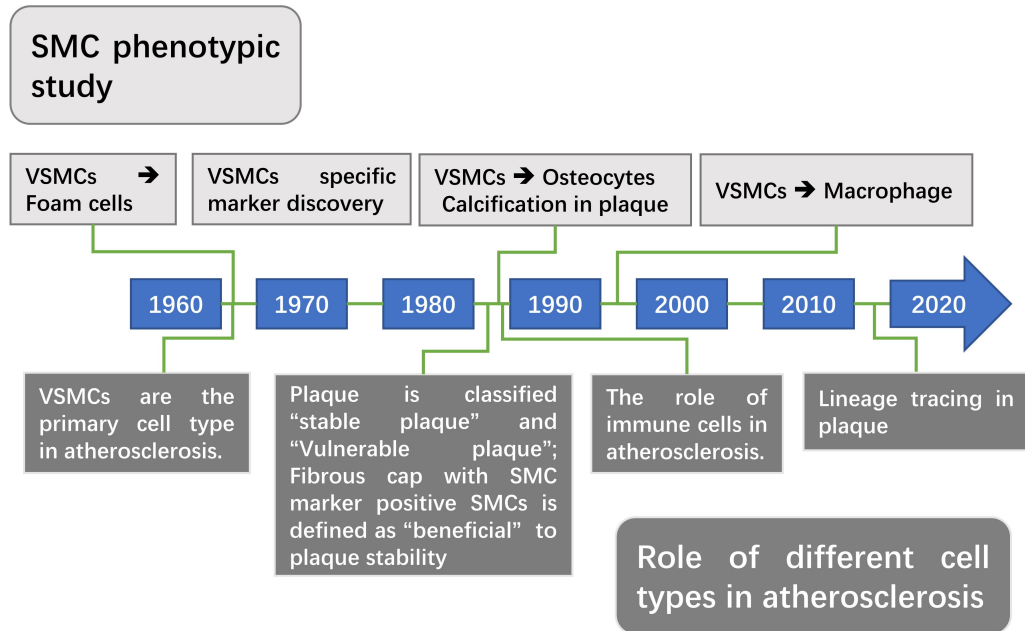


Figure 1.15: Chronology of SMC phenotypic switching and role of cell types in atherosclerosis

tinely used to identify each cell type within lesions are not exclusive to a single cell type. The major ambiguity from the previous study regarding the question of identification of the origins of many of the major cell types within atherosclerotic lesions subsequently led to lineage-tracing studies.

#### 1.3.4 SMC Lineage

Studies of SMC phenotypes have led to the belief in the atherosclerosis field that the role of vascular SMCs in advanced lesions is rather limited. The role of SMCs has generally been viewed as beneficial overall due to the cells' involvement in extracellular matrix production, which contributes to fibrous cap formation and thus to plaque stabilization and reduction of rupture risk. However, vascular SMCs have considerable phenotypic plasticity in atherosclerosis, which is often accompanied by marked changes in morphology and the expression of 'SMC-specific' markers. Therefore, identifying the cell types within atherosclerotic lesions on the basis of morphology or 'specific' markers is problematic. Indeed, basing conclusions on presumably 'SMC-specific' biomarkers has probably confounded appreciation of the full role of SMCs in atherosclerosis [9][10][106] and in other SMC-related diseases.

In the last decade, experiments using fate mapping and lineage tracing strategies have

shown the drawbacks of relying on 'SMC-specific' function-associated markers to infer SMC identity [11][9][10]. In addition, they have demonstrated the degree to which the use of these markers may contribute to false-negative and false-positive detection of SMCs, as well as the oversimplification of SMC heterogeneity and roles in atherosclerotic plaques.

Both fate mapping and lineage tracing have shown (Fig.1.16) that the majority of cells within plaque are SMC-derived. importantly,  $\sim 82\%$  of SMCs within atherosclerotic lesions (YFP<sup>+</sup> DAPI + cells) have been reported to have lost their 'SMC-specific' markers, such as ACTA2(SM- $\alpha$ actin) (Fig. 1.16a), thus underscoring the notion that the majority of SMCs within lesions cannot be reliably identified on the basis of traditional SMC markers.

### 1.3. SPECIFIC FOCUS: SMOOTH MUSCLE CELLS

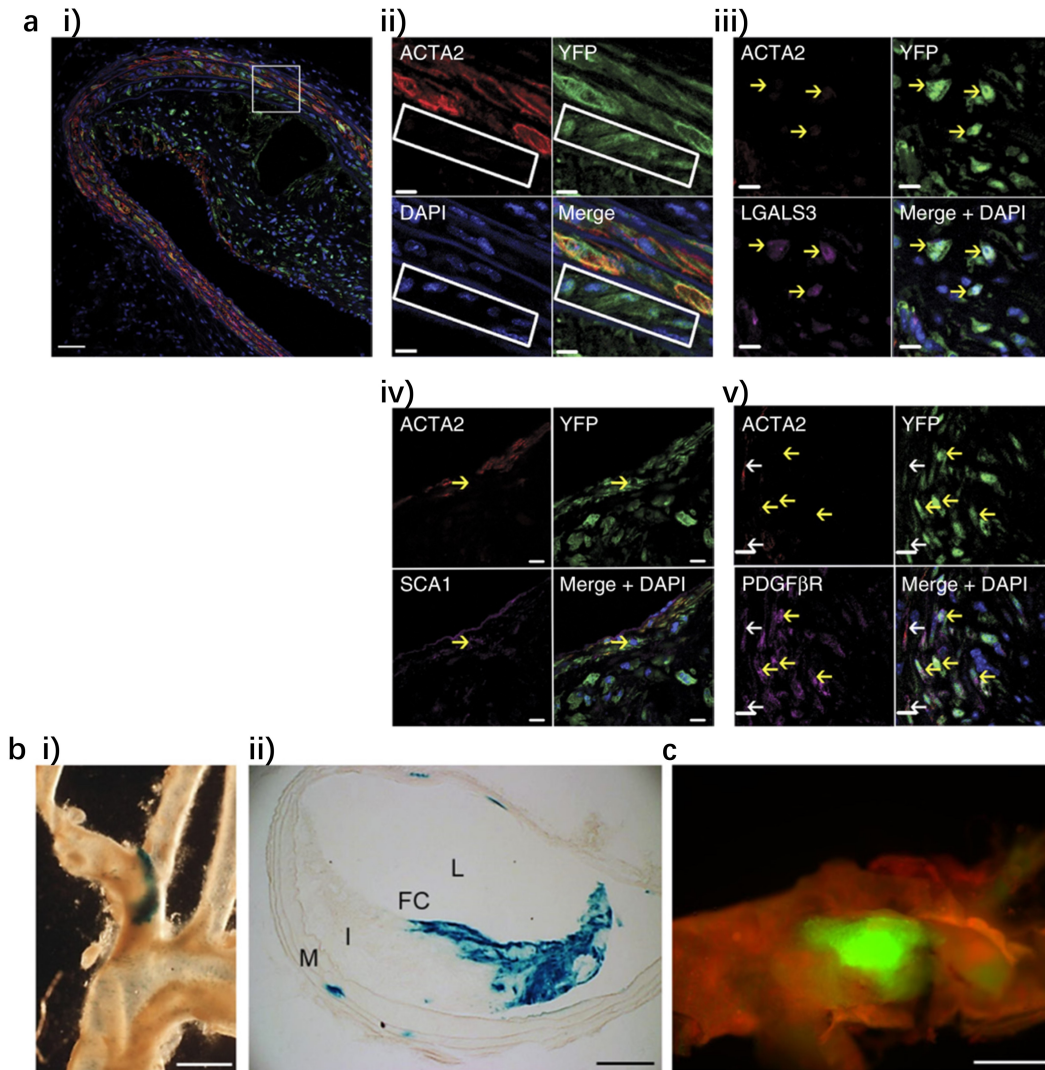


Figure 1.16: Original tracing of cells in plaque. a: Lineage tracing findings provide support for large populations of phenotypically modulated SMCs in lesions. Representative immunofluorescence staining results of brachiocephalic arteries from SMC  $YFP^{+/+}$   $ApoE^{-/-}$  mice fed a Western diet for 18 weeks. The boxed region in i) is shown at higher magnification in ii)-v). Panel a is adapted from[9] b: Fate mapping results from mice aortas as illustrated by X-Gal stained whole mounts in b i) and sections in b ii) of the respective X-Gal-positive atherosclerotic lesions. Note that in addition to the large X-Gal-positive cell patches inside plates, there was only sparse labeling of the vessel in other regions (b i) including in each lesion's underlying media (b ii). Scale bars, 1 mm (b i)) and 100  $\mu$ m (b ii)) c: Total mount of an aortic lesion isolated from a R26R-mT/mG mouse. Green fluorescence represents SMC-derived plaque cells. Panels b and c are adapted from[10]

# Chapter 2

## Balloon angioplasty-induced endothelial damage

### 2.1 Introduction

Balloon angioplasty, also called percutaneous transluminal angioplasty (PTA), involves temporarily inserting and inflating a small balloon at the location where an artery is clogged due to atherosclerotic plaque buildup. Although the use of balloon angioplasty is most common in the coronary arteries, it is also performed to open other narrowed vessels, including cerebral arteries [107][108], carotid arteries [109][110], femoral arteries [111], and iliac arteries [112]. Stent implantation, the most common treatment for vascular blockages, also often requires balloon angioplasty [113]. Due to the widespread use of angioplasty in the past three decades, there has been a considerable amount of basic and clinical research in this field around vascular occlusion and angioplasty [114][115], especially the treatment results and the long-term complication outcomes [107][116][117]. Although many *in vivo* studies both in humans and in various animal models have demonstrated that balloon angioplasty causes significant damage to the arterial wall including endothelial desquamation [118], how exactly this damage occurs remains unclear.

The endothelium is expected to encounter different types of mechanical stresses during the balloon angioplasty procedure. One stress is pressure acting normal to the endothelial surface due to balloon inflation. Another stress is the tangential shear stress due to possible balloon sliding (axial translation) along the arterial wall, and a third stress is possible scratching of the endothelium by the deflated balloon during its removal following completion of the angioplasty procedure. It is unknown to what extent each of these different stresses contributes to balloon-induced endothelial injury. It also is unknown if the relative contributions of these different stresses change depending on

the rigidity of the atherosclerotic plaque that is being treated.

Here, we used endothelialized soft- and hard-wall arterial mimics developed in our laboratory in conjunction with automated image analysis tools to quantify the extent of endothelial damage induced by balloon inflation pressure, balloon tangential displacement, and mechanical scratching from a deflated balloon.

### 2.1.1 Methods

#### *Balloon catheters*

The balloon catheters in all experiments were those used to deploy the BuMA Supreme Bare Metal Stent (SINOMED, Beijing, China) (Fig.). The diameter of the inflated balloon is 3.00 mm. The pressure added during balloon inflation is 15 atm, which leads to a maximum inflated diameter of 3.30 mm. Because the diameter of our arterial mimics is 3 mm, the balloon imposes a 10% over-expansion of the artery.

#### *Collagen arterial mimic*

Previous work in our group had reported the development of a physiologically relevant coronary artery mimic within which endovascular devices such as balloons and stents can be deployed and cellular responses monitored at high resolution in real time[119]. The wall of this arterial mimic consists of a collagen hydrogel within which SMCs can be embedded, and its luminal surface is lined with an endothelial cell (EC) monolayer (seeded typically at  $\sim 2.4$  million cells)(Fig. 2.1b). The arterial mimic has physiological dimensions (luminal diameter of 3 mm) and flow conditions with a pulsatile waveform as well as Reynolds of 360 and Womersely numbers of 16 that resemble those of coronary arteries [119]. The final flow rate applied to the *in vitro* artery was designed for hydrodynamic similarity with the flow of blood in the human coronary artery. This system was used previously in combination with automated image analysis routines developed in our group to quantitatively determine endothelial wound healing rates following the deployment of stents [119] [Rodriguez-Garcia et al. submitted] . In the present work, the arterial mimic was used to assess the extent of endothelial damage induced by the deployment of a balloon catheter.

#### *PDMS arterial mimic*

The PDMS arterial mimic consists of a 3 mm-diameter PDMS tube whose inner wall is coated with fibronectin. Endothelial cells (ECs) were seeded into the mimic and allowed to adhere. The cell seeding density and flow rate were identical to those in the collagen arterial mimic. Similar to the collagen mimic, the PDMS mimic allows control of the imposed flow and enables high resolution cellular imaging. The PDMS is considerably stiffer than the collagen hydrogel of the collagen mimic (elastic moduli

of  $\sim 5\text{-}10$  MPa vs.  $\sim 0.2\text{-}0.5$  kPa, respectively), thus providing an arterial wall that is structurally more stable.

### *Cell culture*

Bovine aortic ECs (BAECs; gift of C. Boulanger, Georges Pompidou Hospital, Paris, France) were used in this study. The cells were cultured at  $37^\circ\text{C}$  and 95% air/5%  $\text{CO}_2$ . BAECs were cultured in Dulbecco’s modified Eagle’s medium (DMEM; Invitrogen, Invitrogen, Waltham, Massachusetts, USA) supplemented with 10% fetal bovine serum (Invitrogen) and 1% penicillin/streptomycin (Cell Applications, San Diego, CA, USA) and were used in passages 4 to 10. The cells were fluorescently labelled 30 min before using by incubation with live-cell tracker dye (Cell tracker, Invitrogen, Waltham, Massachusetts, USA) for 20 mins, then washed with PBS.

### *Image acquisition*

Cell coverage was captured using imaging on a motorized stage epifluorescence microscope (Ti-E, Nikon),  $1280 \times 1024$  CCD camera (Retiga 1300C, Qimaging) and  $4\times$  magnification (1.66 mm pix21) Images were acquired before and after balloon insertion, respectively. Phase contrast and fluorescence images were acquired at each location of the  $20 \times 3$  grid with 5 % overlap in x–y spanning the whole *in vitro* artery. Each series of images was acquired with the focal plane either in the middle of the channel or in the plane tangent to the lumen. Image analysis was carried out in FIJI and a customized Matlab routine.

### *Fluorescence intensity analysis*

Evaluation of the extent of endothelial coverage was obtained from the intensity of the fluorescence signal within the arterial mimic. The intensity of the signals prior to and following balloon insertion were compared to quantify the extent of balloon-induced endothelial damage. The difference between these two intensities was denoted as the “damage signal” and is considered a measure of cellular damage. The “damage ratio” is defined as the ratio of the damage signal to the initial signal intensity.

## 2.1.2 Results

### **Endothelial damage quantification in arterial mimics**

Examples of the balloon, collagen arterial mimic and PDMS arterial mimic used in this study are shown in (Figure 2.1a). In the collagen arterial mimics, the endothelial monolayer is seeded on the collagen hydrogel, whereas in the PDMS mimic, the ECs are seeded on fibronectin-coated PDMS surfaces. Both collagen and PDMS arterial mimics

## 2.1. INTRODUCTION

---

have a 3 mm luminal diameter and a length of 6 cm. This size allows performing a variety of balloon operations on the same mimic by focusing on separate 2 cm-long sections at a time.

Examples of fluorescent images taken pre and post balloon angioplasty are shown in (Figure 2.1b). The fluorescence signal represents live and adherent ECs on the arterial wall. In the pre-angioplasty phase, the fluorescence signal is homogeneous over the entire length of the artery. In contrast, in the post-angioplasty phase, only a few cells remain on the arterial wall. The black zone inside the arterial region indicates that the cells have been damaged and have detached.

To quantify cell coverage in the arterial lumen, we sum up the intensity of each pixel along each horizontal line, which leads to the intensity profiles of the fluorescence signal for the different rows shown in Fig.2.1c. In this graph, the three curves represent three different intensity profiles for the same artery. The green curve represents the EC signal before angioplasty, while the red one represents the EC signal after angioplasty. The blue curve represents the difference between the green and red curves and thus represents the global endothelial damage. The distribution of endothelial damage can be seen in the histogram of damage ratios (Figure2.1d). The global damage ratio of is calculated from the integral based on the damage ratio histograms.

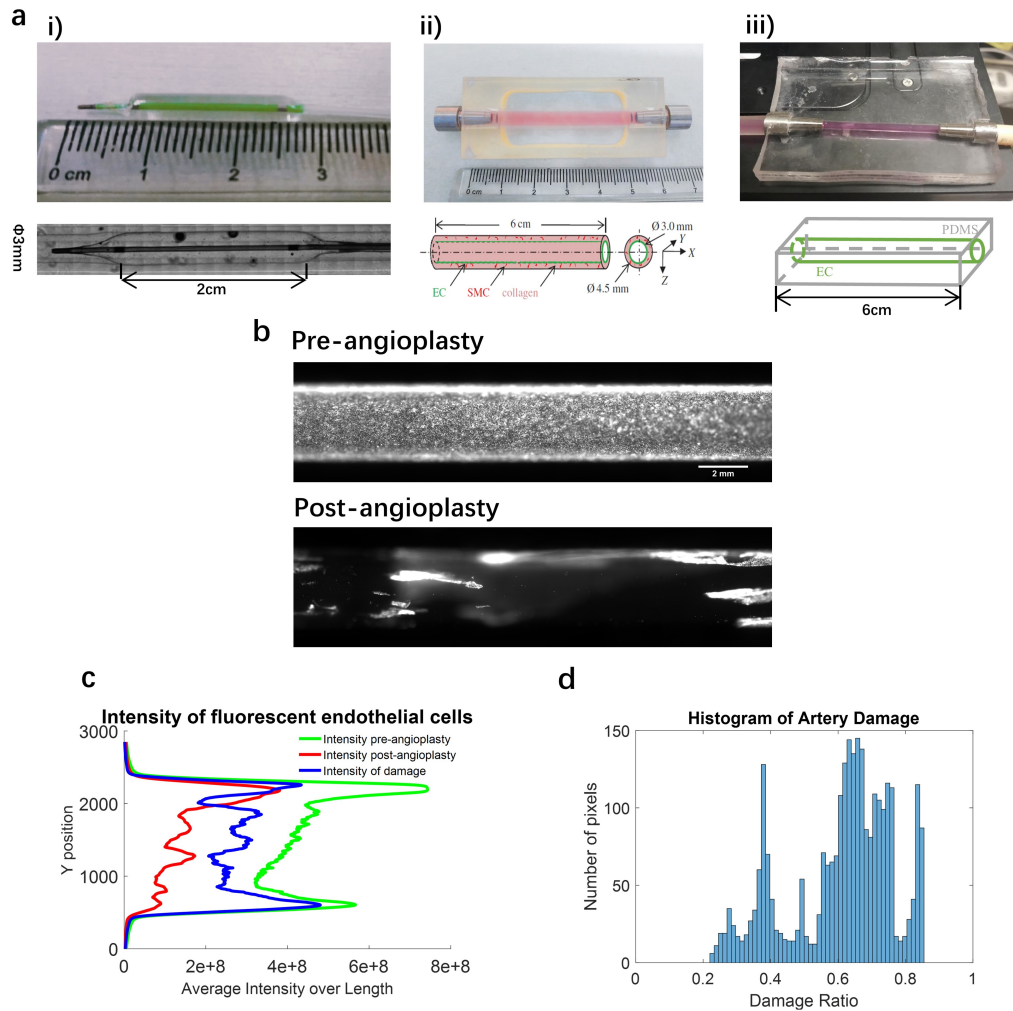


Figure 2.1: a: Photographs of balloon and arterial mimics. i) Photo of inflated balloon alone (top) and inflated balloon in arterial mimic during *in vitro* angioplasty (bottom). ii) Collagen arterial mimic (top) and schematic image (bottom). iii) PDMS arterial mimic (top) with schematic image (bottom). b: Fluorescence microscope images of PDMS artery. The pre-angioplasty artery has an intact endothelium. The post-angioplasty has a massively damaged endothelium. Fluorescence signal represents fluorescently labeled bovine aortic endothelial cells. Once there is damage, the endothelial cells detach from the arterial wall. Scale bar: 2 mm. c: Quantification of fluorescence signal. Green curve represents the fluorescence intensity of pre-angioplasty artery. Red curve represents the post-angioplasty artery. Blue curve represents the damage calculated from the difference between the pre- and post-angioplasty intensity curves. d: Histogram of damage to the endothelial cells. The damage ratio for each line in the picture is calculated as the ratio of the damage intensity (blue curve) to the pre-angioplasty intensity (green curve).

### Damage from different balloon movements

The effect of different clinically-relevant balloon movements on the endothelium was tested in 9 collagen and 9 PDMS arterial mimics. More specifically, we investigated balloon-induced damage to the endothelial layer resulting from the following three movements: 1) deflated balloon scratching, representing damage that would be induced either during balloon navigation to the target lesion or after completion of balloon angioplasty during balloon retraction; 2) balloon inflation and 3) inflated balloon translation, resulting from a common gesture used during the clinical procedures. For each movement, three separate experiments were conducted in each type of arterial mimic.

Figure 2.2) depicts an example of balloon-induced endothelial damage for each of the three balloon movements described above. The results are next described in more detail.

***Balloon inflation.*** Angioplasty involves balloon inflation at the target arterial lesion both in the case of simple balloon angioplasty as well as balloon-mediated stent implantation. Here, we inserted a deflated balloon into the arterial mimics and then inflated it by applying a pressure level consistent with what is used clinically ( $\sim 15$  atm). From the fluorescence images, it became apparent that the most severe damage in response to inflation is observed at the two ends of the balloon, consistent with its inflated shape (Figure 2.2)b i)). This result is attributable to the fabrication process of the balloon whereby the diameter of the inflated balloon at its head and tail is slightly larger than that in the middle portion. Moreover, we observed significant deformation of the soft collagen arterial wall during balloon inflation. Because of the deformation of the arterial wall and the lubrication of the medium, it was difficult to keep the inflated balloon completely in place at the target site in the case of the collagen artery. Balloon inflation invariably resulted in some level of balloon axial translation.

***Inflated balloon translation.*** This movement occurs when an inflated balloon is pulled while inflated (Figure 2.2b ii)). This movement creates not only pressure but also shear stress on the arterial wall. Thus, the damaged regions in this case are seen to be longer than the balloon inflation case. The balloon is pulled and pushed to complete the forward-backward movement in the collagen artery.

***Scratching.*** In clinical use, balloons are brought to the target lesion in a deflated state. During navigation to the target site, the folded edge is likely to contact the arterial wall. Furthermore, upon completion of angioplasty, the deflated balloon may also come in contact with the arterial wall during the process of balloon retraction. In the scratching experiments, each artery was subjected to 3 episodes of balloon back-and-forth movement. The balloon was maintained in the deflated state throughout the entire process. The linear form of damage, corresponding to the trajectory of balloon movement, clearly shows the contact between the deflated balloon edge and the arterial wall (Figure 2.2b iii)).

## Damage to arterial walls of different stiffness

The elastic modulus of a typical healthy arterial wall is  $\sim 1.5$  MPa, whereas for an atherosclerotic artery with calcified plaque, this value can be as high as  $\sim 4$  MPa [120]. Atherosclerotic arteries have been reported to experience 44% more stress and undergo 35% less strain on average compared to healthy ones [120]. Here, we used two types of artery mimics, a soft collagen and a harder PDMS, in order to assess the effect of wall stiffness on balloon-induced endothelial injury. The collagen hydrogel we used is very soft, with an elastic modulus of 0.2-0.5 kPa. It is recognized that this stiffness level is considerably below that encountered physiologically; however, the collagen stiffness could not be increased further due to experimental limitations. More specifically, one way to increase hydrogel stiffness would have been to increase the collagen concentration beyond the 6 mg/ml used here; however, increasing the collagen concentration renders it very difficult to mix the collagen sufficiently thoroughly to have a homogeneous mixture. The PDMS artery elastic modulus is 5-10 MPa, a much more physiologically relevant value.

***PDMS arterial mimic.*** Damage from the three different balloon movements in the PDMS artery is illustrated in the left column of Figure 2.2b. Balloon inflation and translation result in almost complete loss of cells. At the position of contact with the head and tail of the balloon, the damage is more thorough. Translation of the balloon creates longer damage than inflation. Balloon scratching creates a linear damage in the endothelial layer, which is caused by the contact with the edge of the deflated balloon.

***Collagen arterial mimic.*** In the collagen artery mimic (right column of Figure 2.2b), obvious damage can only be observed in the case of balloon scratching. The linear injury of the scratch appears similar to that in the PDMS arterial mimic case. In both balloon inflation and translation, very little damage is observed (Fig.2.2b). The pressure against the balloon appears to be almost fully absorbed by the highly elastic and soft arterial wall, which protects the endothelial layer. It should be noted that the collagen artery is deformed significantly due to the inflated balloon pressure.

***Statistical analysis*** Figure 2.3 provides a summary of the endothelial damage results. In the soft collagen artery, only balloon scratching led to any noticeable cellular damage, whereas balloon inflation and translation had virtually no effect on the cells as the stresses were readily absorbed by wall deformation. In the PDMS arterial mimic, on the other hand, balloon inflation and translation induced massive endothelial damage, while balloon scratching had a moderate effect.

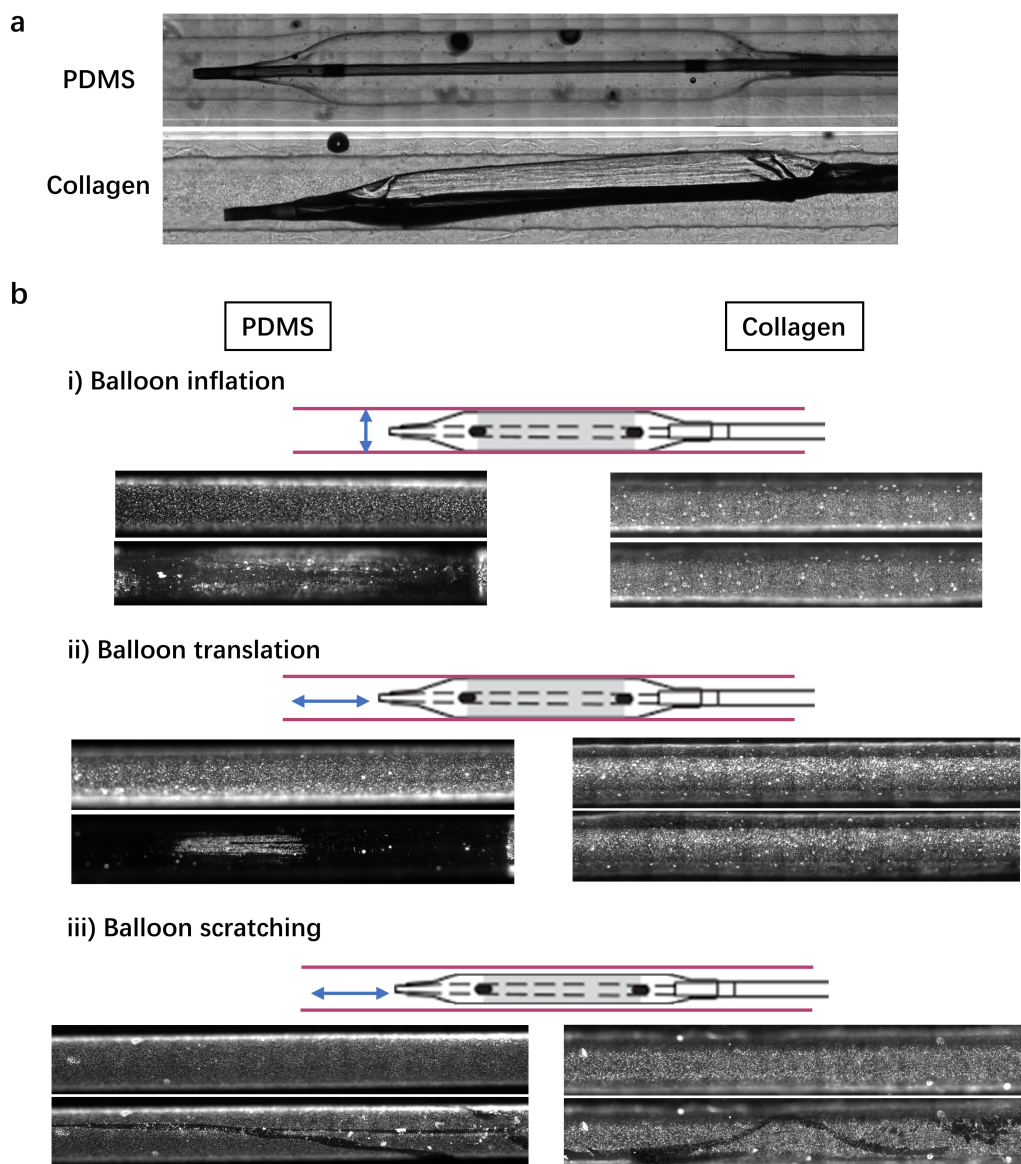


Figure 2.2: Balloon damage to the endothelial layer under different conditions in the PDMS and collagen arterial mimics. a: Bright field images of balloon in arterial mimic. Top: Inflated balloon in a PDMS arterial mimic. Bottom: Deflated balloon in a collagen arterial mimic. The balloon is 15 mm long and has a diameter of 3.3 mm when fully inflated. b: Fluorescence image of endothelial damage for the three different movements in the two types of arterial mimic. i) Balloon inflation. ii) Inflated balloon translation within the arterial mimic. iii) Deflated balloon scratching within the arterial mimic. Left: PDMS arterial mimics. Right: collagen arterial mimics. The pre-angioplasty and post-angioplasty fluorescence images are shown at the top and bottom, respectively

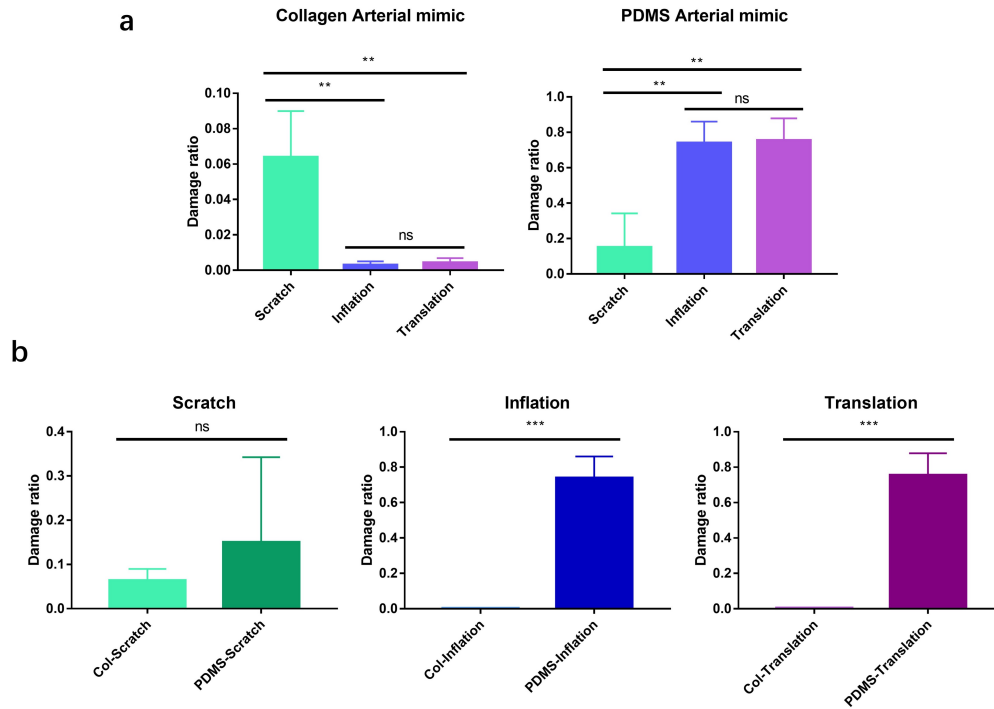


Figure 2.3: Balloon-induced endothelial damage. a: Statistical analysis grouped by arterial mimic type. b: Statistical analysis grouped by balloon movement type.

### 2.1.3 Discussion

Direct experimental testing and visualization constitute a valuable tool for studying the physiological state as well as the injury of soft tissues in response to different challenges [121]. There is little doubt that considerable damage occurs in the arterial wall in response to interventional devices [118]. Indeed, endothelial damage is linked to the occurrence of restenosis [35] and thrombosis [122] post balloon angioplasty and stent deployment. Most investigations of endothelial injury and complications of balloon angioplasty have thus far been performed using computational modeling [123], animal experiments [118], or clinical follow-up studies [124][125]. In animal experiments, visualization of the endothelial layer is impossible without sacrificing the animal. Despite certain limitations, the arterial mimics described here provide a valuable tool for quantitatively assessing the effect of endovascular interventions on the arterial wall.

The current study only focused on immediate damage caused by balloon angioplasty to the vascular endothelium. Naturally, an important consideration is the longer-term implications of this damage. As such, it would be important in the future to extend the study to also probe endothelial wound healing rates that would ensue after the damage reported here.

The present results have shown that the stiffness of the arterial wall is an important consideration in the extent of balloon-induced endothelial damage. While the extent of damage due to balloon scratching was found to be significant for the collagen and PDMS mimics, balloon inflation and translation caused considerably more damage in the stiffer PDMS mimic. If applicable to the *in vivo* case, these results suggest that endothelial damage would be more extensive for calcified plaques than for softer lesions. On the other hand, several studies have reported faster endothelial migration on stiffer substrates [126]; therefore, while endothelial damage is expected to be greater in the case of calcified plaques, endothelial wound healing might also be expected to be faster. It remains to be determined which effect is dominant under which physiological and pathological conditions. This is an issue that certainly merits future investigation.

Because endothelial scratching during insertion and retraction of a deflated balloon appears to constitute a real risk in all cases, efforts aimed at reducing balloon-wall contact during balloon navigation would certainly be worthwhile.

### 2.1.4 Conclusions

This study used PDMS and collagen arterial mimics to investigate EC injury induced by different movements likely to occur during balloon angioplasty. In the PDMS artery mimic, all types of balloon movements created much more extensive damage to the endothelium than in the soft collagen artery mimic. Balloon inflation and translation were observed to damage virtually the entire balloon-contacting area in the case of the PDMS artery. The results of this study can provide useful information that can serve as a reference for the effects of different types of balloon manipulations on endothelial damage.

### Code

See Appendix [6.2](#).

# Chapter 3

## Contractility-induced self-organization of smooth muscle cells

*The phenomenon was observed accidentally when I first cultured SMCs at a higher seeding density.*

### 3.1 Introduction

Smooth muscle cells (SMCs) populate the walls of many tissues where they play a vital contractile function. Abnormalities in SMC organization are observed in many chronic diseases including vascular disease, asthma, and uterine fibroid. Several groups have reported that SMCs cultured on flat surfaces can spontaneously form three-dimensional clusters whose organization resembles that encountered in disease. Remarkably, how these clusters form remains unknown. Using *in vitro* experiments and mathematical modeling, we describe the precise sequence of events that leads to cluster formation and show that the dynamics of these clusters can be described by balancing the cells' contractile forces, adhesion forces, and fluid-like viscosity. We propose that these clusters can be used as model systems for studying various diseases.

## 3.2 Article submitted

### Contractility-induced self-organization of smooth muscle cells

#### Authors

Xiuyu Wang<sup>1</sup>, David Gonzalez-Rodriguez<sup>2</sup>, Thomas Vourc'h<sup>3+</sup>, Pascal Silberzan<sup>3</sup>, Abdul I. Barakat<sup>1\*</sup>

#### Affiliations

<sup>1</sup>LadHyX, CNRS, Ecole Polytechnique, Institut Polytechnique de Paris, Palaiseau, France

<sup>2</sup>Université de Lorraine, LCP-A2MC, Metz, France

<sup>3</sup>Laboratoire PhysicoChimie Curie, Institut Curie, PSL Research University, Paris, France

<sup>+</sup>Current Address: Université Clermont Auvergne, SIGMA Clermont, Institut Pascal, BP 10448, F-63000 Clermont-Ferrand, France

<sup>\*</sup>Correspondence: Abdul I. Barakat - [abdul.barakat@polytechnique.edu](mailto:abdul.barakat@polytechnique.edu)

### 3.2.1 Abstract

Smooth muscle cells (SMCs) are mural cells that play a vital contractile function in many tissues. Abnormalities in SMC organization are associated with many diseases including atherosclerosis, asthma, and uterine fibroid. Various studies have reported that SMCs cultured on flat surfaces can spontaneously form three-dimensional clusters whose organization resembles that encountered in some of these pathological settings. Remarkably, how these structures form remains unknown. Here we combine *in vitro* experiments and physical modeling to show that three-dimensional clusters initiate when cellular contractile forces induce a hole in a flat SMC sheet, a process that can be modeled as the brittle fracture of a viscoelastic material. The subsequent evolution of the nascent cluster can be modeled as an active dewetting process with cluster shape evolution driven by a balance between cluster surface tension, arising from both cell contractility and adhesion, and cluster viscous dissipation. The description of the physical mechanisms governing the spontaneous emergence of these intriguing three-dimensional clusters offers insight into SMC-related disorders.

### 3.2.2 Introduction

Smooth muscle cells (SMCs) are contractile cells that populate the walls of many hollow tissues and organs including blood vessels, pulmonary airways, and the gastrointestinal and urogenital systems[127][128]. *In vivo*, SMCs regulate tissue tone and synthesize a host of extracellular matrix proteins. Aberrant SMC proliferation and organization are the hallmarks of many chronic pathologies including atherosclerosis[129], hypertension[130], asthma[131], uterine fibroid[132] (UFs), and obstructive gastrointestinal diseases[133]. In normal tissue, SMCs are typically organized in a multi-layered structure with highly aligned cells whose architecture is tailored for optimal contractile function. Abnormalities in this organization are associated with a number of disorders. A prominent example is the case of UFs, common benign smooth muscle tumors that afflict up to 60-80% of all women[134], where SMCs organize into three-dimensional spheroid-like structures. The factors driving the changes in SMC organization during UF formation remain unclear.

A number of studies over the past few decades have reported that SMCs cultured on flat surfaces can under certain conditions spontaneously form three-dimensional structures that have alternately been referred to as hills, mounds, or hill-and-valley (HV) patterns[135][136][137]. These structures have been reported in SMCs from different species including human[138], pig[139], rat[140][141][142], and cow[143]. In some cases, the HV patterns transition to spherical “ball-like” clusters[144] that can either remain adherent to the substrate from which they emerged or become suspended in the culture medium. Interestingly, ball-like structures that originate from SMCs derived from human UFs revert back to HV patterns upon treatment with gonadotrophin releasing hormone (GnRH) in culture[145], suggesting that these three-dimensional structures may constitute a useful *in vitro* model for fibroids. Remarkably, despite the repeated and widespread observations, the physical mechanisms governing the spontaneous emergence of these intriguing three-dimensional SMC clusters and the dynamics of their evolution remain unexplained.

Here we use a combination of *in vitro* experiments and physical modeling to elucidate the mechanisms governing the spontaneous emergence and dynamics of three-dimensional SMC clusters from flat two-dimensional SMC layers. We show that the clusters initiate when SMC contractile forces overcome adhesion forces to the substrate, which only occurs once a critical SMC density has been attained. We also show that cluster formation occurs through a precise sequence of physical events whose dynamics we characterize both experimentally and using models that rely upon the well-established analogy between the spreading of cellular aggregates and the dewetting phenomena of liquid droplets[146][147].

### 3.2.3 Results

Culturing SMCs on a fibronectin-coated flat glass surface leads to the spontaneous emergence of three-dimensional clusters once a sufficiently high cell density is attained (Supplementary Movie 1). The cluster diameter varies over a wide range of  $\sim 100\mu\text{m}$  to  $\sim 3\text{mm}$ . As shown in Figure 3.1 1a and schematized in Figure 3.1 1c, SMCs within clusters exhibit two distinct patterns of organization. Along the peripheral region of the cluster, particularly in the bottom portion, cells are oriented radially, have elongated nuclei, and express abundant F-actin, consistent with radial force generation associated with the anchoring to the surrounding SMC layer. On the other hand, SMCs in the inner region of the cluster assume an architecture that resembles a bird nest with nuclei oriented circumferentially and strikingly low levels of F-actin expression, suggesting minimal force exertion. Interestingly, the centermost portion of the cluster often contains a zone of lower cell density (Fig.3.1 1a, b) that spans a portion of the height of the cluster. Live/dead staining revealed that the vast majority of the cells were viable (Supplementary Fig.1).

Time-lapse imaging revealed that cluster formation occurs through the following sequence of specific physical events (Fig.3.1 1d): 1) contractility-induced formation of a breach or hole in the flat SMC layer (Supplementary Movie 2), presumably due to an imbalance in the exerted contractile forces as a result of a locally elevated SMC concentration; 2) cellular retraction after hole formation, leading to a bumpy SMC “aggregate” that nevertheless remains fully attached to the substrate over its entire contour (Supplementary Movie 3); 3) additional contraction of the aggregate until a portion of it tears off from the substrate, giving rise to a well-defined three-dimensional cluster (Supplementary Movie 4); 4) rounding-up of the typically oblong cluster into a hemispherical shape (Supplementary Movie 5); 5) cluster stabilization in its final hemispherical shape until the end of the observation (Supplementary Movie 6). Two clusters that come in contact are sometimes observed to fuse into a single cluster (Supplementary Movie 7). The physics of each of the five steps outlined above are described next.

**Hole development in the SMC layer and aggregate formation.** We investigated cluster formation at three different SMC seeding densities: low, medium and high corresponding respectively to 40,000, 80,000, and 160,000 cells/cm<sup>2</sup> (see Methods). For the high-density group, cluster formation initiates within 24 h of seeding with the spontaneous development of holes in the SMC layer (Fig. 3.2a). In the early stages, the hole may still be partially covered with cells under high strain due to contractile forces from surrounding cells (Fig. 3.2a).

We quantified the velocity field in the cell sheet surrounding the hole using particle image velocimetry (PIV) (Fig. 3.2b, c). The hole widens as cells pull in opposite directions with a progressively increasing velocity. When the cell velocity on either side of the hole attains a peak (typically  $\sim 150\mu\text{m}/\text{h}$ ), the cells extending over the hole tear

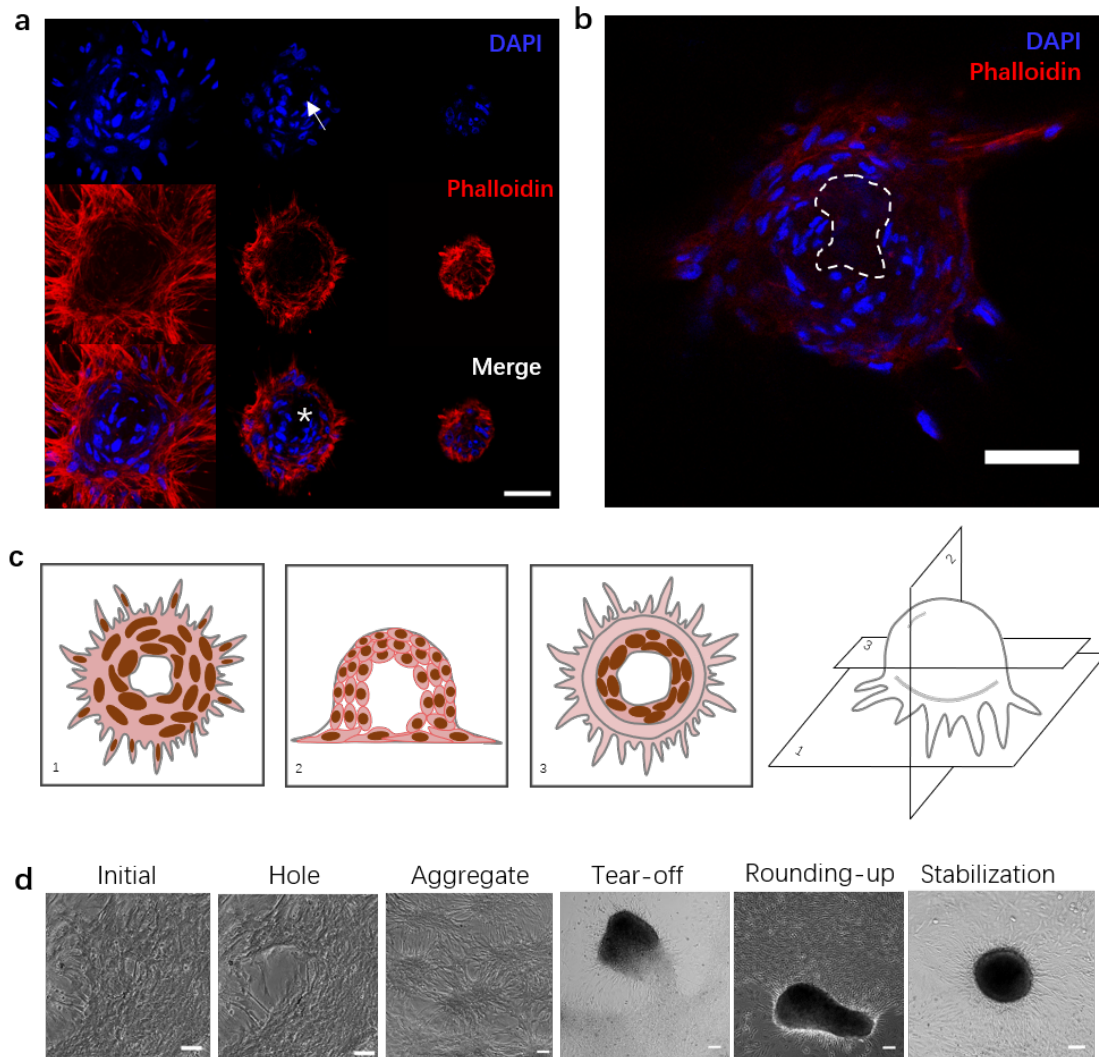


Figure 3.1: Cellular organization in SMC clusters and sequence of steps leading to cluster formation. a: Confocal images of cellular organization within a cluster. From left to right: z-stack from bottom to top of a cluster for the nucleus (DAPI channel; top row), F-actin (phalloidin channel; middle row), and both channels combined (bottom row). Note the lower cell density zone in the center of the cluster (white arrow on DAPI image; white \* on merge image). Scale bar: 50  $\mu\text{m}$ . b: A confocal optical section through the midplane of a cluster to more clearly illustrate the lower cell density zone in the center (dashed contour). Scale bar: 50  $\mu\text{m}$ . c: Schematic of cellular organization within SMC clusters. d: Phase contrast images of the sequence of five distinct events leading to cluster formation. From left to right: initial condition, crack development, aggregate formation, aggregate tear-off, cluster rounding-up from oblong to circular cross-section, and cluster stabilization. Scale bars: 100  $\mu\text{m}$ .

off, which has the effect of releasing the tension and stabilizing the hole width. This is accompanied with an overall reduction in cell velocity below  $\sim 20\mu m/h$ .

We also characterized the evolution of the size and shape of the hole (Fig. 3.2d-f). This evolution can be modeled as the brittle fracture of a viscoelastic material where the dynamics are dominated by elasticity, similar to the work of Tabuteau et al.[148] The profile of the hole can be described by a parabola of equation  $y = A\sqrt{x}$ , where the symmetry axis  $y$  of the parabola is aligned with the direction of hole propagation and the constant  $A \sim \sqrt{\frac{G}{E}}$  depends on the adhesion energy  $G \sim 10^{-2} J/m^2$  [149] and the SMC elastic modulus  $E \sim 10^4 Pa$  [150]. Modeling the cell sheet as an elastic sheet, the opening dynamics of the hole width  $a$  are governed by a balance between cell elastic recoil and friction with the substrate, which leads to 3.1:

$$a = a_{max}[1 - \exp(-Ct)] \quad (3.1)$$

where  $C \sim \frac{E}{kR_c}$  is a constant,  $k$  is the cell-substrate friction, and  $R_c$  is the cell size. By fitting the experimental data (Fig. 2e), we obtain experimentally  $a_{max} \sim 200\mu m \sim R_c$  and  $C \sim 2 \cdot 10^{-3} s^{-1}$ , which enables us to estimate a cell-substrate friction coefficient of  $k \approx 2 \cdot 10^{10} Pa.s.m^{-1}$ , comparable to albeit slightly larger than a friction coefficient value reported previously<sup>25,26</sup>. Along its length, the hole opens in successive phases, corresponding approximately to one cell length<sup>27</sup> (Fig.3.2f). According to our theoretical interpretation, the time to advance one phase should then scale as the stretching time  $\frac{1}{C} \sim 500s$ , which is consistent with the observations. This hole development phenomenon is strongly reminiscent of the dewetting of a cell monolayer described by Douezan et al.<sup>28</sup>, although here the dominant driving force is cell elastic recoil, rather than intercellular adhesion.

An established hole represents a valley in the commonly described HV SMC pattern. Once the hole expands, it ultimately forms a ring, leading to a topological transition with the formation of an ‘‘aggregate’’, a multi-layer hill-like structure with a dense central portion and radially outward-pointing cells at the periphery (Supplementary Movie 3 and Supplementary Fig. 2a). These aggregates are highly dynamic as a result of gradients in cell pulling forces. PIV analysis revealed considerably higher cellular velocities in the monolayer ( $\sim 30\mu m/h$ ) opposite to the direction of aggregate movement (Supplementary Fig. 2b, c).

**Cluster rounding and stabilization.** Driven by cell contraction, aggregates subsequently tear off from the substrate and form independent clusters (Supplementary Fig. 3). These clusters are mobile on the substrate as they progressively round up (Fig. 3a). We analyzed the evolution of cluster size and shape during this rounding-up process as well as cluster motion (Supplementary Fig. 4 and Supplementary Note 1) by imaging the cluster every 20min (Supplementary Note 2). Cluster morphometric data were obtained through automatic detection of the bright contour in the images (Fig. 3a). Over 24 h, the cluster projected area decreases by about 40% and its circularity (defined

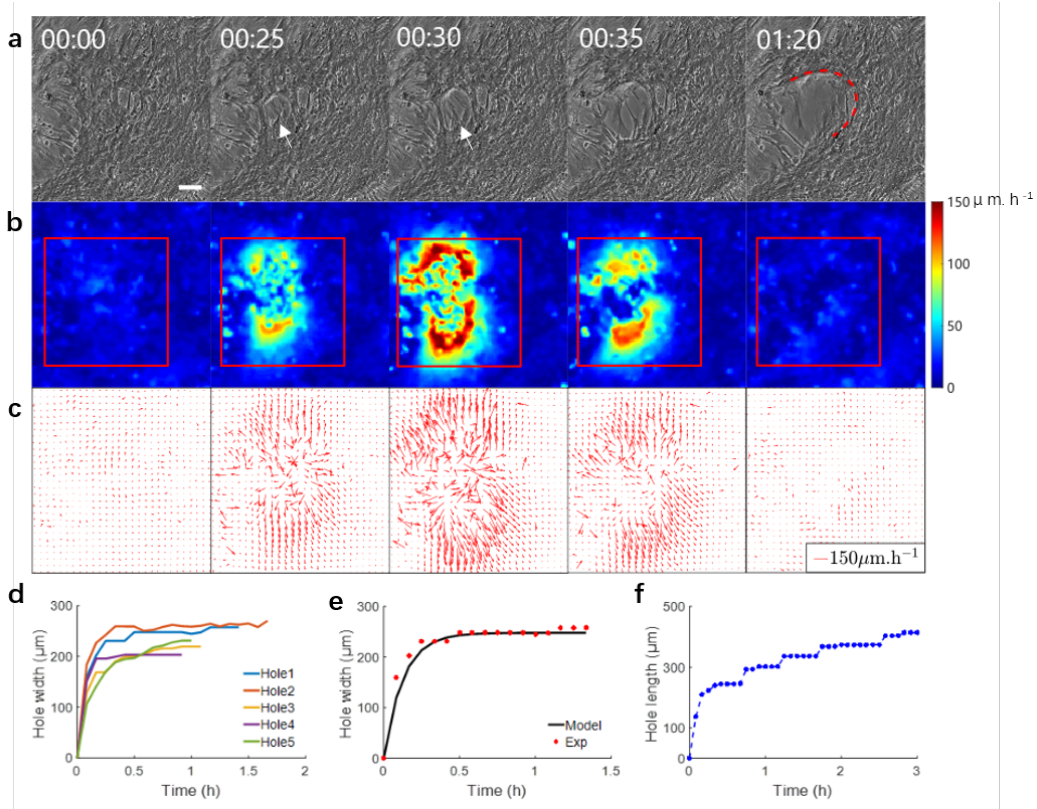


Figure 3.2: Dynamics of hole development. a: Phase contrast images of SMCs at different times pre and post hole development. White arrow denotes the position of hole initiation. Fit of the experimental shape of the hole edge by a parabola (red curve) whose equation is indicated in the text. Times are in hours and minutes. Scale bar:  $100\mu m$ . b: Heat map of SMC tissue speed corresponding to the velocity field shown in panel c. c: Velocity vector field in the SMC tissue showing the larger velocities in the hole vicinity. d: Time evolution of hole width for five different holes. e: Comparison between the mathematical model of hole width evolution (solid black curve) and experimental data (red circles). f: Length development for one representative hole. Note the successive phases of hole opening.

as  $4\pi A/P^2$ , where  $A$  is the cluster area and  $P$  is its perimeter), increases from 0.65 to almost 1 (Fig. 3b, c), thus indicating that the cluster becomes more compact and round over time. Similar to previous models<sup>29</sup>, we interpret the dynamics of rounding up as a phenomenon driven by cluster surface tension, arising from both cell contractility and adhesion, and resisted by cluster viscous dissipation. Mathematically,

$$\gamma \dot{S} = -\eta \int_V \vec{\nabla} \vec{u} : \vec{\nabla} \vec{u} dV \quad (3.2)$$

where  $\gamma$  is the surface tension coefficient,  $\eta$  the cluster viscosity,  $S$  and  $V$  the cluster surface area and volume, and  $\vec{u}$  is the velocity field within the cluster. We assume the

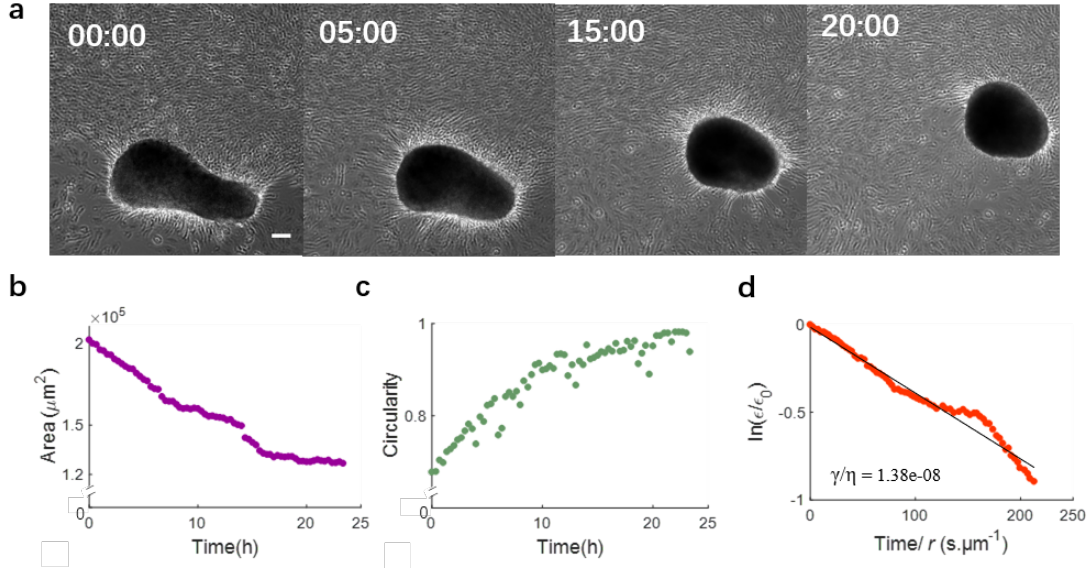


Figure 3.3: Cluster rounding dynamics. a: Phase contrast images of a SMC cluster at different times showing progressive rounding. Times are in hours. Scale bar:  $100\mu m$ . b: Time evolution of cluster projected area. c: Time evolution of cluster circularity. d: Normalized cluster/spheroid anisotropy, allowing determination of the value of the ratio of surface tension to viscosity ( $\gamma/\eta$ ). Equation is indicated in the text.

cluster shape to be a prolate spheroid of major axis  $a$  and minor axis  $c$ . By considering the spheroid to be sufficiently close to a sphere, we can obtain an expression for the velocity field and obtain a closed-form approximate solution to 3.2 (Supplementary Note 3):

$$\ln\left(\frac{\epsilon}{\epsilon_0}\right) = -\frac{15}{56} * \frac{\gamma}{\eta} * \frac{t}{r} \quad (3.3)$$

where we have defined  $\epsilon = \frac{c-a}{c+a}$  and  $r = \frac{2a+c}{3}$ . A fit of 3.3 to the experimental data is shown in Fig. 3d, yielding  $\gamma/\eta \approx 10^{-8}m/s$ , comparable to that reported for the rounding up of cellular aggregates of other cell types<sup>28</sup>. Once clusters round up, they stabilize in size and shape (Supplementary Fig. 5, Supplementary Note 4) unless they fuse with other clusters.

**Cluster fusion.** The interaction of two clusters that are sufficiently close to one another often leads to fusion (Fig.3.4a). The fused cluster subsequently goes through the “rounding-up” and “stabilization” steps described above for single clusters.

To analyze the fusion process, we quantify the evolution of the “neck” radius  $\rho$ , i.e., the radius of the contact region between two adjacent clusters as seen in projection on the experimental images. The observed neck evolution is reasonably fitted by equation 3.4

of the sintering theory proposed by Douezan and Brochard29:

$$\frac{\rho^2}{R_0} = \frac{\gamma}{\eta} * t \quad (3.4)$$

Here,  $R_0$  is the cluster radius,  $R_0 = \sqrt{\frac{A_1+A_2}{2\pi}}$ , with  $A_1$  and  $A_2$  the initial cluster areas,  $\gamma/\eta$  is the ratio of surface tension to viscosity, and  $t$  is the elapsed time since the beginning of the fusion process (Fig.3.4b, c). By fitting the experimental observations of aggregate fusion, we obtain a value of  $\gamma/\eta$  of the order of  $1 - 3 \times 10^{-9}m/s$ . Taking into account possible scaling factors that arise from our simplified geometrical treatment of the problem, this value of  $\gamma/\eta$  appears consistent with that obtained for rounding-up. Our findings thus suggest that both phenomena, “rounding-up” and “fusion”, are governed by the same physics of an effective surface tension driving the morphological change, whose speed of evolution is limited by viscous dissipation.

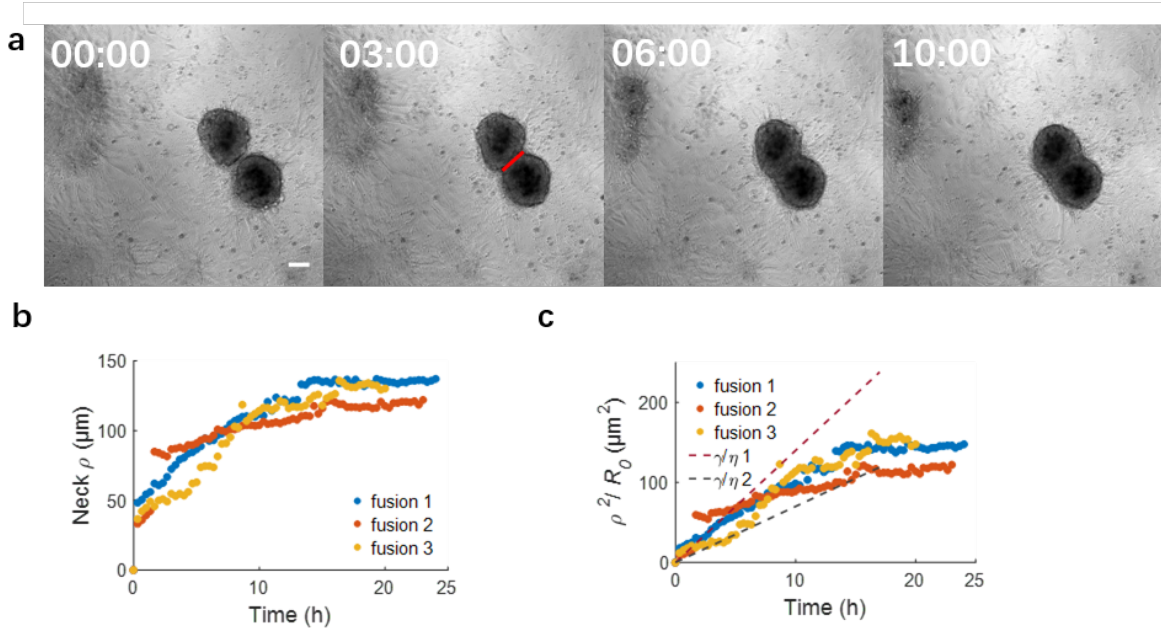


Figure 3.4: Cluster fusion. a: Phase contrast images of two fusing SMC clusters at different times. Times are in hours. Red line:  $2\rho$ , where  $\rho$  is the “neck” radius. Scale bar:  $100 \mu\text{m}$ . b: Time evolution of “neck” radius  $\rho$ . c: Time evolution of the normalized neck radius.  $\gamma/\eta_1 = 3.5 \times 10^{-9}m/s$ ,  $\gamma/\eta_2 = 1.2 \times 10^{-9}m/s$ . Equation is indicated in the text.

**Prerequisite conditions for SMC cluster formation.** The occurrence of SMC cluster formation as detailed above requires two prerequisite conditions: a sufficiently high cell density and sufficient levels of SMC contractility. The role of each of these two conditions is characterized next.

**Role of cell density.** SMC density determines both the dynamics of cluster formation and the pre-cluster organization of SMC sheets necessary for initiating a cluster.

(i) Dynamics of cluster formation: We investigated the dynamics of cluster formation for the three different cell seeding densities tested (40,000, 80,000, and 160,000 *cells/cm*<sup>2</sup>) (Supplementary Fig. 6). We divide the clusters into two types (Supplementary Fig. 7): “developed clusters”, which have a clear and complete contour, and “developing clusters”, which have a partially developed contour. Not surprisingly, cluster formation occurs most rapidly at the highest cell seeding density for both types of clusters (Fig. 3.5a, b and Supplementary Fig. 6b). Furthermore, cluster formation at the lower seeding densities occurs only after a delay, suggesting that a critical cell density needs to be attained via cell proliferation for cluster formation to initiate. For both types of clusters, the number of clusters increases for several days until it reaches a maximum and then decreases before ultimately stabilizing at a plateau. For developing clusters, the increase is due to cluster formation because of cell proliferation, whereas the decrease corresponds to developing clusters maturing into developed clusters. For developed clusters, the increase is driven by the maturing developing clusters, while the decrease is due to cluster fusion once cluster density becomes sufficiently high for neighboring clusters to interact. The time evolution of the total number of clusters (i.e. developing and developed) exhibits similar overall behavior (Fig. 3.5c) once a shift of 3 days has been introduced for the low and medium seeding densities, so that  $t = 0$  for all experiments is the time when cluster formation starts. With this shift, all experimental curves are approximately similar. This master curve first rapidly increases to reach a maximum, and then decreases to finally stabilize at a plateau.

The master curve in Figure 3.5c can be described by the following population dynamics differential equation 3.5:

$$\frac{dN}{dt} = p_1 - \alpha(t)p_2N \quad (3.5)$$

where  $N$  is the total number of clusters at time  $t$ ,  $p_1$  is the rate of cluster formation, and  $p_2$  the rate of (relative) cluster number reduction, mainly arising from cluster fusion. The time-dependent parameter  $\alpha(t)$  is introduced to account for a reduced rate of cluster number at short time, due to the time required for clusters to meet each other and fuse. We assume a linear increase of the dissociation rate over time,  $\alpha(t) = \min(t/t_s, 1)$ , with  $t_s$  being a certain stabilization time. The solution to this differential equation agrees closely with the experimentally observed shape. Figure 5c shows a comparison between the computational fit and the experimental data with fitted model parameter values of  $p_1 = 50$  clusters/day,  $p_2 = 1.5 \text{ day}^{-1}$  and  $t_s = 8$  days.

(ii) Pre-cluster SMC organization: It would be instructive to characterize the organization of our SMC layers prior to cluster formation for the different cell densities. To this end, we quantify the extent of actin stress fiber alignment by computing the scalar

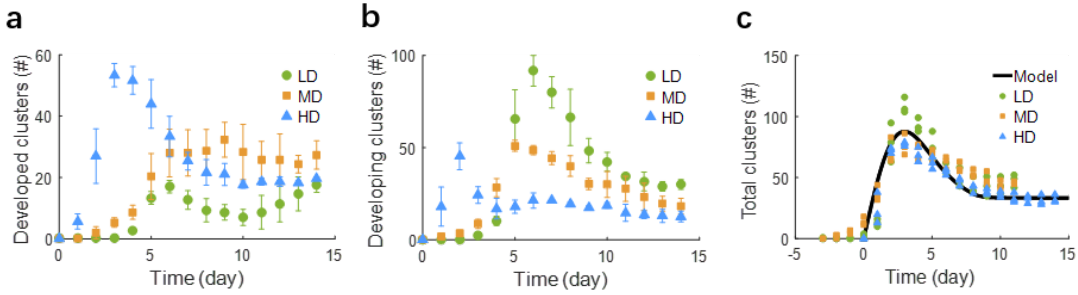


Figure 3.5: Dynamics of cluster evolution. a: Time evolution of the number of developed clusters for the different cell seeding densities. The maximum number of developed clusters is reached at days 14, 9 and 4 for the low (LD), medium (MD), and high (HD) seeding densities, respectively. Error bars are SEM of three independent experiments. b: Time evolution of the number of developing clusters for the different cell seeding densities. The maximum number of developing clusters is reached at days 6, 5 and 2 for the low (LD), medium (MD), and high (HD) seeding densities, respectively. Error bars are SEM of three independent experiments. c: Time evolution of total number of clusters (sum of developed and developing clusters) and physical model fit. Three experiments for each density are shown.

order parameter  $Q$  for non-polar particles<sup>30</sup> (Supplementary Fig. 8):

$$Q = \sqrt{\langle \cos 2\theta \rangle^2 + \langle \sin 2\theta \rangle^2} \quad (3.6)$$

where  $\theta$  is the angle between the stress fiber direction and a reference direction (the horizontal direction in this case).  $Q$  ranges from 0 for a completely disordered case to 1 for a perfect nematic order where all stress fibers are aligned in the same direction. At low cell density, SMCs exhibit a wide range of orientations (Fig. 6a) as indicated by the small value of  $Q=0.12$ . At medium density, SMCs coordinate with local alignment of stress fibers, leading to considerably increased order ( $Q = 0.69$ ). At high density, SMCs rapidly form multiple layers, typically three (Fig. 6b), prior to cluster formation, and actin stress fibers within each layer are highly aligned (Fig. 6b, c), with an order parameter approximately equal to unity ( $Q = 0.95$ ). These findings are consistent with previous studies<sup>30-32</sup>.

**Role of contractility.** Our results indicate that SMC cluster formation only initiates once a critical cell density is attained and the cells have formed several layers. However, cell density *per se* is not sufficient to initiate cluster formation. The additional required component is a sufficiently elevated cell contractility in order to overcome cell-substrate adhesion as depicted schematically in Fig. S9a. Such force disequilibrium would lead to the tearing-off of the SMC cell sheet from the substrate. In support of this model, SMC contractility inhibition using blebbistatin ( $5 \mu M$ ) significantly slows down cell detachment from the substrate and delays the formation of clusters (Supplementary Fig. 9b), confirming the important role that SMC contractility plays in cluster formation.

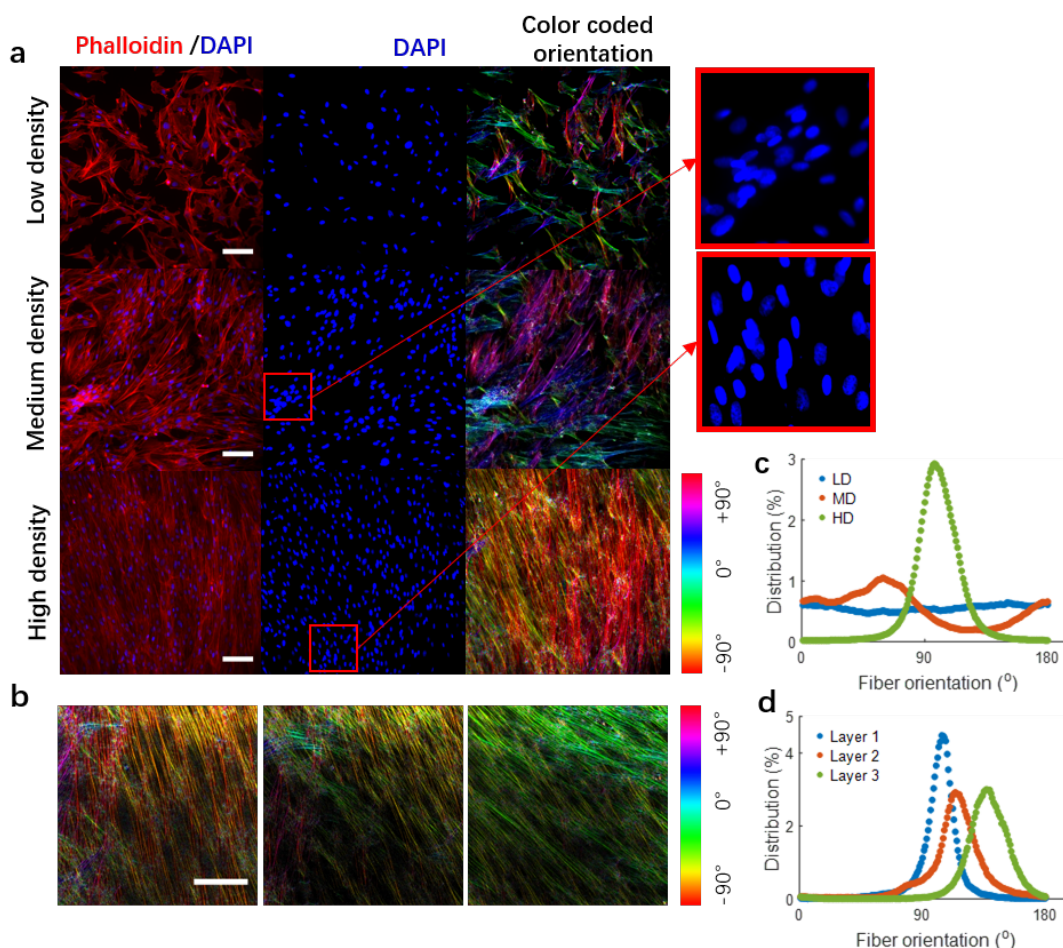


Figure 3.6: Pre-cluster SMC actin stress fiber organization. a: Immunostaining images of samples with different seeding density 24 h post-seeding. DAPI (blue) shows SMC nuclei, while phalloidin (red) shows F-actin. Nuclear overlap in some regions (see insets) demonstrates that cells begin to form local multi-layer zones at the medium density. Scale bars:  $100 \mu\text{m}$ . b: Maps of F-actin orientation of one three-layer sample at high cell seeding density obtained by confocal microscopy. Left: bottom layer; middle: second layer; right: top layer. Scale bar:  $50 \mu\text{m}$ . c: F-actin orientation histograms for the low (LD), medium (MD), and high (HD) seeding density samples, showing progressively increasing orientation. d: F-actin orientation distributions for the three-layer sample in panel b.

A higher dose of blebbistatin ( $10 \mu\text{M}$ ) further reduces the area of cellular detachment (more than 20 times smaller than the untreated controls).

As an additional test, we investigated the dynamics of SMC cluster formation when the cells were cultured on very soft gels (Young's modulus of  $2 \text{ kPa}$ ) on which their ability to generate large contractile forces is greatly diminished. The results demonstrated that

when plated at the same seeding density, cluster formation on the soft gel required 3 days longer than on plastic (Young’s modulus = 2.7 GPa). Applying the model described in the “Rounding-up” section for the dynamics of cluster formation yields a value of  $\gamma/\eta$  that is 3 to 4 times smaller for the soft gel than for plastic (Fig. S9c), consistent with a slower rate of cluster formation. These findings are consistent with the central role for contractility as the driving force for SMC cluster formation.

### 3.2.4 Discussions and conclusions

The spontaneous formation of three-dimensional SMC clusters, referred to elsewhere as HV patterns and ball-like structures, from flat cellular layers has been described qualitatively in many studies over the past few decades; however, the physical processes giving rise to these clusters have not been described. The present study provides the first detailed quantitative characterization and physical modeling of the events leading to the formation of SMC clusters.

Our experiments indicate that cluster formation occurs through a sequence of physical events whose dynamics and underlying mechanisms we characterize by conceptualizing SMC clusters and their precursor structures (referred to as aggregates) as active liquid droplets. This physical formulation allows us to explain the observed dynamics of: (i) hole development in the flat SMC layer, analogous to brittle viscoelastic fracture followed by dewetting, (ii) cluster shape evolution, analogous to droplet rounding-up, and (iii) cluster fusion, analogous to droplet coalescence. The model’s predictions are in agreement with observations and provide estimates of the material properties of SMC clusters. At a population scale, we describe the evolution of the number of clusters by a population dynamics model that accounts for cluster formation and cluster fusion.

Cells in SMC clusters are oriented radially along the periphery of the cluster and circumferentially in the interior region with a near “cell-free” zone in the center. This organization also shares some similarities with that of UFs that have been reported to exhibit regions of radial and circumferential cell orientation. Moreover, the cell-free zone of SMC clusters appears to resemble the core region of atherosclerotic plaque-like mounds in cultures of aortic SMCs reported back in 1975 as well as the loose, water-laden myxoid tissue alternately called “necrotic core” in UFs. It would be particularly interesting to probe if SMC clusters may serve as a useful *in vitro* model for studying UF development and density-driven SMC hypertrophy and hyperplasia.

### 3.2.5 Materials and methods

*Cell culture*

Bovine aortic smooth muscle cells (SMCs; Cell Applications, Inc., San Diego, CA, USA) in passages 3-10 were cultured using standard procedures in bovine SMC growth medium (Cell Applications) and maintained at 37°C and 95% air/5% CO<sub>2</sub>.

#### *SMC cluster formation and visualization*

Cells were seeded on either tissue culture-treated well plates (Costar, Corning Inc., New York, NY, USA) or fibronectin-coated glass surfaces at either “low”, “medium”, or “high” density, corresponding respectively to 40,000, 80,000, or 160,000 cells/cm<sup>2</sup>. The low density is considered the baseline seeding density and yielded a confluent SMC monolayer after 24 h. The medium density corresponds to a confluent monolayer upon cell adhesion, whereas the high density results immediately in 2 to 3 overlapping cell layers. Except for the different initial densities, all experiments were performed under the same conditions. Cellular evolution was monitored over 14 days.

Bright-field images were acquired using an inverted microscope (Nikon ECLIPSE Ti2, Tokyo, Japan) equipped with a 10X objective. The acquisition rate was 1 frame every 20 min for most observations and 1 frame every 5 min for the “hole development” experiments whose dynamics were faster. Images (2048 × 2044 pixels) were exported in TIFF format and analyzed using FIJI.

#### *Preparation of coated glass substrates*

Small (7 mm-diameter) holes were drilled into a 1 cm-thick polydimethylsiloxane (PDMS; Sylgard-to-catalyst ratio of 10:1) sheet to accommodate thin glass coverslips. The PDMS and coverslips were sterilized in ethanol for 5 min, dried at room temperature, plasma treated for 45 sec, and then assembled together by pressure application. The assembly was then sterilized in ethanol for 5 min and dried at room temperature. The 7 mm wells so created were coated with a 0.1 mg.mL<sup>-1</sup> solution of GIBCO™ Fibronectin Bovine Protein (Thermo Fisher Scientific, Boston, MA, USA) in PBS (pH 7.4) for 45 min at room temperature. The coated surfaces were then rinsed with PBS (pH 7.4) and used within 2 h.

#### *Preparation of coated gel substrates*

Soft gel substrates were prepared using the DOWSIL™ CY 52-276 A&B gel formulation (Dow Corning, ratio 1:1) according to the manufacturer’s specifications, leading to a gel with an elastic modulus of 1-3 kPa. The gel was poured into 48-well plates and maintained at 75°C for 10 h. The gel surfaces were sterilized in ethanol for 5 min and dried at room temperature before coating with a 0.1 mg.mL<sup>-1</sup> solution of GIBCO™ Fibronectin Bovine Protein (Thermo Fisher Scientific) in PBS (pH 7.4) for 45 min at room temperature. The coated surfaces were then rinsed with PBS (pH 7.4) and used within 2 h.

*SMC cluster internal structure imaging*

The 3D organization of SMC clusters was imaged using a confocal microscope (Leica SP8, Wetzlar, Germany) equipped with a 63 $\times$  objective. The cells were stained with DAPI and phalloidin to visualize nuclei and F-actin. Images were exported in TIFF format and analyzed using FIJI.

*Image analysis*

Cluster outlines were defined by their bright contours in phase contrast images. Cluster contours were tracked using the Analyze Particles FIJI plug-in. Cluster morphometric parameters including area, perimeter, centroid position, major axis length, and minor axis length were quantified using a custom-made MATLAB code.

*PIV analysis*

Particle image velocimetry (PIV) was used to obtain the velocity fields of SMC tissue. The PIV analysis was performed using the Matpiv package in MATLAB(<https://www.mn.uio.no/math/english/people/aca/jks/matpiv/>). A three-pass computation using a final window of 32  $\times$  32 pixels (20.8  $\times$  20.8  $\mu m$ ) was used. The overlap was set at 0.5. Aberrant vectors were detected and removed from the analysis when their magnitude exceeded the local mean value by three times the standard deviation ( $\sim 5\%$  of the data). The time interval between consecutive images was 5 min in the “hole development” experiments and 20 min in the other cases. For each frame, we computed the root-mean squared-velocity as  $V_{rms} = \sqrt{\langle V^2 \rangle}$ , where V is the magnitude of the velocity and the brackets denote an average over the entire field.

*Immunostaining*

Samples are fixed with 4% paraformaldehyde for 15 min and rinsed with PBS three times and then permeabilized with 0.1% triton solution in PBS (PBST) for 15 min. Non-specific binding was blocked using 3% BSA in PBST. Nuclei were stained with DAPI (SigmaAldrich, St. Louis, MO, USA; 1:20,000) and F-actin with Phalloidin594 (LifeTechnologies, Carlsbad, CA, USA; 1:200). The incubation time was 1 h.

*Statistical analysis*

A minimum of three experiments were performed. All data are expressed as mean  $\pm$  SEM. Differences were assumed to be statistically significant for  $p < 0.05$ . Statistical comparison for the data on substrate rigidity data was performed using the Student t-test. All statistical analyses were conducted using MATLAB.

### **Acknowledgments**

The authors acknowledge all members of the Barakat group for their constructive input to the preparation of the manuscript. This work was funded by an endowment in Cardiovascular Bioengineering from the AXA Research Fund (to A.I.B.) and a doctoral fellowship from Ecole Polytechnique (to X.W.).

### **Conflict of interest**

The authors declare no competing or financial interests.

### **Author contributions**

X.W. and A.I.B. conceived the study. X.W. designed and conducted the experiments. X.W. developed the computational analysis tool. X.W. analyzed the experimental results with the help of D.G.R. D.G.R. developed the theoretical models. T.V. conducted the PIV analysis. X.W. wrote the manuscript with the help of D.G.R. All authors participated in the review of the manuscript.

### 3.3 Supplementary documents

#### 3.3.1 Supplementary Figures

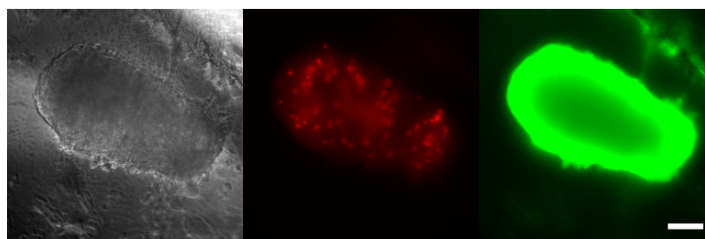


Figure 3.7: SF1. Left: Brightfield image of a SMC cluster. Right: Live-dead staining of SMCs in a cluster. Red: dead cells; green: live cells. The vast majority of the cells are viable, indicating that the cluster is a living organoid. Scale bar:  $100 \mu m$ .

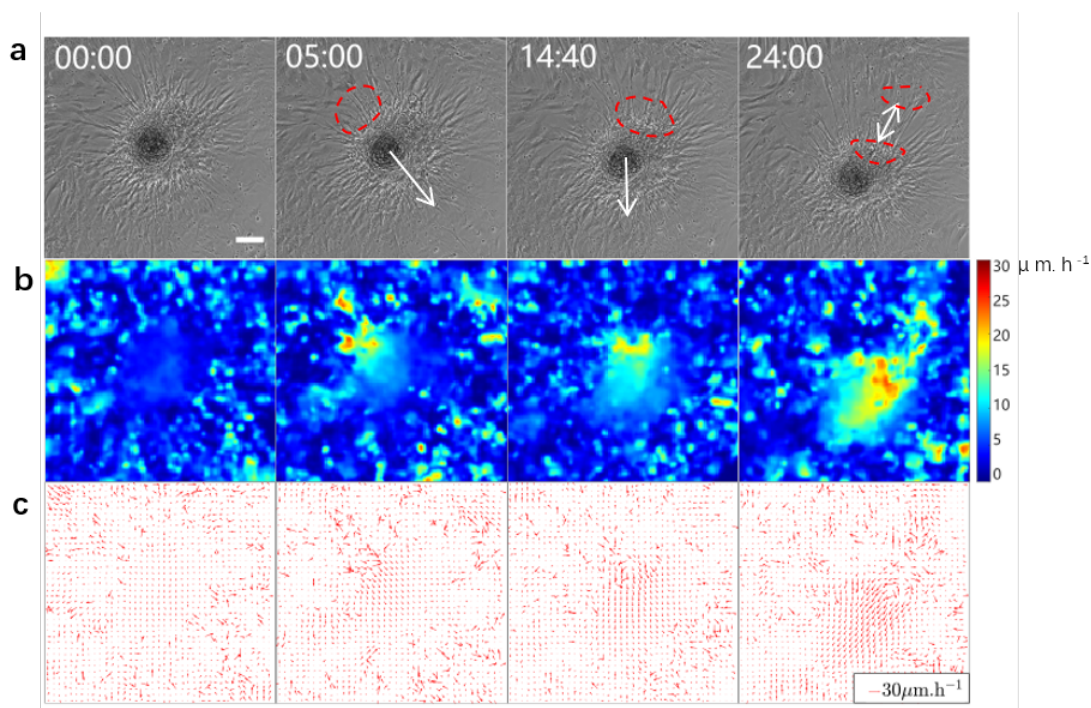


Figure 3.8: SF2. Cellular dynamics around SMC aggregates. a: Gradients in contractile forces around an aggregate lead to net pulling forces and aggregate displacement in the directions of the arrows. The red dashed contours demarcate zones of highly stretched cells as a result of the high pulling forces. Times shown are in hours and minutes. Scale bar:  $100 \mu m$ . b and c: PIV maps demonstrating particularly elevated cellular velocities in the regions of the stretched cells.

### 3.3. SUPPLEMENTARY DOCUMENTS

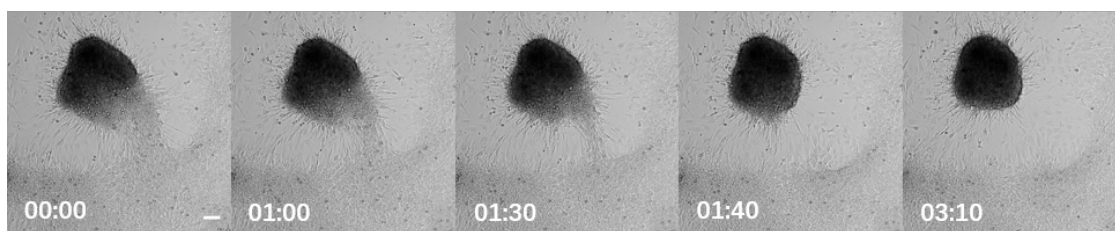


Figure 3.9: SF3. SMCs at the periphery of aggregates tear off progressively. Once the aggregate loses the last bundle of cell-substrate adhesion, it balls up into a developing cluster that eventually becomes a developed cluster with a complete contour. Scale bar:  $100 \mu\text{m}$ .

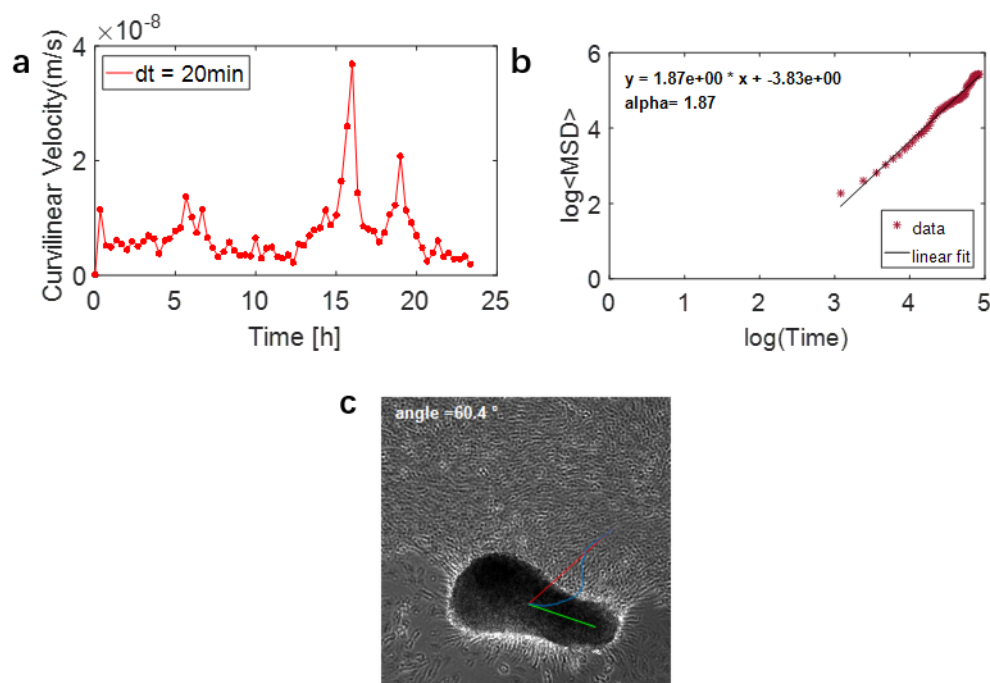


Figure 3.10: SF4. Cluster movement during the rounding-up process. a: Curvilinear velocity of a representative cluster as a function of time. b: Time evolution of the mean square displacement (MSD) for the same cluster. c: Cluster gets pulled by the higher SMC density on one side. Blue line denotes the cluster trajectory. Green line denotes the instantaneous direction of the cluster major axis. Red line denotes connects the initial position of the center of mass to its final position.

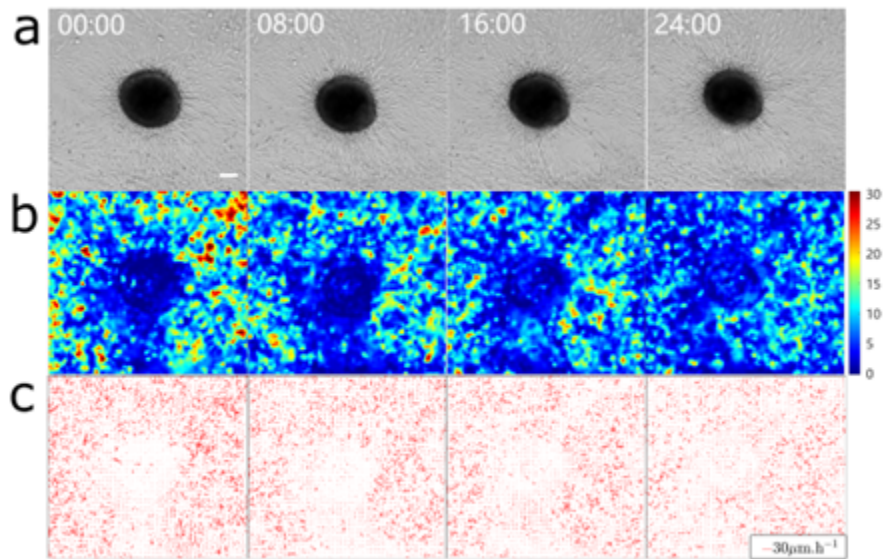


Figure 3.11: SF5. Cluster equilibrium upon stabilization. a: Clusters show minimal change in position after stabilization. Time points are in hours. Scale bar:  $100 \mu\text{m}$ . b and c: PIV of the velocity field after stabilization. The velocities are generally low and largely symmetric around the cluster.

### 3.3. SUPPLEMENTARY DOCUMENTS

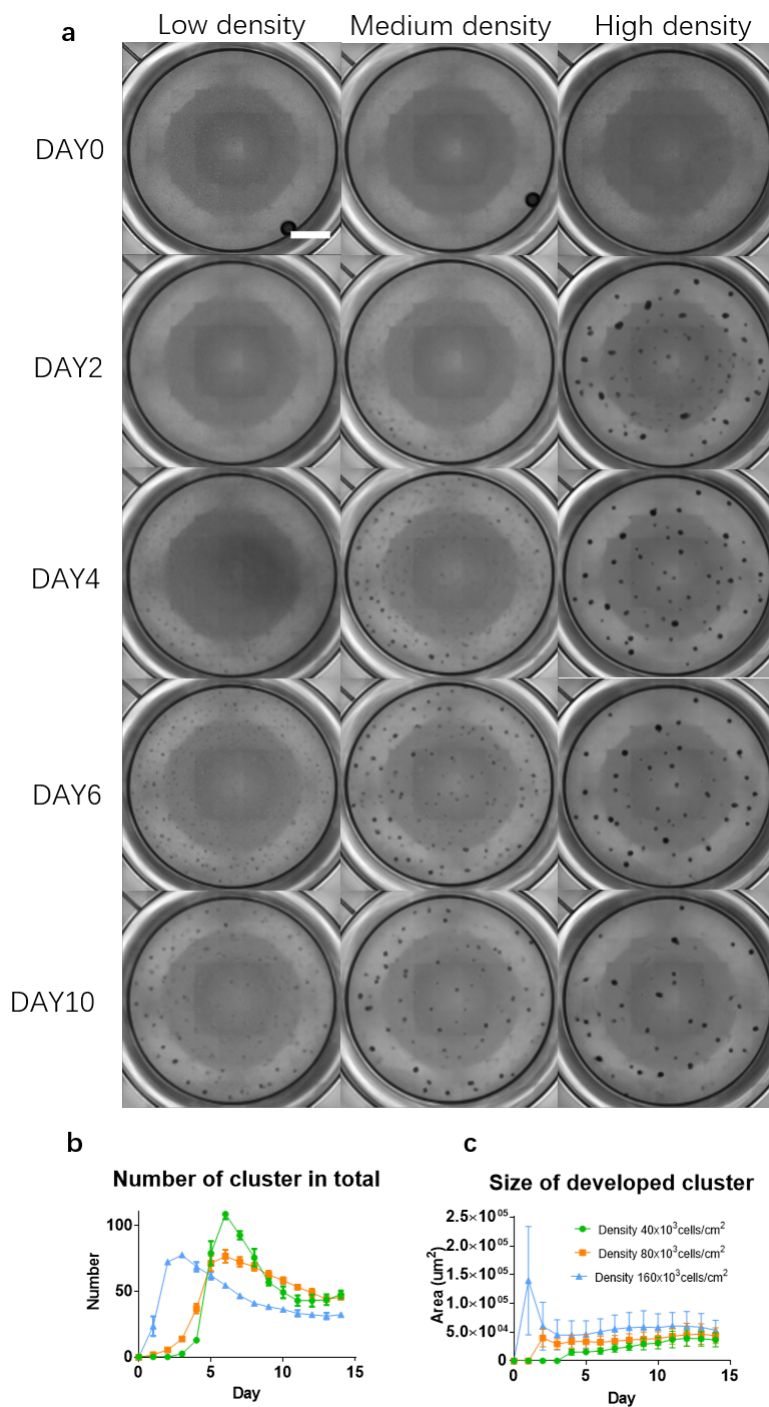


Figure 3.12: SF6. Dynamics of cluster formation at the three different cell seeding densities. a: Phase contrast images of cluster evolution in well-plates. Scale bar: 2 mm. b: Time evolution of the total number of clusters. The increase is due to cluster formation, whereas the decrease is due to cluster fusion. c: Time evolution of the area of developed clusters.

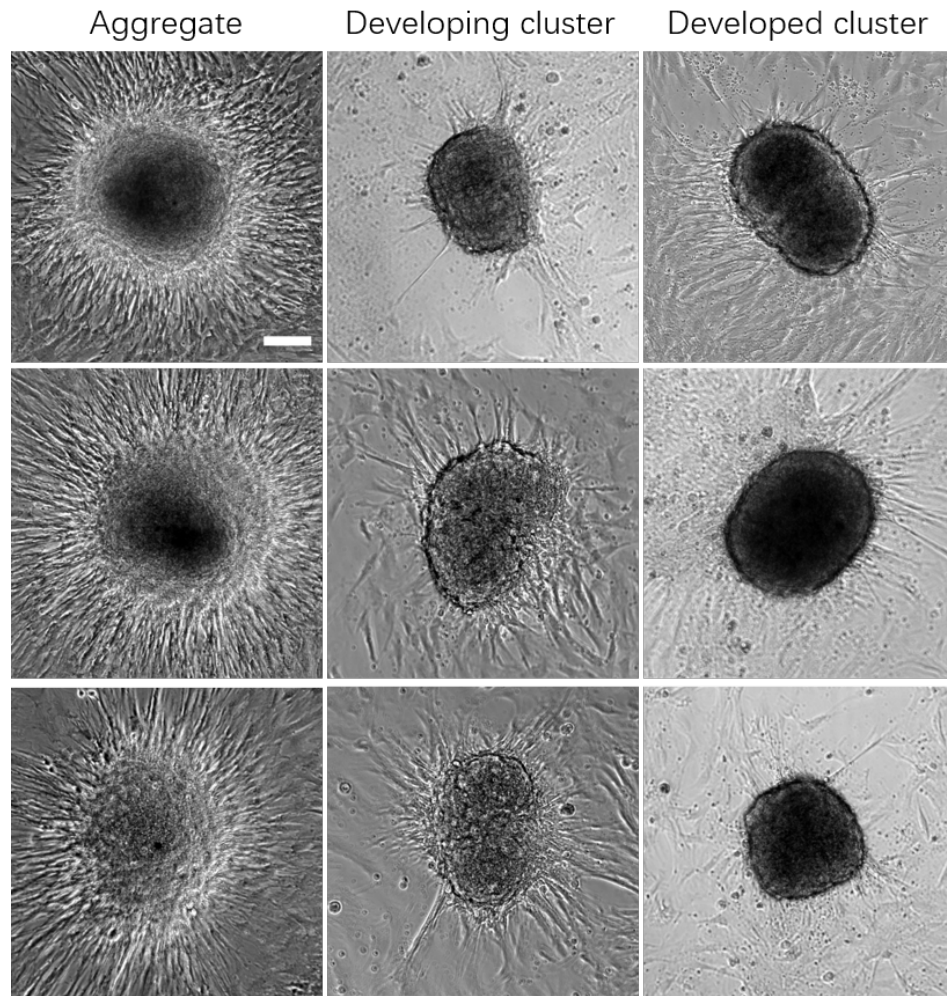


Figure 3.13: SF7. Three examples of aggregates, developing clusters and developed clusters. Aggregates, developing clusters, and developed clusters are three states seen at different times of the spontaneously arising three-dimensional SMC structures. Scale bar: 100  $\mu m$ .

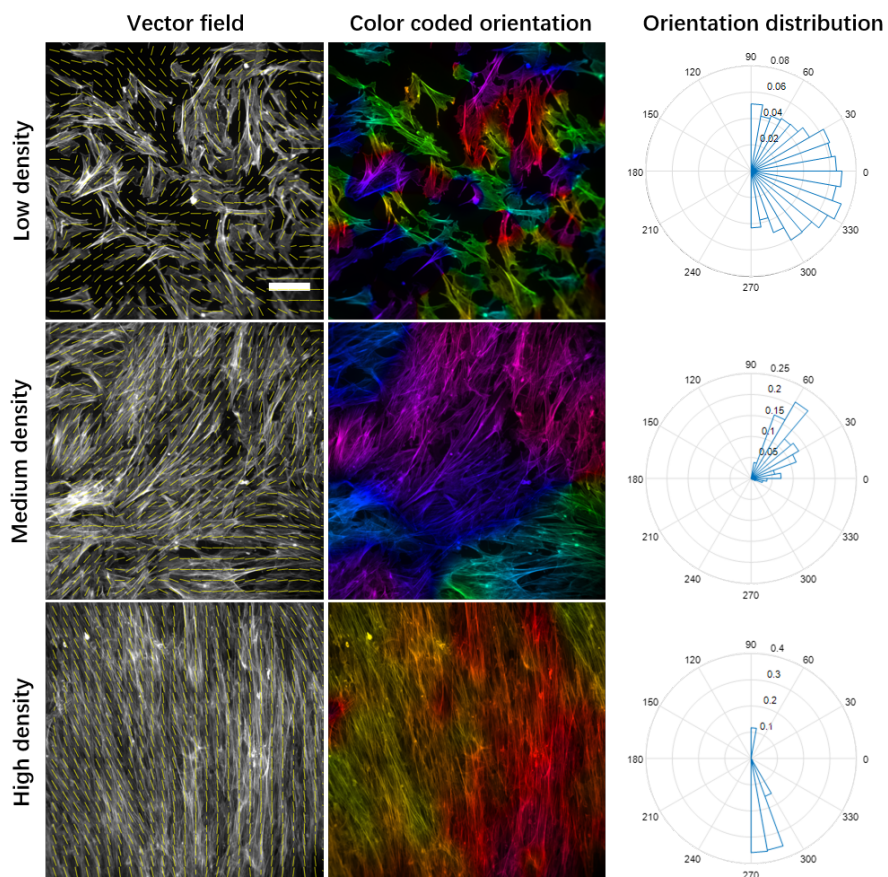


Figure 3.14: S8. Different representations of F-actin orientation for the three different cell densities studied. Left panels: vector field of orientations. Scale bar:  $100 \mu m$ . Middle panels: color-coded orientation maps. Right panels: orientation rose diagrams (polar histograms). The order parameter values for the low, medium, and high densities are as follows:  $Q_{LD} = 0.12$ ,  $Q_{MD} = 0.69$ ,  $Q_{HD} = 0.95$ .

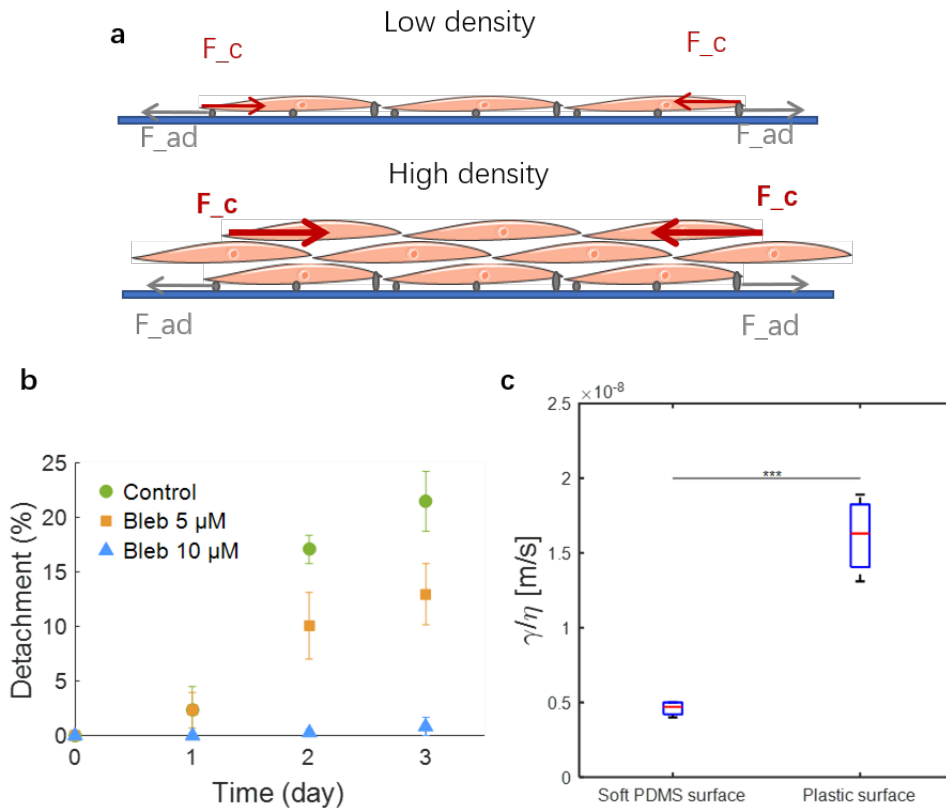


Figure 3.15: SF9. Role of contractility in SMC cluster formation. a: Hypothesized mechanism of cluster formation: clusters initiate when contractile forces become sufficiently large to overcome substrate adhesion forces. b: Contractility inhibition using blebbistatin diminishes SMC tissue detachment and cluster formation. c: SMCs on a soft gel where contractility is diminished exhibit a significantly smaller  $\gamma/\eta$  value, indicative of a much longer time for cluster formation than for cells on a plastic surface.

### 3.3.2 Supplementary Notes

#### Note 1: Dynamics of event “Rounding-up”

To characterize the motion, we measured the curvilinear velocity (Fig.3.10a) of the center of mass and the mean-square displacement (MSD) (Fig. 3.10b) of the cluster trajectory over a period of 24 h. The mean curvilinear velocity  $U = 7.2 \times 10^{-3} \mu\text{m}/\text{s}$  has the same order of magnitude as that of SMCs in a monolayer and is also comparable to that reported for the motion of aggregates of a different cell type. With an exponent  $\alpha = 1.87$ , a value close to 2, the MSD dependence on time indicates that the SMC cluster performs a persistent walk. We followed the cluster trajectory (Fig.3.10c) and found that the direction of persistent motion is largely orthogonal to the cluster’s major axis. The cluster is often positioned between a cell-rich and a cell-free zone, and it is pulled towards the cell-rich zone by cell contraction. The contractile force exerted on a cluster is  $F = kr^2U$ , where  $r$  is the equivalent radius of the projected cluster area, defined above. For the measured value of  $U$  and for  $k \approx 2 \cdot 10^{10} \text{Pa.s.m}^{-1}$ , as deduced from the hole opening dynamics above, we obtain  $F \approx 5\mu\text{N}$ , which corresponds to a contractile tension  $\gamma \sim F/r \approx 10\text{mN}/\text{m}$ , a value comparable to the surface tension reported for contractile cell aggregates[151].

**Note 2: Cluster movement during the rounding-up process**

**Curvilinear velocity:** To analyze the temporal displacement of SMC clusters, it is necessary to define an appropriate interval between successive frames for the analysis. To this end, we tested time intervals of 5, 20, and 60 min. Figure B.1 depicts the temporal evolution of the curvilinear velocity (i.e. distance raveled per unit time) of the center of mass of a representative SMC cluster over a period of 24 h for the three time intervals, while Table 1 provides the time-average curvilinear velocity and directionality for the same cluster.

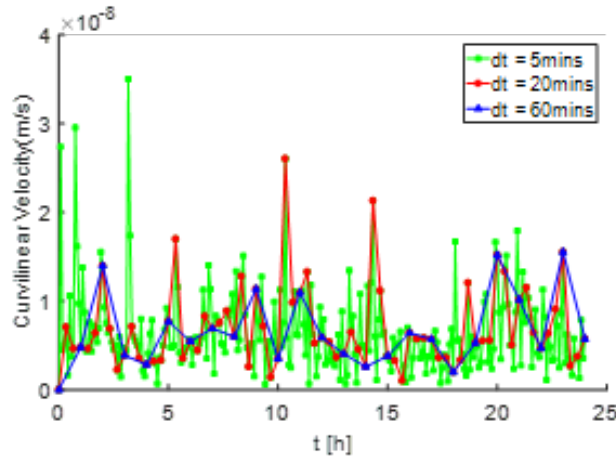


Figure 3.16: N1. Curvilinear velocity of the centroid of a representative SMC cluster as a function of time for the three time intervals selected of 5, 20, and 60 min.

Time Interval (min)	Average curvilinear velocity (m/s)	Directionality/Persistence
5	$6.45e^{-9}$	0.43
20	$6.87e^{-9}$	0.69
60	$6.58e^{-9}$	0.80

These results demonstrate that the average curvilinear velocities calculated with the different time intervals are very close to one another. However, the directionality only becomes stable for time intervals of 20 min or longer. Thus, a time interval of 20 min was used in all subsequent data analysis.

**Note 3: Mathematical modeling of cluster rounding-up** We interpret the dynamics of rounding as a phenomenon driven by cluster surface tension, arising from both cell contractility and adhesion, and resisted by cluster viscosity. Mathematically,

$$\gamma\dot{S} = -\eta \int_V \vec{\nabla}\vec{u} : \vec{\nabla}\vec{u} dV \quad (3.7)$$

where  $\gamma$  is the surface tension coefficient,  $\eta$  the cluster viscosity,  $S$  and  $V$  the cluster surface and volume, and  $\vec{u}$  is the velocity field within the cluster, which we assume of the form

$$\vec{u} = \left( \frac{\rho}{R}\dot{R}, 0, 0 \right) \quad (3.8)$$

where  $R(\theta)$  is the cluster radius and  $(\rho, \theta, \phi)$  are the spherical coordinates. We obtain:

$$\vec{\nabla}\vec{u} : \vec{\nabla}\vec{u} = \left( \frac{\dot{R}}{R} \right)^2 + \left[ \frac{\partial}{\partial\theta} \left( \frac{\dot{R}}{R} \right) \right]^2 \quad (3.9)$$

We assume the cluster shape to be a prolate spheroid, of major axis  $a$  and minor axis  $c$ . We further assume the spheroid to be sufficiently close to a sphere of radius  $r$ . We call  $\varepsilon$  the relative size of the geometric perturbation. By imposing that the deformation of the spheroid conserves a total volume equal to  $\frac{4}{3}\pi r^3$ , we obtain  $a = r(1 - \varepsilon + \frac{2}{3}\varepsilon^2)$  and  $c = r(1 + 2\varepsilon + \frac{5}{3}\varepsilon^2)$ , where we neglect terms of order  $\varepsilon^3$ . The radius of a prolate spheroid is  $R^2(\theta) = a^2\cos^2\theta + c^2\sin^2\theta$ . Replacing the expressions of  $a$  and  $c$ , we obtain

$$R = r[1 + \varepsilon f(\theta) + \varepsilon^2 g(\theta) + O(\varepsilon^3)] \quad (3.10)$$

where  $f(\theta) = 2\sin^2\theta - \cos^2\theta$  and  $g(\theta) = -1/2(2\sin^2\theta - \cos^2\theta)^2 + 7/6\cos^2\theta + 9/3\cos^2\theta$ . Replacing equation 3.10 into equation 3.9 and performing the integral in equation 3.7, we obtain the equation of the round-up dynamics,

$$\gamma\varepsilon = -\frac{56}{15}\mu r\dot{\varepsilon} \quad (3.11)$$

To obtain the dynamical equation 3.10, we have supposed that the round-up occurs without changing the total aggregate volume, i.e.,  $\dot{r} = 0$ . This is an acceptable approximation if the change in volume is small as compared to the change in shape. Solving the differential equation 3.10 leads to the evolution equation in the article's main text.

**Note 4: Description of “stabilization” event** Clusters undergo changes in both shape and position during the “rounding-up” phase before eventually reaching a stable state. The cluster surface tension, arising from both cell contractility and adhesion, is balanced by cluster internal viscosity, leading to the stability in shape. The displacement of a cluster is driven by the imbalance in contraction force around it. During the “stabilization” step, the “adhering cells” around the cluster are quite homogenous, which greatly reduces the displacement of the cluster (Fig. 3.11a). We used PIV analysis to quantify the speed and direction of migrating “adhering cells” (Fig. 3.11b and c). The speed is generally below  $30 \mu\text{m}/\text{h}$ . From the average velocity of cells at each time point, we compare the dynamics of cells from different states.

### Code

See Appendix.

# Chapter 4

## SMC organization within clusters

*After telling the story of the last chapter, I still wanted to verify some hypotheses in an attempt to answer certain questions despite very limited time.*

### 4.1 Introduction

In the previous chapter, I carefully studied the sequence of events leading to the formation and development of SMC clusters steps, starting with hole opening all the way to cluster stabilization. Two major factors that drive cluster formation are cell contractility and cell density. In fact, these two factors simultaneously determine the total contraction force of the SMC cell sheet. Thus, understanding the role of contractility at the different steps of cluster formation is key to elucidating the underlying mechanisms of this phenomenon.

Contractility is the principal function of SMCs[152]. The contractile SMC phenotype is typically viewed as the "healthy" state of SMCs, as opposed to the synthetic phenotype which often characterizes dysfunctional or diseased SMCs[153]. As is commonly done, I studied SMC contractility by studying the expression levels of specific protein biomarkers using both immunostaining and Western blotting in an effort to obtain results that are as quantitative as possible. Protein expression can only provide information on whether or not the cells are contractile, but it is not able to quantify the contractile force generated by the cells. Therefore, I used traction force microscopy (TFM) to quantify the actual force levels associated with SMC contractility under different conditions.

In the previous chapter, I had shown SMC morphological differences within clusters, suggesting potential phenotypic variations within clusters. Apart from cell morpho-

logical differences, in many clusters, the "core" of the cluster has a lower cell density than the peripheral zone. In some cases, the core appears virtually cell-free. I used the micro-injection method to address the following question: is the core of a cluster truly cell-free and simply a fluid-filled space?

In this chapter, I will present results using four methods: immunostaining, Western blots, TFM force measurement and micro-injection. The experiments are very different from the previous study, so I will first present each method then show the results.

## 4.2 Methods

### Immunostaining

In biochemistry, immunostaining is the use of an antibody-based method to detect a specific protein in a sample. The term "immunostaining" was originally used to refer to the immunohistochemical staining of tissue sections, as first described by Albert Coons in 1941. However, immunostaining now encompasses a broad range of techniques used in histology, cell biology, and molecular biology that use antibody-based staining methods.(Adapted from: <https://en.wikipedia.org/wiki/Immunostaining>)

### Western blot

Blot, in molecular biology and genetics, is a way of transferring protein, DNA or RNA to a carrier membrane. In many cases, this is done during gel electrophoresis, transferring the molecules from the gel onto the specific blotting membrane, and in some other cases, adding the samples directly onto the membrane. Southern, Northern and Western blot are the most commonly seen blot methods for DNA, RNA, and protein quantification, respectively.(Adapted from: [https://en.wikipedia.org/wiki/Blot\\_\(biology\)](https://en.wikipedia.org/wiki/Blot_(biology)))

Western blot is the most widely used method for protein detection. It is used as an analytical method, which here enables quantification of SMC-specific biomarker expression, in order to complement the qualitative results of immunostaining. In Western blotting, proteins are separated by their different molecular weights during the process of electrophoresis. The membrane is subsequently incubated with an antibody and visualized using a color rendering agent.(Adapted from: [https://en.wikipedia.org/wiki/Western\\_blot](https://en.wikipedia.org/wiki/Western_blot))

In my experiments, SMCs are cultured for one day in 6-well plates. The cells are then lysed and analyzed by Western blotting using antibodies against SM- $\alpha$ actin and myosin heavy chain (MHC), two protein biomarkers that are generally considered to charac-

terize SMC phenotype. The same two antibodies were also used for immunostaining (see above 4.2) except for  $\beta$ -actin, which is used as the reference protein. More details of the protocol can be found in 6.1.

### **Traction force microscopy (TFM)**

The results of (Chap. 3) suggested that SMC contractility plays a central role in the development of clusters. When the contraction force is inhibited with blebbistatin, the formation of clusters is significantly slowed down. Upon further investigation, we discovered a second SMC cell line, which shows much more limited cluster formation. Naturally, we hypothesized that this second cell line would be characterized by less contractility. To quantify the contraction forces during cluster formation, I used TFM to measure and compare the traction forces generated by the two distinct cell lines.

TFM is a widely used approach to measure forces generated by cells on their substrates. Briefly, cells are seeded on a substrate that is sufficiently compliant to be deformed by the cells. If the stiffness of the substrate is known, it is then possible to calculate the forces exerted by the cells to deform the substrate. In 1980, Harris et al. first used an elastic silicone substrate that deforms under the action of the cells. The forces exerted by the cells on the substrate could be determined from the wrinkles that the cells induced in the substrate[154]. Later in 1997, Burton and Taylor updated this technique to obtain substrates with well-calibrated mechanical properties; thus, they were able to monitor the forces exerted by daughter cells during division[155]. The "Traction Force Microscopy" (TFM) technique is also based on the use of a cell-deformable substrate[156] : using a polyacrylamide gel makes it possible to control the rigidity of the substrate in a fairly simple manner (adjustment of the proportion of polymer and cross-linking agent), and the inclusion of fluorescent micro beads in the gel enables observation and quantification of the deformation of the transparent gel. Thus, the rigidity of the gel is controllable, and the displacement of the fluorescent beads between the state under stress (gel with cells) and a reference state (gel without cells) is used to calculate the forces exerted by the cells to deform the substrate.

This technique now has many variants:

- - **High-resolution TFM [157]**: improvement of the analysis algorithm to obtain a better reconstruction of the force field from the deformation of the gel. Since calculations are faster, this technique can also be used on videomicroscopy images.
- - **TFM in 3D [158]**: monitoring of gel deformation in the 3 dimensions thanks to confocal imaging. Possibility to calculate the forces exerted not only in X and Y but also in Z.

- - **TFM and adhesive micropatterns [159]:** geometry control adhesion of the cells to the substrate. This technique allows not only to standardize the morphology of the cells and thus be able to compare a cell to another one more easily (for example to average the forces calculated on several cells cultivated on the same micropattern), but also to calculate the forces only from the deformation of the fluorescent pattern (use of fluorescent fibronectin), and thus to free itself from bead imaging.
- - **TFM on adherent cell doublets [160]:** deduction of the forces exerted between the two cells at the adherent junction from the forces exerted by each of the two cells on the substrate. Indeed, during the calculation of forces from the deformation of the gel, the sum of the forces exerted by each of the cells is zero if all the forces exerted by the cell are exerted on the substrate. If certain forces are exerted on the other cell and not on the substrate, the sum of the forces calculated from the deformation of the gel is no longer nil but reflects an imbalance corresponding to the forces exerted between the two cells.

### Micro-injection into SMC 3D spheroids

The use of micro-injection as a biological technique started in the early twentieth century, but it was not widely used until the 1970s. By the 1990s, its use had expanded considerably and is now considered to be a popular laboratory procedure, along with vesicle fusion, electroporation, chemical transfection and viral transduction, for the injection of a small quantity of a material through a small target. (Adapted from: <https://en.wikipedia.org/wiki/Microinjection>)

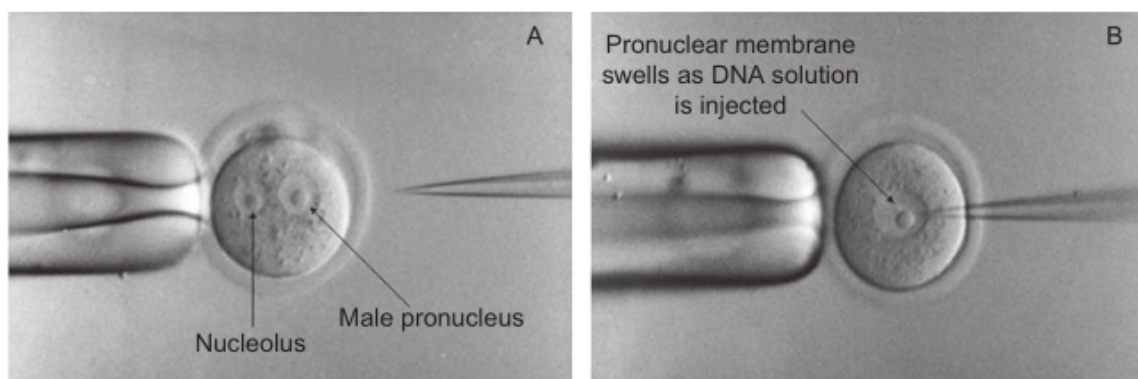


Figure 4.1: Introduction of micro-injection in mouse embryos[161]. A: Mouse embryo prior to micro-injection showing the larger male pro-nucleus and nucleolus. B: Successful micro-injection of the mouse embryo showing swelling of the pronucleus as the DNA is injected.

## 4.2. METHODS

---

Micro-injection is used in the technique of *in vitro* fertilization. It is also very commonly used in the production of transgenic mice and rats. This involves the micro-injection of exogenous DNA into the pronucleus of a single-cell donor embryo stem cell (ESC) at the 0.5-day post-coitus stage of development as depicted in Fig. 4.1 which shows a blastocyst prior to micro-injection, displaying the holding pipette on the left and the micro-injection needle on the right with the ESC. The modulation of the embryo is accomplished using two micromanipulators and joystick controllers on either side of the microscope. One micromanipulator controls the movement of the holding pipette, while the other controls the injection needle, both of which are attached to a precisely regulated pressure system to allow fine control of both the embryo and the injection needle.

Apart from injection into single cells, micro-injection technology is also used to inject fluid into spheroids to probe their internal structure[162]. In Fleming et al.'s work, they demonstrate the uniluminal cavity of a spheroid with an endothelial and SMC co-culture by injecting green fast dye (Fig.4.2).

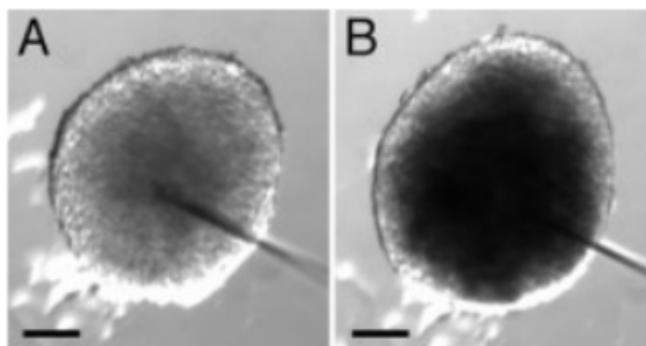


Figure 4.2: Light microscopic images of a spheroid resulting from the fusion of two uniluminal vascular spheroids[162] A: Pre-injection. B: Post green fast dye injection. The increment of time between the image shown in A and B is  $<1$  s. Scale bars:  $100 \mu\text{m}$ .

For the present work, we simplified the experimental setup. SMC clusters are adherent to their substrate, which obviates the need for one micromanipulator and one joystick of pipette holder. The micro-needles are produced in our laboratory using the heating and drawing process of glass capillaries, and the tip of the needle is drawn to a diameter of 5-7 microns. The end of the needle is then heated and bent at an angle of  $45^\circ$ . The micro-needle is filled with fluorescein Figure 4.2.

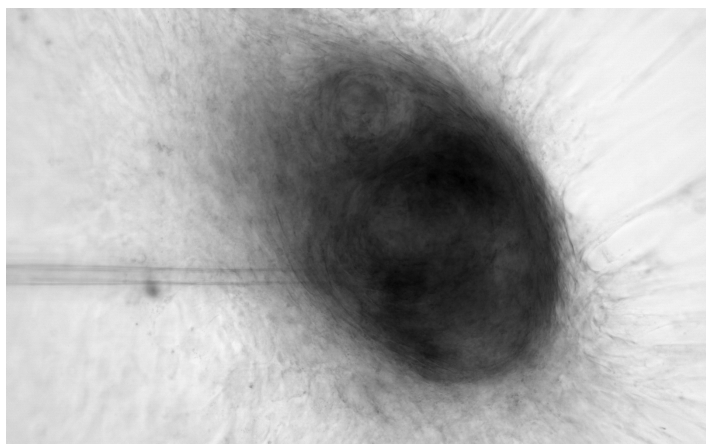


Figure 4.3: Micro-injection into a SMC cluster

A major challenge in micro-injection is overcoming the capillary effect which results from the intermolecular forces between the liquid in the micro-needle and the surrounding rigid surfaces. The capillary effect creates a negative pressure that needs to be overcome by imposing an equivalent positive pressure within the needle. However, introducing this positive pressure into the fluorescein-filled micro-needle prior to penetrating the SMC cluster leads to fluorescein solution everywhere within the cluster, which "pollutes" our Field of view (FOV). On the other hand, not adding this positive pressure risks blockage of the micro-needle due to the negative pressure. These considerations rendered the injection of fluorescein more complicated and less controlled.

Another complication stemmed from the relatively large size of the SMC clusters which rendered focusing and imaging difficult and made it virtually impossible to monitor the micro-needle progression within the cluster. These difficulties in focus and in needle monitoring are clearly visible in Fig. 4.3.

## 4.3 Results

### 4.3.1 Protein quantification

Immunostaining and Western blotting of SMCs are conducted at different cell seeding densities: low density of SMC cell sheet, high density of SMC cell sheet and high density of SMC cluster. Because we wish to investigate the two stable phenotypes of SMCs, the contractile and non-contractile phenotypes, we have a total of six groups. Functionally, the non contractile phenotype is unable to form clusters, presumably due to insufficient contraction forces. To prevent the high density cell sheet group from developing into clusters, the cells were only cultured for one day.

Figure 4.4a depicts the results of the immunostaining on the contractile group for the low density cell sheet, the high density cell sheet, and the high density clusters and for both smooth muscle cell actin and MHC. The results demonstrate clearly that high density cell sheets exhibit higher levels of both smooth muscle actin and MHC. Clusters show the characteristic behavior describe in the previous chapter whereby elongated contractile cells are distributed at the periphery of the cluster while the core has round cells that are considerably less contractile.

The WB results, shown in Figure 4.4b indicate that  $\alpha$ -SMA expression is not dependent of density nor phenotype. It is a specific marker of SMC, but it can not be used to distinguish different phenotypes. However, MHC expression is dependent of both cell phenotype and cell density. MHC expressed at a low level in non contractile cells and even in contractile cell, the expression is not remarkable in the low density groups. Moreover, in contractile group, it turned out to be positively correlated with cell density. The positive correlation between MHC and density indicate the positive correlation between unit cell contractility and density. It enhanced the previous hypothesis that cell density and cell contractility are the two key elements for cluster formation.

The deficiency of MHC in the non-contractile group even in a high density condition is in agreement with the fact that non-contractile SMCs do not form clusters even at sufficiently high density. Without the "motor" of contraction, cells simply pile up on top of one another and form multi-layer flat sheets. For both phenotypes, the expression levels of MHC increase with cell density (Fig. 4.4).

In the previous chapter, we indicated that the two principal elements of cluster formation are cell contractility and cell density. The fact that higher cell density is associated with higher MHC expression levels and thus presumably higher contractility levels leads us to conclude that cluster formation is principally driven by contraction forces.

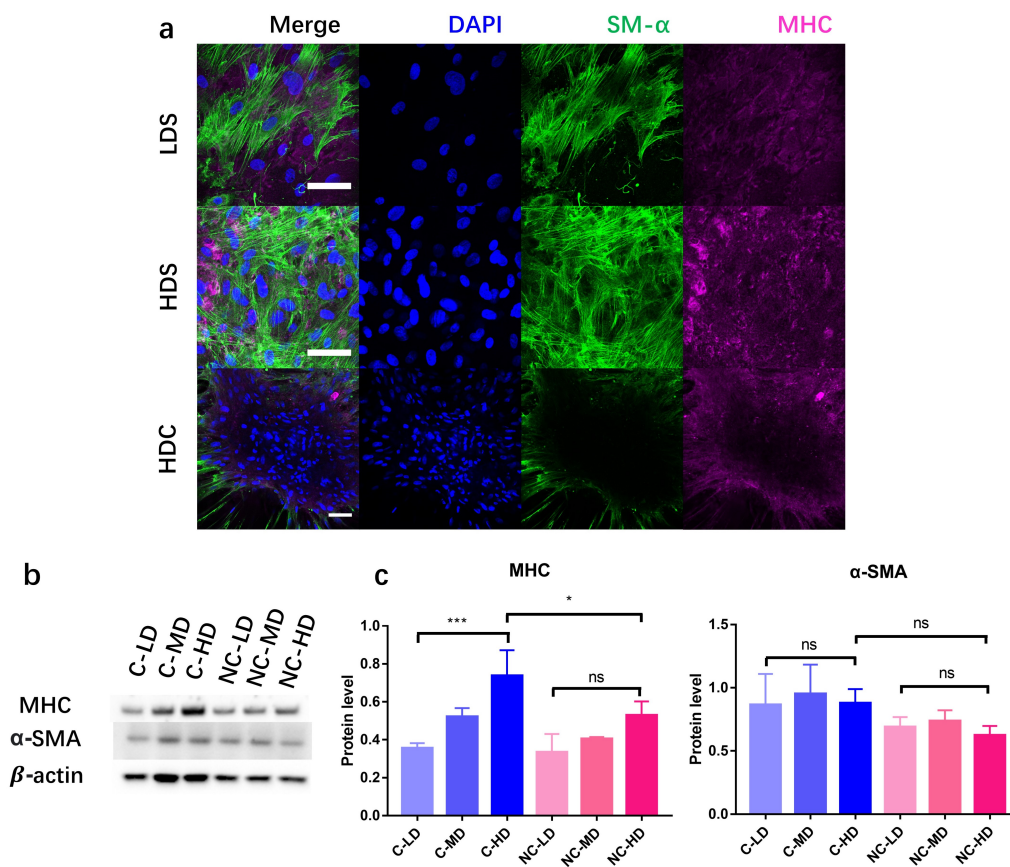


Figure 4.4: SMC protein expression in the different density cases. a: Immunostaining of  $\alpha$ -SMA, MHC in SMC cell sheet and cluster. LDS: low density, 20,000 cells/cm<sup>2</sup> seeding density. HDS: high density, 80,000 cells/cm<sup>2</sup> seeding density. HDC: high density cluster: 160,000 cells/cm<sup>2</sup>. Scale bar: 50  $\mu$ m. b: Western blot for  $\alpha$ -SMA, MHC and  $\beta$ -actin. C: contractile. NC: non-contractile LD: low density, 20,000 cells/cm<sup>2</sup> MD: medium density, 80,000 cells/cm<sup>2</sup> HD: high density, 160,000 cells/cm<sup>2</sup> c Quantification of relative protein level.

### 4.3.2 TFM results

I used TFM to measure the traction forces generated by the contractile and non-contractile SMC phenotypes 4.5. Cells were seeded on the TFM gels at 80,000 cells/cm<sup>2</sup> for 12 hours to allow adhesion to the substrate. The observation of traction forces was conducted for a period of 2-3 hours. In the non-contractile group, the traction stresses were generally homogeneous in the field of view and varied from 0 to  $\sim$  100 Pa (4.5 bottom), and the cells did not have the tendency to form clusters as already described. On the other hand, in the contractile group, an SMC aggregate developed, and traction stresses at the border of the developing aggregate varied from  $\sim$  100 to  $\sim$  400 Pa (4.5

Top). Furthermore, the distribution of traction stresses correlated positively with the location of the SMC aggregate: in the geometry center of the aggregate, the stress levels were low; on the border, on the other hand, the stresses attained their maximum values.

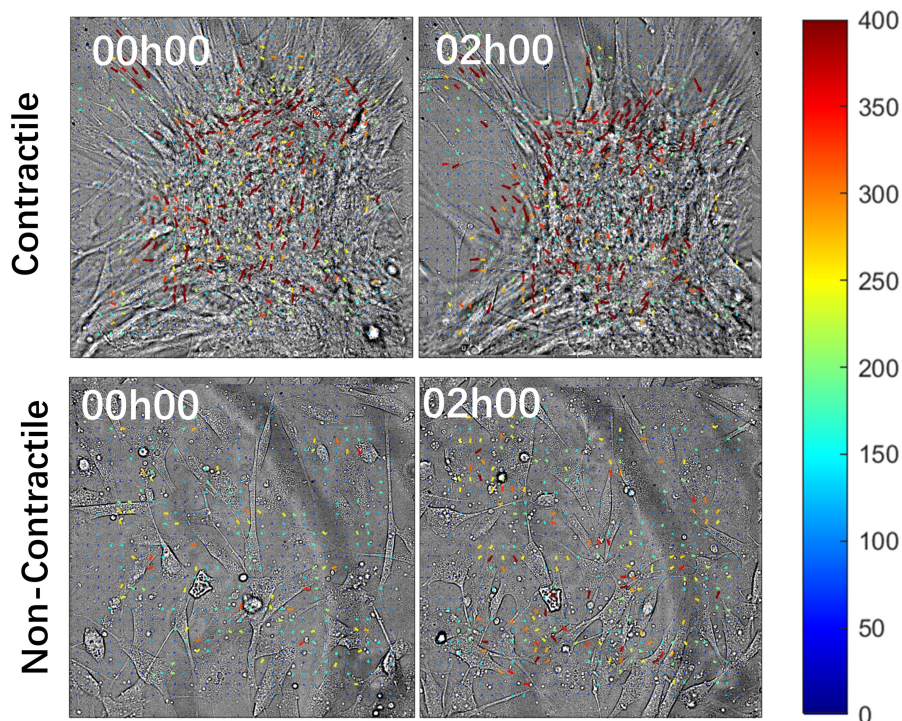


Figure 4.5: **Traction force microscopy results.** a: Traction force representation of contractile SMCs. b: Traction force representation of non-contractile SMCs. Scale bar: 400Pa.

### 4.3.3 Spatial distribution of protein expression within SMC clusters

Immunostaining is used to characterize the spatial distribution of protein expression in SMC clusters. In the previous chapter, we described the heterogeneity of F-actin expression within a SMC cluster. Because of the role of F-actin machinery in generating tension in cells, SMCs expressing low levels of F-actin would be expected to be in a state of low tension. Therefore, I hypothesized that the center of a cluster, where cells exhibit lower F-actin expression, would contain less contractile SMCs. To understand the phenotype of SMCs within a cluster, I investigated the spatial distribution of two of the most representative proteins of contractile SMCs: SM $\alpha$ -actin (SMA) and MHC.

As can be seen in Figure 4.6a, both SMA and MHC are expressed prominently in cells

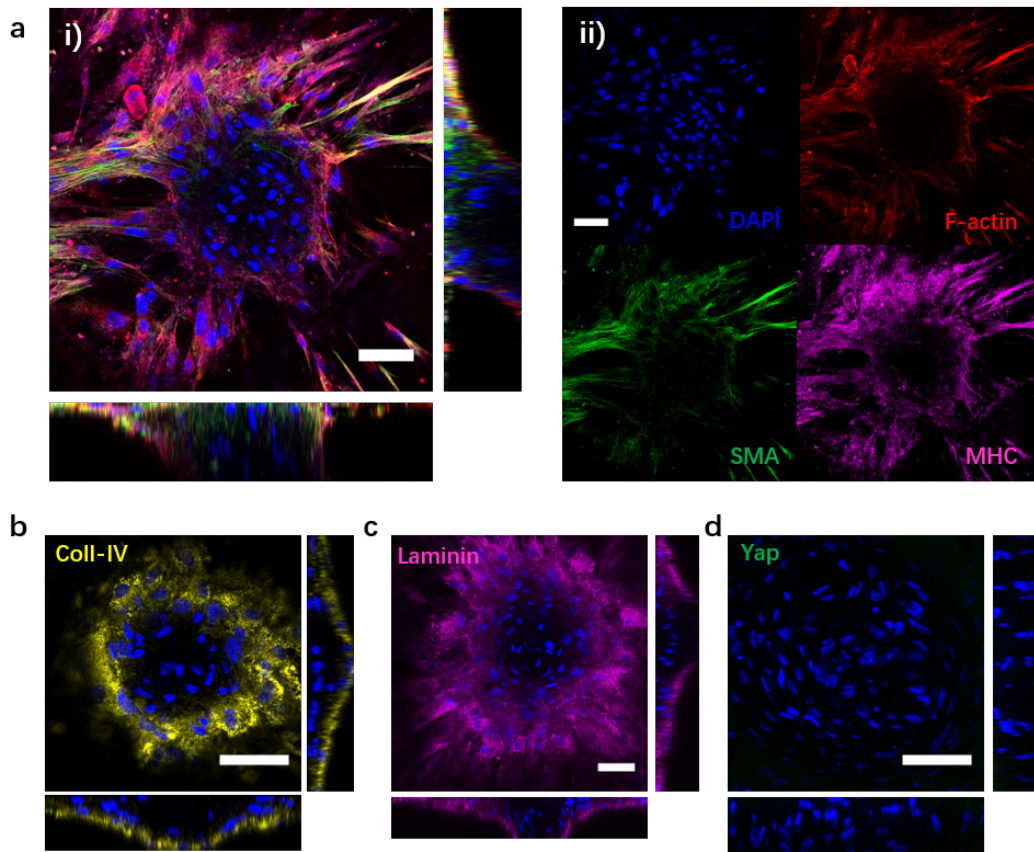


Figure 4.6: Immunostaining of clusters. a: Immunostaining of F-actin, SMA, MHC in a SMC cluster. i) Merge image of F-actin, SMA, MHC with orthogonal views. ii) Split channel of each protein. In the center of the cluster, DAPI is the only fluorescent signal. Note the absence of the most specific proteins of contractile SMCs, namely SMA and MHC, in the center region. The same is true for actin stress fibers. b: Immunostaining for collagen IV. Collagen IV is only expressed in the peripheral zone of a cluster. c: Immunostaining for laminin. Laminin is only expressed in the peripheral zone of a cluster. d: Immunostaining for Yap. Yap is not expressed anywhere in the clusters. Scale bar: 50  $\mu\text{m}$  in all panels.

located at the periphery of clusters. Although the center of the cluster contains cells as can be ascertained from the DAPI (nuclear) staining, the expression of SMA and MHC in that region is very low. This suggests that the SMCs in the center of the cluster are not contractile.

At their functional extremes, SMCs can exhibit either a contractile or a synthetic phenotype. Since the SMCs in the center of the cluster are not contractile, I wondered if they were synthetic. A hallmark of synthetic SMCs is the secretion of extracellular matrix proteins. Therefore, I investigated if the cells in the center of clusters express higher levels of extracellular matrix proteins.

### 4.3. RESULTS

---

Collagen IV and laminin are two vital components of the extracellular matrix that play critical structural roles and regulate cellular differentiation, proliferation and migration. As depicted in Figure 4.6b and c, the core of SMC clusters expresses neither of these two proteins, whereas the contractile cells in the peripheral region certainly do. Since the cells in the center region are viable (Fig. 3.7), I also tested YAP nuclear localization, an indicator of DNA damage, and found it to be absent in all regions of a cluster, from the center to the periphery and from bottom to top.

Therefore, SMCs in the center of clusters appear to be neither contractile nor synthetic. Meanwhile, they are viable and do not seem to exhibit DNA damage. Knowing that mature SMCs still maintain a high differentiation potential, probably, central SMCs differentiated into another type of cells, such as macrophage or foam cells[ref]. The cell covering the surface of cluster, express SMA, MHC, meanwhile, secrete laminin and collagen IV.

These immunostaining results of SMC clusters share some similarities with some published *in vivo* atherosclerosis study [163]. In *ApoE*<sup>(-/-)</sup> mice fed a high fat diet (HFD), plaque initiation starts from week 5. In figure 4.7 b-d, the cores have low or no SMC marker expression (SMA & MHC) but express macrophage marker CD68<sup>+</sup>. Meanwhile, the caps are GFP<sup>+</sup> SMA<sup>+</sup> SMMHC<sup>+</sup>. Furthermore, the cell density in the core decreases compared to that in healthy tissue, as demonstrated by the number of nuclei.

**Integrin  $\beta 3$**  Integrins are heterodimeric receptors that link the extracellular matrix to the cytoskeleton, and deletion of the gene encoding integrin  $\beta 3$  (*Itgb3*) exacerbates atherosclerosis burden in atheroprone mice.

**CD36** is a multifunctional protein that enhances cellular fatty acid (FA) uptake, a key step in energy metabolism, and its dysregulation in multiple tissue sites is central to obesity-linked diabetes, a risk factor for atherosclerosis.

**CD68** is a heavily glycosylated glycoprotein that is highly expressed in macrophages and other mononuclear phagocytes.

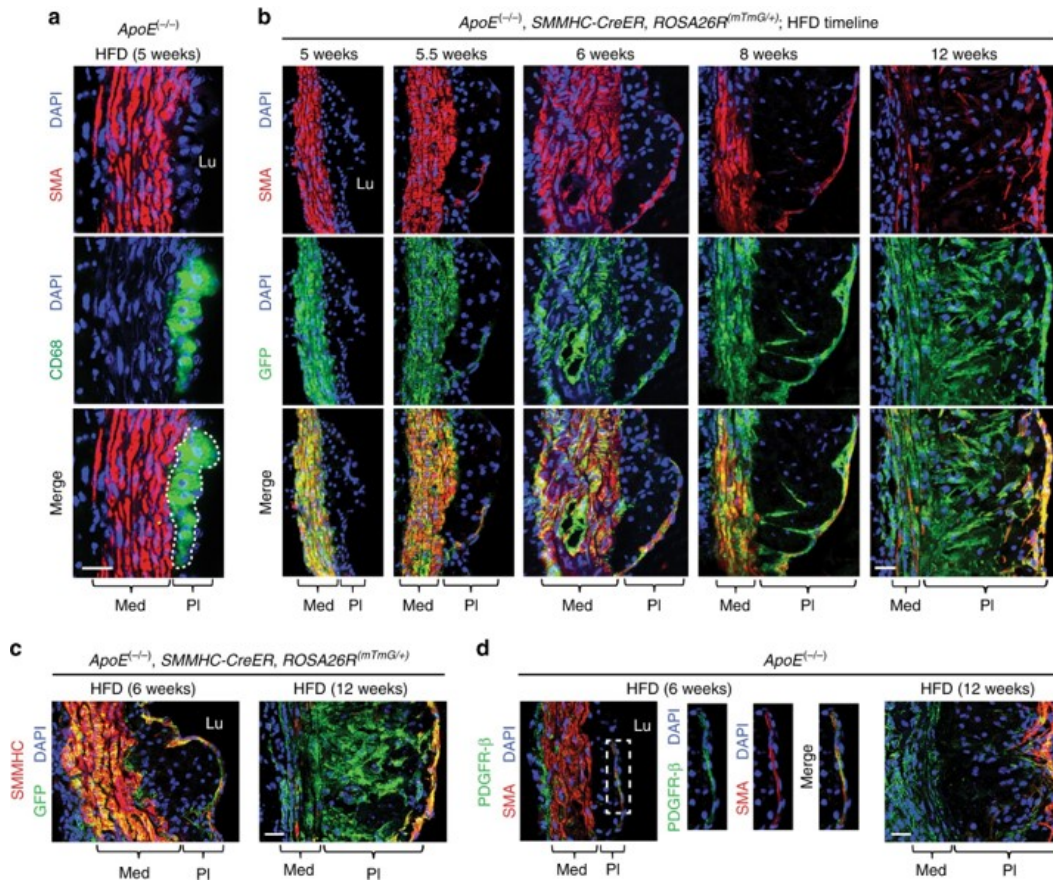


Figure 4.7: Smooth muscle-derived cells initially cover the cap of the plaque and then invade into the core and dedifferentiate [163]. Transverse aortic root sections of mice fed a HFD for 5–12 weeks were immunostained. a, d: Sections from *ApoE*<sup>-/-</sup> mice were stained for SMA, nuclei (DAPI), and either CD68 (a) or PDGFR-β (d). b, c: Prior to the HFD, *ApoE*<sup>-/-</sup>, SMMHC – CreER<sup>T2</sup>, ROSA26R<sup>(mTmG/+)</sup> were induced with tamoxifen, and sections were stained for GFP (fate marker), nuclei (DAPI), and either SMA (b) or SMMHC (c). Results are representative of 5 mice. Lu, aortic lumen; Med, tunica media; Pl, plaque. Scale bars, 25 μm

#### 4.3.4 Micro-injection

In general, the core regions of SMC clusters have lower cell densities. In some clusters, the central zone even appears nucleus-free. Inspired by the study "Fusion of uniluminal vascular spheroid" [162], I wondered if the central zone of the SMC cluster was a uniluminal space. Injection of fluorescein into the SMC & EC spheroid were used to demonstrate the structure has a uniluminal central lumen. To investigate this hypothesis, conducted fluid micro-injection studies within clusters.

#### Injection in clusters

SMCs were cultured on fibronectin-coated flat tissue culture plastic surfaces for three days to allow cluster formation. Large clusters with diameters of  $\sim 200\text{-}1000 \mu\text{m}$  were selected for micro-injection in order to facilitate the procedure. We observed that the injected fluorescein solution remained confined to the internal space of the cluster for a certain period of time. The fluorescence intensity decreased gradually, indicating slow dye leakage from the cluster. The leakage rate within the cluster was approximately 3 times slower than for free diffusion as defined by fluorescein injected outside of the cluster (Fig. 4.8b). These results suggest that dye transport within clusters is characterized by hindered diffusion.

In one micro-injection experiment, the cluster happened to have a leaky portion at the entrance of the micro-needle. This provided a perfect opportunity to directly compare the fluorescence intensity evolution for the two diffusion modes in the same cluster. The kymograph results from respectively outside and inside of the cluster are shown in Figure 4.8a. In the leaky section, the fluorescein injected into the cluster leaks out, leading to the fluorescence signal outside the cluster increasing rapidly (within two seconds). The maximum intensity levels of the signals both inside and outside of the clusters was comparable (approximately  $\sim 200$  units). The fluorescence signal outside the cluster rapidly dissipated, whereas the signal within the cluster remained at a relatively high level for at least 10 seconds longer. These observations demonstrate that the transport of fluid injected into a SMC cluster is hindered, so that the dissipation rate of the fluorescence signal is clearly slower than that for fluid outside the cluster. The effect is illustrated in Figure 4.8 b, which shows that the fluorescence intensity in the cluster remains at 100 units for over 100s, whereas the equivalent value outside the cluster is  $\sim 35$ s.

The diffusion and dissipation of fluorescein in the core of the cluster demonstrated that there is a confined liquid-like space inside clusters. The fact that fluorescein can diffuse homogeneously (Fig. 4.8 a,b) in the internal space in a few seconds suggests the presence of a "liquid-like" core. Moreover, the dissipation rate inside a cluster is at least 3 times slower than that of a free-injection in the outside medium (Fig. 4.8 b). It can be inferred that the leaking is limited. The kymograph shows that there is no leaking at the cluster wall. The only possible leak is at the bottom of a cluster.

The results above lead me to the hypothesis that there is an internal cell-free space in the core of the cluster. This inference is similar to a report dating back to 1975 [164] where the authors showed a cross sectional view of a SMC cluster and reported a cellular "cap" and an acellular "core" (Fig. 4.8c).

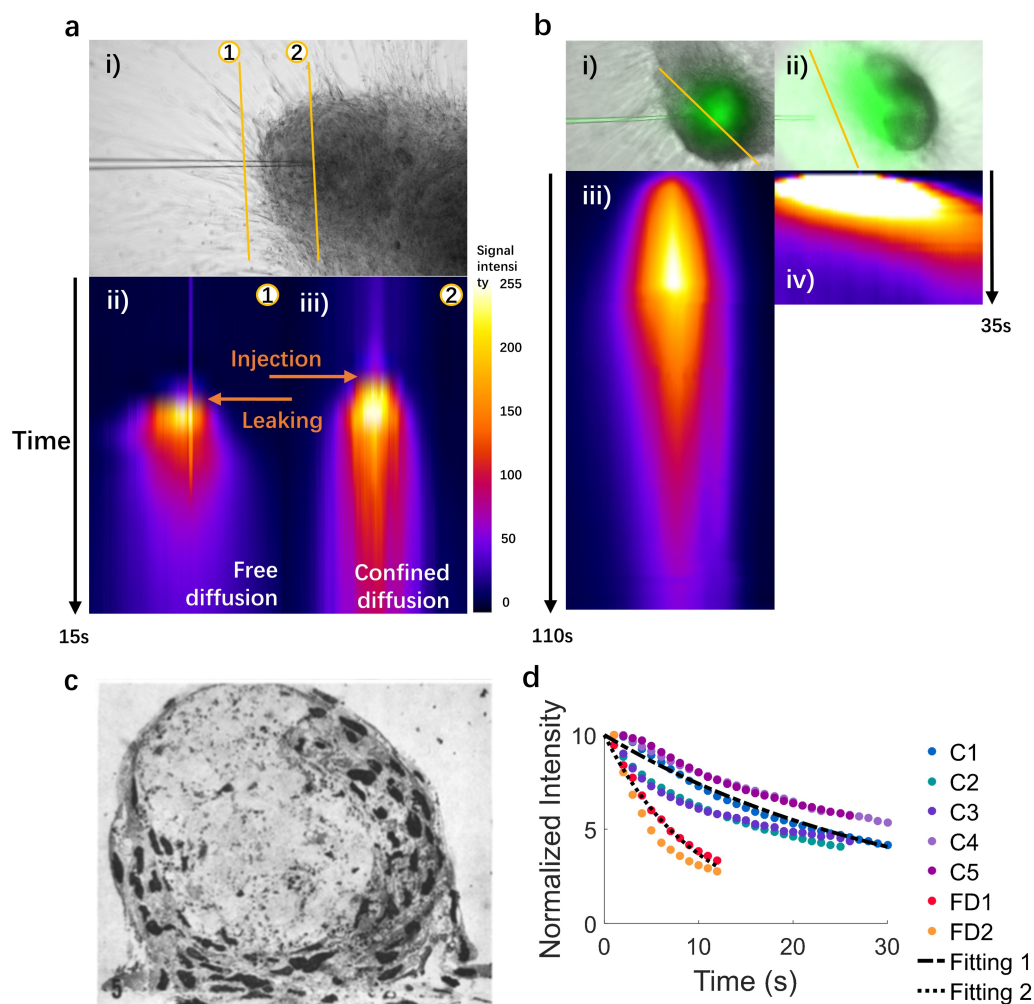


Figure 4.8: Injection in a cluster. a: Injection in a cluster with leaking at the needle entrance spot. i) Bright field image of the analyzed cluster. ii) Kymograph of the outside of the cluster (free diffusion). iii) Kymograph of the inside of the cluster (diffusion in cluster). b: Comparison between the diffusion in a cluster and free diffusion. i) Merge image of the injection in a cluster. ii) Merge image of the injection at the outside of a cluster. iii) Kymograph of the cut in a cluster. iv) Kymograph of the cut outside a cluster (free diffusion). c: Cross section of a mound, stained with silver nitrate. Darkly stained nuclei help to distinguish the cellular layer of the "cap" from the acellular "core". Adapted from [164]. d: Time evolution of the fluorescein signal intensity within and outside several clusters. Also included are the results from two fits of the compartment model described in the text. Fit 1 is for transport in a confined tank. Fit 2 is transport in the case of free diffusion.

### A cluster with two compartments

During the micro-injection experiments, we found one cluster with two compartments, presumably due to yet incomplete fusion of two clusters. When we injected the fluorescein solution into the center of one cluster, we observed that the fluorescein also appeared in the other cluster even though there was no visible link or physical connection between the two compartments. The signal intensity in center 2 increased during the process of injection into center 1. We note that fluorescence was also observed in the region outside the clusters, presumably due to fluorescein leakage. However, the fluorescence intensity of center 2 was always higher than that of the region outside the clusters. These results suggest a level of communication between the two compartments.

We characterized the evolution of the fluorescence signals in the two compartments. This evolution can be understood by using the following multi-compartment model [165]:

$$\dot{\mathbf{q}} = \mathbf{K}\mathbf{q} + \mathbf{u} \quad (4.1)$$

where  $\mathbf{q}$  is the mass of solute,  $\mathbf{K}$  is the proportionality and  $\mathbf{u}$  is the input. Most commonly, the mathematics of multi-compartment models is simplified to provide only a single parameter. Here, it is the concentration of fluorescein within a compartment. Modeling the fluorescein exchanges between the two centers as the liquid concentration of two compartments, the signal is governed by the equations:

$$\begin{aligned} \dot{y}_1 &= c(y_1 - y_2) - \xi_1 y_1 + \omega(t) \\ \dot{y}_2 &= c(y_2 - y_1) - \xi_2 y_2 \end{aligned} \quad (4.2)$$

where  $c$  is the exchange at the interface,  $\xi_1, \xi_2$  are viscous dissipation for center 1 and center 2, respectively and  $\omega(t)$  is the input. By fitting the experimental data (Fig. 4.9c), we obtain experimentally  $c \sim -0.03(s^{-1})$  and  $\xi_1, \xi_2 \sim 0.03(s^{-1})$ . There is a 5 s delay between peak 1 and peak 2, which are the maximum of the fluorescence signals of clusters 1 and 2, respectively. Along the major axis of the cluster, the kymograph (Fig. 4.9d) showed that the intensity of cluster 2 increased after that of cluster 1 and that considerable intensity changes only occurred in the inner regions of the clusters. The intensity in the cluster eventually dissipates due to fluid leakage from the cluster; however, this leakage does not occur at the lateral SMC wall (Fig. 4.9b e). The kymograph results at three different zones show clearly that the intensity is lowest at the wall are the lowest, even lower than the outside signal intensity (Fig. 4.9e). The results of two center clusters again suggests that there is liquid-like space exist in the center of SMC spheroids, which facilitate a spacial connection. The two centers are probably results from a not completely fused cluster.

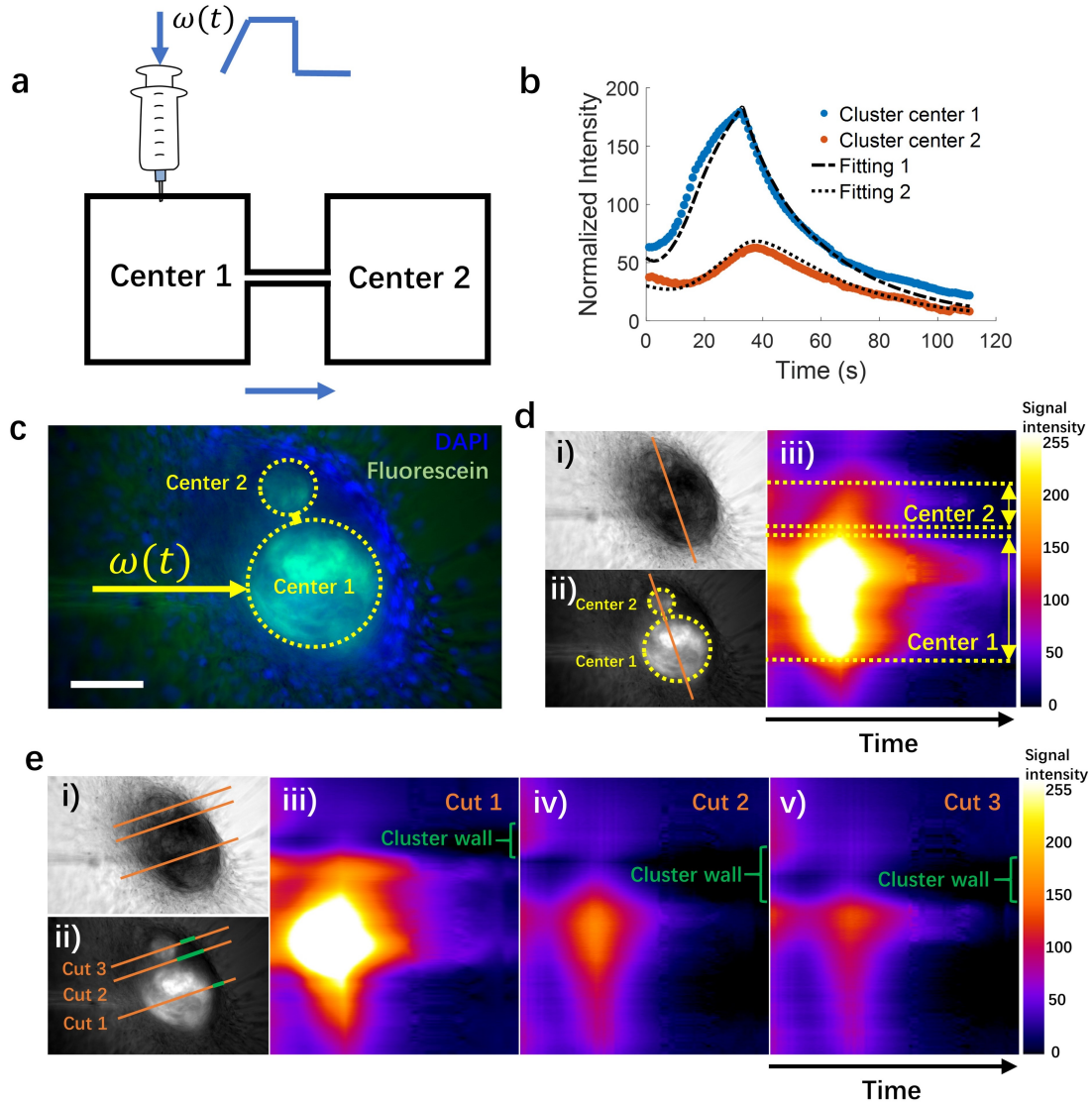


Figure 4.9: Injection in a cluster with two circular centers. a: Schematic panel of tank diffusion model. b: Fluorescent image of cluster post-injection. Scale bar:  $100 \mu m$ . c: Signal intensity evolution of two centers with corresponding computational fitting. d: Kymograph along the major axis of cluster. i) Bright-field image of cluster. ii) Fluorescent image of cluster. iii) Kymograph of the orange line in i) and ii). Center 2 has a delay of signal increase. e: Kymograph of three lines, along the direction of the minor axis. i) Bright-field image of cluster. ii) Fluorescent image of cluster. iii) Kymograph of cut 1. iv) Kymograph of cut 2. v) Kymograph of cut 3. The wall of the cluster shows the lowest signal intensity.

## 4.4 Discussion and conclusions

In this chapter, we have developed a better understanding of SMC clusters from the standpoint of three specific aspects: spatial distribution of protein expression, spatial structure/organization and traction force levels. Using a combination of immunostaining and Western blotting, it is shown that SMC underwent phenotypic switching during cluster formation, and cells in the acellular "core" of the cluster did not exhibit SMC-specific markers. Micro-injection experiments, along with a diffusion model, confirmed the hypothesis that the acellular "core" has some unobstructed liquid space.

# Chapter 5

## Conclusions

In Chapter 1, I presented the background information relevant to the field of my research. Atherosclerosis is at the heart of the three projects I pursued during my PhD. I discussed the concept of collective cell behavior, which is important in the studies I conducted. For instance, the cluster formation studies described in later chapters can be thought of in terms of a collective morphological transition. In the last part of the chapter, I presented some important information on smooth muscle cells (SMCs).

In Chapter 2, I used arterial mimics previously developed in our laboratory to quantify the damage to the endothelial layer induced by balloon angioplasty. The results provided me with an understanding of which types of balloon movement induce cellular damage. They also provided me with an appreciation for the importance of wall mechanical rigidity in determining the extent of endothelial damage induced by a balloon.

Chapter 3 described the most significant part of my PhD: the description of contractility-induced SMC cluster formation. The fact that SMCs cultured in vitro can spontaneously form specific 3D patterns has been well known since the 1970s. These 3D structures have been given various names, including mounds, aggregates, clusters and hill-valley patterns. However, the physical events that give rise to these clusters and the physical mechanisms that govern their formation had not been previously described. In my project, combined with a dewetting model, we first described all sequences of this collective 2D to 3D transition, and we then interpreted this phenomenon in terms of cell contractility and cell density. Observing phenomena, formulating hypotheses, designing experiments, building analytical tools, analyzing data, writing and reviewing articles, this project has enabled me to acquire the full set of competencies of a researcher.

Chapter 4 presented some preliminary results aimed at addressing certain questions that arose from the previous chapter: i) What is the internal structure of the SMC clusters? ii) What is the contraction force levels generated by SMCs to initiate cluster

---

formation? Due to the limited time of my thesis and the impact of the pandemic, the scope of this work is limited. However, I was able to design, conduct and analyze some new experiments in a short period of two months to answer these interesting questions. Although the content of the results is clearly not sufficient for publication, I felt they were sufficiently interesting to include as they can form the basis of future studies.

# References

- [1] Peter Libby, Paul M Ridker, and Göran K Hansson. “Progress and challenges in translating the biology of atherosclerosis”. In: *Nature* 473.7347 (2011), pp. 317–325.
- [2] C Velican. “A dissecting view on the role of the fatty streak in the pathogenesis of human atherosclerosis: culprit or bystander?”. In: *Medecine interne* 19.4 (1981), p. 321.
- [3] MacRae F Linton et al. “The role of lipids and lipoproteins in atherosclerosis”. In: *Endotext [Internet]*. MDText. com, Inc., 2019.
- [4] Renu Virmani et al. “Lessons from sudden coronary death: a comprehensive morphological classification scheme for atherosclerotic lesions”. In: *Arteriosclerosis, thrombosis, and vascular biology* 20.5 (2000), pp. 1262–1275.
- [5] Herbert C Stary et al. “A definition of advanced types of atherosclerotic lesions and a histological classification of atherosclerosis: a report from the Committee on Vascular Lesions of the Council on Arteriosclerosis, American Heart Association”. In: *Circulation* 92.5 (1995), pp. 1355–1374.
- [6] Delphine Gomez and Gary K Owens. “Smooth muscle cell phenotypic switching in atherosclerosis”. In: *Cardiovascular research* 95.2 (2012), pp. 156–164.
- [7] James X Rong et al. “Transdifferentiation of mouse aortic smooth muscle cells to a macrophage-like state after cholesterol loading”. In: *Proceedings of the National Academy of Sciences* 100.23 (2003), pp. 13531–13536.
- [8] Elena R Andreeva, Inna M Pugach, and Alexander N Orekhov. “Subendothelial smooth muscle cells of human aorta express macrophage antigen in situ and in vitro”. In: *Atherosclerosis* 135.1 (1997), pp. 19–27.
- [9] Laura S Shankman et al. “KLF4-dependent phenotypic modulation of smooth muscle cells has a key role in atherosclerotic plaque pathogenesis”. In: *Nature medicine* 21.6 (2015), pp. 628–637.
- [10] Susanne Feil et al. “Transdifferentiation of vascular smooth muscle cells to macrophage-like cells during atherogenesis”. In: *Circulation research* 115.7 (2014), pp. 662–667.

## REFERENCES

---

- [11] Delphine Gomez et al. “Detection of histone modifications at specific gene loci in single cells in histological sections”. In: *Nature methods* 10.2 (2013), pp. 171–177.
- [12] SC Bergheanu, MC Bodde, and JW Jukema. “Pathophysiology and treatment of atherosclerosis”. In: *Netherlands Heart Journal* 25.4 (2017), pp. 231–242.
- [13] Hendrick B Barner. “Operative treatment of coronary atherosclerosis”. In: *The Annals of thoracic surgery* 85.4 (2008), pp. 1473–1482.
- [14] G Antonakoudis et al. “Blood pressure control and cardiovascular risk reduction”. In: *Hippokratia* 11.3 (2007), p. 114.
- [15] Cheuk-Man Yu et al. “Long-term changes in exercise capacity, quality of life, body anthropometry, and lipid profiles after a cardiac rehabilitation program in obese patients with coronary heart disease”. In: *American Journal of Cardiology* 91.3 (2003), pp. 321–325.
- [16] Bryan Williams. *Drug treatment of hypertension: Most patients will need a treatment cocktail—including a thiazide diuretic*. 2003.
- [17] ROBERT C TARAZI, HARRIET P DUSTAN, and EDWARD D FROHLICH. “Long-term thiazide therapy in essential hypertension: evidence for persistent alteration in plasma volume and renin activity”. In: *Circulation* 41.4 (1970), pp. 709–717.
- [18] Hiromi Rakugi et al. “Induction of angiotensin converting enzyme in the neointima after vascular injury. Possible role in restenosis.” In: *The Journal of clinical investigation* 93.1 (1994), pp. 339–346.
- [19] Ellen O Weinberg et al. “Angiotensin-converting enzyme inhibition prolongs survival and modifies the transition to heart failure in rats with pressure overload hypertrophy due to ascending aortic stenosis.” In: *Circulation* 90.3 (1994), pp. 1410–1422.
- [20] Heribert Schunkert et al. “Evidence for tissue-specific activation of renal angiotensinogen mRNA expression in chronic stable experimental heart failure.” In: *The Journal of clinical investigation* 90.4 (1992), pp. 1523–1529.
- [21] SOLVD Investigators\*. “Effect of enalapril on survival in patients with reduced left ventricular ejection fractions and congestive heart failure”. In: *New England Journal of Medicine* 325.5 (1991), pp. 293–302.
- [22] Sylvia Heeneman, Judith C Sluimer, and Mat JAP Daemen. “Angiotensin-converting enzyme and vascular remodeling”. In: *Circulation research* 101.5 (2007), pp. 441–454.
- [23] Daiana Weiss, Dan Sorescu, and W Robert Taylor. “Angiotensin II and atherosclerosis”. In: *The American journal of cardiology* 87.8 (2001), pp. 25–32.
- [24] Carlos M Ferrario et al. “Effect of angiotensin-converting enzyme inhibition and angiotensin II receptor blockers on cardiac angiotensin-converting enzyme 2”. In: *Circulation* 111.20 (2005), pp. 2605–2610.

- 
- [25] A Fleckenstein et al. “The role of calcium in the pathogenesis of experimental arteriosclerosis”. In: *Trends in Pharmacological Sciences* 8.12 (1987), pp. 496–501.
- [26] Michael Schachter. “Vascular smooth muscle cell migration, atherosclerosis, and calcium channel blockers”. In: *International journal of cardiology* 62 (1997), S85–S90.
- [27] David Waters et al. “A controlled clinical trial to assess the effect of a calcium channel blocker on the progression of coronary atherosclerosis.” In: *Circulation* 82.6 (1990), pp. 1940–1953.
- [28] Hermann Esterbauer et al. “Biochemical structural and functional properties of oxidized low-density lipoprotein”. In: *Chemical research in toxicology* 3.2 (1990), pp. 77–92.
- [29] John W Gofman et al. “The role of lipids and lipoproteins in atherosclerosis”. In: *Science* 111.2877 (1950), pp. 166–186.
- [30] Shinya Okazaki et al. “Early statin treatment in patients with acute coronary syndrome: demonstration of the beneficial effect on atherosclerotic lesions by serial volumetric intravascular ultrasound analysis during half a year after coronary event: the ESTABLISH Study”. In: *Circulation* 110.9 (2004), pp. 1061–1068.
- [31] Akira Endo. “A historical perspective on the discovery of statins”. In: *Proceedings of the Japan Academy, Series B* 86.5 (2010), pp. 484–493.
- [32] Allen Shek and Mary J Ferrill. “Statin—fibrate combination therapy”. In: *Annals of Pharmacotherapy* 35.7-8 (2001), pp. 908–917.
- [33] Aim-High Investigators. “Niacin in patients with low HDL cholesterol levels receiving intensive statin therapy”. In: *New England Journal of Medicine* 365.24 (2011), pp. 2255–2267.
- [34] Robert H Knopp et al. “Contrasting effects of unmodified and time-release forms of niacin on lipoproteins in hyperlipidemic subjects: clues to mechanism of action of niacin”. In: *Metabolism* 34.7 (1985), pp. 642–650.
- [35] Raimund Erbel et al. “Coronary-artery stenting compared with balloon angioplasty for restenosis after initial balloon angioplasty”. In: *New England Journal of Medicine* 339.23 (1998), pp. 1672–1678.
- [36] Campbell Rogers et al. “Balloon-artery interactions during stent placement: a finite element analysis approach to pressure, compliance, and stent design as contributors to vascular injury”. In: *Circulation research* 84.4 (1999), pp. 378–383.
- [37] Robert A Byrne, Michael Joner, and Adnan Kastrati. “Stent thrombosis and restenosis: what have we learned and where are we going? The Andreas Grüntzig Lecture ESC 2014”. In: *European heart journal* 36.47 (2015), pp. 3320–3331.

- [38] Patrick W Serruys et al. “Percutaneous coronary intervention versus coronary-artery bypass grafting for severe coronary artery disease”. In: *New England journal of medicine* 360.10 (2009), pp. 961–972.
- [39] Ashish Saxena et al. “Effect of carotid artery stenosis on neck skin tissue heat transfer”. In: *International Journal of Thermal Sciences* 145 (2019), p. 106010.
- [40] J-L Deneubourg et al. “The self-organizing exploratory pattern of the argentine ant”. In: *Journal of insect behavior* 3.2 (1990), pp. 159–168.
- [41] Máté Nagy et al. “Hierarchical group dynamics in pigeon flocks”. In: *Nature* 464.7290 (2010), pp. 890–893.
- [42] Kolbjørn Tunstrøm et al. “Collective states, multistability and transitional behavior in schooling fish”. In: *PLoS Comput Biol* 9.2 (2013), e1002915.
- [43] John RG Dyer et al. “Consensus decision making in human crowds”. In: *Animal Behaviour* 75.2 (2008), pp. 461–470.
- [44] Christos C Ioannou, Vishwesh Guttal, and Iain D Couzin. “Predatory fish select for coordinated collective motion in virtual prey”. In: *Science* 337.6099 (2012), pp. 1212–1215.
- [45] Ariana Strandburg-Peshkin et al. “Shared decision-making drives collective movement in wild baboons”. In: *Science* 348.6241 (2015), pp. 1358–1361.
- [46] Kenneth M Yamada and Edna Cukierman. “Modeling tissue morphogenesis and cancer in 3D”. In: *Cell* 130.4 (2007), pp. 601–610.
- [47] Peter Friedl and Darren Gilmour. “Collective cell migration in morphogenesis, regeneration and cancer”. In: *Nature reviews Molecular cell biology* 10.7 (2009), pp. 445–457.
- [48] Casey M Kraning-Rush et al. “The role of the cytoskeleton in cellular force generation in 2D and 3D environments”. In: *Physical biology* 8.1 (2011), p. 015009.
- [49] Jonathan Stricker, Tobias Falzone, and Margaret L Gardel. “Mechanics of the F-actin cytoskeleton”. In: *Journal of biomechanics* 43.1 (2010), pp. 9–14.
- [50] Margaret L Gardel et al. “Traction stress in focal adhesions correlates biphasically with actin retrograde flow speed”. In: *Journal of Cell Biology* 183.6 (2008), pp. 999–1005.
- [51] Grégory Giannone et al. “Lamellipodial actin mechanically links myosin activity with adhesion-site formation”. In: *Cell* 128.3 (2007), pp. 561–575.
- [52] K Kruse et al. “Contractility and retrograde flow in lamellipodium motion”. In: *Physical biology* 3.2 (2006), p. 130.
- [53] Lan Lu et al. “Mechanical properties of actin stress fibers in living cells”. In: *Biophysical journal* 95.12 (2008), pp. 6060–6071.
- [54] Guillaume T Charras et al. “Reassembly of contractile actin cortex in cell blebs”. In: *The Journal of cell biology* 175.3 (2006), pp. 477–490.

- 
- [55] Takashi Kato et al. “Liquid-crystalline physical gels”. In: *Chemical Society Reviews* 36.12 (2007), pp. 1857–1867.
- [56] Amin Doostmohammadi et al. “Active nematics”. In: *Nature communications* 9.1 (2018), pp. 1–13.
- [57] M Cristina Marchetti et al. “Hydrodynamics of soft active matter”. In: *Reviews of Modern Physics* 85.3 (2013), p. 1143.
- [58] Tim Sanchez et al. “Spontaneous motion in hierarchically assembled active matter”. In: *Nature* 491.7424 (2012), pp. 431–434.
- [59] Thuan Beng Saw et al. “Topological defects in epithelia govern cell death and extrusion”. In: *Nature* 544.7649 (2017), pp. 212–216.
- [60] Kyogo Kawaguchi, Ryoichiro Kageyama, and Masaki Sano. “Topological defects control collective dynamics in neural progenitor cell cultures”. In: *Nature* 545.7654 (2017), pp. 327–331.
- [61] Dmitri Volfson et al. “Biomechanical ordering of dense cell populations”. In: *Proceedings of the National Academy of Sciences* 105.40 (2008), pp. 15346–15351.
- [62] Yonit Maroudas-Sacks et al. “Topological defects in the nematic order of actin fibers as organization centers of Hydra morphogenesis”. In: *bioRxiv* (2020).
- [63] LS Penrose. “Dermatoglyphic topology”. In: *Nature* 205.4971 (1965), pp. 544–546.
- [64] M-A Fardin and B Ladoux. “Living proof of effective defects”. In: *Nature Physics* (2020), pp. 1–2.
- [65] Guillaume Duclos et al. “Topological defects in confined populations of spindle-shaped cells”. In: *Nature Physics* 13.1 (2017), pp. 58–62.
- [66] TR Elsdale. “Parallel orientation of fibroblasts in vitro”. In: *Experimental cell research* 51.2-3 (1968), pp. 439–450.
- [67] Ralf Kemkemer et al. “Elastic properties of nematoid arrangements formed by amoeboid cells”. In: *The European Physical Journal E* 1.2-3 (2000), pp. 215–225.
- [68] Thomas E Angelini et al. “Glass-like dynamics of collective cell migration”. In: *Proceedings of the National Academy of Sciences* 108.12 (2011), pp. 4714–4719.
- [69] Kenekwuw David Nnetu et al. “The impact of jamming on boundaries of collectively moving weak-interacting cells”. In: *New Journal of Physics* 14.11 (2012), p. 115012.
- [70] Jin-Ah Park et al. “Unjamming and cell shape in the asthmatic airway epithelium”. In: *Nature materials* 14.10 (2015), pp. 1040–1048.
- [71] Amin Doostmohammadi et al. “Stabilization of active matter by flow-vortex lattices and defect ordering”. In: *Nature communications* 7.1 (2016), pp. 1–9.

## REFERENCES

---

- [72] Luca Giomi et al. “Defect dynamics in active nematics”. In: *Philosophical Transactions of the Royal Society A: Mathematical, Physical and Engineering Sciences* 372.2029 (2014), p. 20130365.
- [73] LM Pismen. “Dynamics of defects in an active nematic layer”. In: *Physical Review E* 88.5 (2013), p. 050502.
- [74] Stéphane Douezan et al. “Spreading dynamics and wetting transition of cellular aggregates”. In: *Proceedings of the National Academy of Sciences* 108.18 (2011), pp. 7315–7320.
- [75] Grégory Beaune et al. “Reentrant wetting transition in the spreading of cellular aggregates”. In: *Soft Matter* 13.45 (2017), pp. 8474–8482.
- [76] Stéphane Douezan and Françoise Brochard-Wyart. “Active diffusion-limited aggregation of cells”. In: *Soft Matter* 8.3 (2012), pp. 784–788.
- [77] Peter Friedl et al. “Classifying collective cancer cell invasion”. In: *Nature cell biology* 14.8 (2012), pp. 777–783.
- [78] Grégory Beaune et al. “How cells flow in the spreading of cellular aggregates”. In: *Proceedings of the National Academy of Sciences* 111.22 (2014), pp. 8055–8060.
- [79] David Gonzalez-Rodriguez et al. “Detachment and fracture of cellular aggregates”. In: *Soft Matter* 9.7 (2013), pp. 2282–2290.
- [80] Russell Ross and John A Glomset. “Atherosclerosis and the arterial smooth muscle cell”. In: *Science* 180.4093 (1973), pp. 1332–1339.
- [81] Earl P Benditt and John M Benditt. “Evidence for a monoclonal origin of human atherosclerotic plaques”. In: *Proceedings of the National Academy of Sciences* 70.6 (1973), pp. 1753–1756.
- [82] Christopher Ward et al. “Airway inflammation, basement membrane thickening and bronchial hyperresponsiveness in asthma”. In: *Thorax* 57.4 (2002), pp. 309–316.
- [83] Masahito Ebina et al. “Cellular hypertrophy and hyperplasia of airway smooth muscle underlying bronchial asthma”. In: *Am Rev Respir Dis* 148 (1993), pp. 720–726.
- [84] Elizabeth A Stewart. “Uterine fibroids”. In: *The Lancet* 357.9252 (2001), pp. 293–298.
- [85] Elizabeth A Stewart et al. “Uterine fibroids”. In: *Nature reviews Disease primers* 2.1 (2016), pp. 1–18.
- [86] Jason M Tarkin et al. “Imaging atherosclerosis”. In: *Circulation research* 118.4 (2016), pp. 750–769.
- [87] Stephen T Holgate. “Asthma: Clinical Aspects and Mucosal Immunology”. In: *Mucosal Immunology*. Elsevier, 2015, pp. 1833–1856.

- 
- [88] E Serdar and MD Balun. “Uterine fibroids”. In: *N Engl J Med* 369 (2013), pp. 1344–55.
- [89] Rodolfo Montironi et al. “Morphological diagnosis of urothelial neoplasms”. In: *Journal of clinical pathology* 61.1 (2008), pp. 3–10.
- [90] Tuqa Saleh Al-Shehabi, Rabah Iratni, and Ali H Eid. “Anti-atherosclerotic plants which modulate the phenotype of vascular smooth muscle cells”. In: *Phytomedicine* 23.11 (2016), pp. 1068–1081.
- [91] Nataliya A Pidkovka et al. “Oxidized phospholipids induce phenotypic switching of vascular smooth muscle cells in vivo and in vitro”. In: *Circulation research* 101.8 (2007), pp. 792–801.
- [92] Frédéric Dandré and Gary K Owens. “Platelet-derived growth factor-BB and Ets-1 transcription factor negatively regulate transcription of multiple smooth muscle cell differentiation marker genes”. In: *American Journal of Physiology-Heart and Circulatory Physiology* 286.6 (2004), H2042–H2051.
- [93] Nathalie Clément et al. “Notch3 and IL-1 $\beta$  exert opposing effects on a vascular smooth muscle cell inflammatory pathway in which NF- $\kappa$ B drives crosstalk”. In: *Journal of cell science* 120.19 (2007), pp. 3352–3361.
- [94] Catherine M Shanahan et al. “High expression of genes for calcification-regulating proteins in human atherosclerotic plaques.” In: *The Journal of clinical investigation* 93.6 (1994), pp. 2393–2402.
- [95] Catherine M Shanahan et al. “Identification of osteoglycin as a component of the vascular matrix: differential expression by vascular smooth muscle cells during neointima formation and in atherosclerotic plaques”. In: *Arteriosclerosis, thrombosis, and vascular biology* 17.11 (1997), pp. 2437–2447.
- [96] Julie H Chamley et al. “Distinction between smooth muscle, fibroblasts and endothelial cells in culture by the use of fluoresceinated antibodies against smooth muscle actin”. In: *Cell and Tissue Research* 177.4 (1977), pp. 445–457.
- [97] Allen M Gown et al. “A smooth muscle-specific monoclonal antibody recognizes smooth muscle actin isozymes.” In: *The Journal of cell biology* 100.3 (1985), pp. 807–813.
- [98] Catherine M Shanahan and Peter L Weissberg. “Smooth muscle cell heterogeneity: patterns of gene expression in vascular smooth muscle cells in vitro and in vivo”. In: *Arteriosclerosis, thrombosis, and vascular biology* 18.3 (1998), pp. 333–338.
- [99] JULIE Chamley-Campbell, GORDON R Campbell, and RUSSELL Ross. “The smooth muscle cell in culture”. In: *Physiological reviews* 59.1 (1979), pp. 1–61.
- [100] Goran K Hansson et al. “Immune mechanisms in atherosclerosis.” In: *Arteriosclerosis: An Official Journal of the American Heart Association, Inc.* 9.5 (1989), pp. 567–578.

## REFERENCES

---

- [101] Goran K Hansson. “Immune mechanisms in atherosclerosis”. In: *Arteriosclerosis, thrombosis, and vascular biology* 21.12 (2001), pp. 1876–1890.
- [102] Jack C Geer, Henry C McGill Jr, and Jack P Strong. “The fine structure of human atherosclerotic lesions”. In: *The American journal of pathology* 38.3 (1961), p. 263.
- [103] H Imai et al. “Atherosclerosis in rabbits: architectural and subcellular alterations of smooth muscle cells of aortas in response to hyperlipemia”. In: *Experimental and Molecular Pathology* 5.3 (1966), pp. 273–310.
- [104] Diane Proudfoot et al. “Calcification of human vascular cells in vitro is correlated with high levels of matrix Gla protein and low levels of osteopontin expression”. In: *Arteriosclerosis, thrombosis, and vascular biology* 18.3 (1998), pp. 379–388.
- [105] Catherine M Shanahan et al. “Medial localization of mineralization-regulating proteins in association with Monckeberg’s sclerosis: evidence for smooth muscle cell-mediated vascular calcification”. In: *Circulation* 100.21 (1999), pp. 2168–2176.
- [106] Kazuyuki Yahagi et al. “Pathophysiology of native coronary, vein graft, and in-stent atherosclerosis”. In: *Nature Reviews Cardiology* 13.2 (2016), p. 79.
- [107] Takahisa Mori et al. “Follow-up study after intracranial percutaneous transluminal cerebral balloon angioplasty”. In: *American Journal of Neuroradiology* 19.8 (1998), pp. 1525–1533. ISSN: 0195-6108.
- [108] Toshihiro Ueda et al. “Long-term outcome of balloon angioplasty without stenting for symptomatic middle cerebral artery stenosis”. In: *Journal of Stroke Cerebrovascular Diseases* 27.7 (2018), pp. 1870–1877. ISSN: 1052-3057.
- [109] Jacques G Theron et al. “Carotid artery stenosis: treatment with protected balloon angioplasty and stent placement”. In: *Radiology* 201.3 (1996), pp. 627–636. ISSN: 0033-8419.
- [110] Michael J Pentecost et al. “Guidelines for peripheral percutaneous transluminal angioplasty of the abdominal aorta and lower extremity vessels. A statement for health professionals from a special writing group of the Councils on Cardiovascular Radiology, Arteriosclerosis, Cardio-Thoracic and Vascular Surgery, Clinical Cardiology, and Epidemiology and Prevention, the American Heart Association”. In: *Circulation* 89.1 (1994), pp. 511–531. ISSN: 0009-7322.
- [111] Martin Schillinger et al. “Balloon angioplasty versus implantation of nitinol stents in the superficial femoral artery”. In: *New England Journal of Medicine* 354.18 (2006), pp. 1879–1888.
- [112] K Wayne Johnston. “Iliac arteries: reanalysis of results of balloon angioplasty.” In: *Radiology* 186.1 (1993), pp. 207–212.

- 
- [113] Campbell Rogers et al. “Balloon-artery interactions during stent placement: a finite element analysis approach to pressure, compliance, and stent design as contributors to vascular injury”. In: *Circulation research* 84.4 (1999), pp. 378–383. ISSN: 0009-7330.
- [114] David Martin and Fergal Boyle. “Finite element analysis of balloon-expandable coronary stent deployment: Influence of angioplasty balloon configuration”. In: *International journal for numerical methods in biomedical engineering* 29.11 (2013), pp. 1161–1175. ISSN: 2040-7939.
- [115] Houman Zahedmanesh, Daniel John Kelly, and Caitriona Lally. “Simulation of a balloon expandable stent in a realistic coronary artery—Determination of the optimum modelling strategy”. In: *Journal of Biomechanics* 43.11 (2010), pp. 2126–2132. ISSN: 0021-9290.
- [116] David L Fischman et al. “A randomized comparison of coronary-stent placement and balloon angioplasty in the treatment of coronary artery disease”. In: *New England Journal of Medicine* 331.8 (1994), pp. 496–501. ISSN: 0028-4793.
- [117] Patrick W Serruys et al. “A comparison of balloon-expandable-stent implantation with balloon angioplasty in patients with coronary artery disease”. In: *New England Journal of Medicine* 331.8 (1994), pp. 489–495. ISSN: 0028-4793.
- [118] Peter M Steele et al. “Balloon angioplasty. Natural history of the pathophysiological response to injury in a pig model.” In: *Circulation Research* 57.1 (1985), pp. 105–112.
- [119] Elizabeth E Antoine, François P Cornat, and Abdul I Barakat. “The stentable in vitro artery: an instrumented platform for endovascular device development and optimization”. In: *Journal of The Royal Society Interface* 13.125 (2016), p. 20160834.
- [120] Alireza Karimi et al. “Measurement of the uniaxial mechanical properties of healthy and atherosclerotic human coronary arteries”. In: *Materials Science and Engineering: C* 33.5 (2013), pp. 2550–2554.
- [121] Brian D Stemper et al. “Mechanics of fresh, refrigerated, and frozen arterial tissue”. In: *Journal of Surgical Research* 139.2 (2007), pp. 236–242.
- [122] Donald E Cutlip et al. “Stent thrombosis in the modern era: a pooled analysis of multicenter coronary stent clinical trials”. In: *Circulation* 103.15 (2001), pp. 1967–1971.
- [123] G Jan Willem Bech et al. “Usefulness of fractional flow reserve to predict clinical outcome after balloon angioplasty”. In: *Circulation* 99.7 (1999), pp. 883–888.
- [124] P Syamasundar Rao et al. “Five-to nine-year follow-up results of balloon angioplasty of native aortic coarctation in infants and children”. In: *Journal of the American College of Cardiology* 27.2 (1996), pp. 462–470.

## REFERENCES

---

- [125] Scott E Fletcher et al. “Balloon angioplasty of native coarctation of the aorta: midterm follow-up and prognostic factors”. In: *Journal of the American College of Cardiology* 25.3 (1995), pp. 730–734.
- [126] Valérie M Laurent et al. “Gradient of rigidity in the lamellipodia of migrating cells revealed by atomic force microscopy”. In: *Biophysical journal* 89.1 (2005), pp. 667–675.
- [127] Elaine Nicpon Marieb and Katja Hoehn. *Human anatomy & physiology*. Pearson education, 2007. ISBN: 0321372948.
- [128] Lindsay M Biga et al. *Anatomy & physiology*. OpenStax & Oregon State University, 2020.
- [129] Amanda C. Doran, Nahum Meller, and Coleen A. McNamara. “Role of smooth muscle cells in the initiation and early progression of atherosclerosis”. In: *Arteriosclerosis, thrombosis, and vascular biology* 28.5 (2008), pp. 812–819. ISSN: 1524-4636 1079-5642. DOI: [10.1161/ATVBAHA.107.159327](https://doi.org/10.1161/ATVBAHA.107.159327).
- [130] AA Geisterfer, Michael J Peach, and Gary K Owens. “Angiotensin II induces hypertrophy, not hyperplasia, of cultured rat aortic smooth muscle cells”. In: *Circulation research* 62.4 (1988), pp. 749–756. ISSN: 0009-7330.
- [131] SJ Hirst. “Airway smooth muscle cell culture: application to studies of airway wall remodelling and phenotype plasticity in asthma”. In: *European Respiratory Journal* 9.4 (1996), pp. 808–820. ISSN: 0903-1936.
- [132] Oksana Shynlova et al. “Myometrial Apoptosis: Activation of the Caspase Cascade in the Pregnant Rat Myometrium at Midgestation1”. In: *Biology of Reproduction* 74.5 (2006), pp. 839–849. ISSN: 0006-3363. DOI: [10.1095/biolreprod.105.048124](https://doi.org/10.1095/biolreprod.105.048124). URL: <https://doi.org/10.1095/biolreprod.105.048124>.
- [133] Kenton M Sanders et al. “Regulation of gastrointestinal motility—insights from smooth muscle biology”. In: *Nature reviews Gastroenterology and hepatology* 9.11 (2012), p. 633. ISSN: 1759-5053.
- [134] Carter Owen and Alicia Y Armstrong. “Clinical management of leiomyoma”. In: *Obstetrics and Gynecology Clinics* 42.1 (2015), pp. 67–85. ISSN: 0889-8545.
- [135] B. G. Brown, R. Mahley, and G. Assmann. “Swine aortic smooth muscle in tissue culture. Some effects of purified swine lipoproteins on cell growth and morphology”. In: *Circ Res* 39.3 (1976), pp. 415–24. ISSN: 0009-7330 (Print) 0009-7330. DOI: [10.1161/01.res.39.3.415](https://doi.org/10.1161/01.res.39.3.415).
- [136] Russell Ross et al. “A platelet-dependent serum factor that stimulates the proliferation of arterial smooth muscle cells in vitro”. In: *Proceedings of the National Academy of Sciences* 71.4 (1974), pp. 1207–1210. ISSN: 0027-8424.

- 
- [137] John J Albers and Edwin L Bierman. “The effect of hypoxia on uptake and degradation of low density lipoproteins by cultured human arterial smooth muscle cells”. In: *Biochimica et Biophysica Acta (BBA)-Lipids and Lipid Metabolism* 424.3 (1976), pp. 422–429. ISSN: 0005-2760.
- [138] O. Benzakour et al. “Evidence for cultured human vascular smooth muscle cell heterogeneity: isolation of clonal cells and study of their growth characteristics”. In: *Thromb Haemost* 75.5 (1996), pp. 854–8. ISSN: 0340-6245 (Print) 0340-6245.
- [139] Hiroyuki Hao et al. “Heterogeneity of smooth muscle cell populations cultured from pig coronary artery”. In: *Arteriosclerosis, thrombosis, and vascular biology* 22.7 (2002), pp. 1093–1099. ISSN: 1079-5642.
- [140] Richard A Majack. “Beta-type transforming growth factor specifies organizational behavior in vascular smooth muscle cell cultures”. In: *The Journal of cell biology* 105.1 (1987), pp. 465–471. ISSN: 0021-9525.
- [141] C. M. Walthers et al. “Smooth muscle strips for intestinal tissue engineering”. In: *PLoS One* 9.12 (2014), e114850. ISSN: 1932-6203. DOI: [10.1371/journal.pone.0114850](https://doi.org/10.1371/journal.pone.0114850). URL: <https://www.ncbi.nlm.nih.gov/pmc/articles/PMC4259486/pdf/pone.0114850.pdf>.
- [142] N. Endlich et al. “Culture of vascular smooth muscle cells from small arteries of the rat kidney”. In: *Kidney Int* 57.6 (2000), pp. 2468–75. ISSN: 0085-2538 (Print) 0085-2538. DOI: [10.1046/j.1523-1755.2000.00105.x](https://doi.org/10.1046/j.1523-1755.2000.00105.x).
- [143] MG Frid et al. “Smooth muscle cells isolated from discrete compartments of the mature vascular media exhibit unique phenotypes and distinct growth capabilities”. In: *Circulation research* 81.6 (1997), pp. 940–952. ISSN: 0009-7330.
- [144] James F May et al. “The induction of atherosclerotic plaque-like mounds in cultures of aortic smooth muscle cells”. In: *Virchows Archiv B* 18.1 (1975), p. 205. ISSN: 0340-6075.
- [145] Y. Kobayashi et al. “Effects of a GnRH analogue on human smooth muscle cells cultured from normal myometrial and from uterine leiomyoma tissues”. In: *Molecular human reproduction* 3.2 (1997), pp. 91–9. ISSN: 1360-9947 (Print) 1360-9947. DOI: [10.1093/molehr/3.2.91](https://doi.org/10.1093/molehr/3.2.91).
- [146] D. Gonzalez-Rodriguez et al. “Soft matter models of developing tissues and tumors”. In: *Science* 338.6109 (2012), pp. 910–7. ISSN: 1095-9203 (Electronic) 0036-8075 (Linking). DOI: [10.1126/science.1226418](https://doi.org/10.1126/science.1226418).
- [147] C Redon, F Brochard-Wyart, and F Rondelez. “Dynamics of dewetting”. In: *Physical review letters* 66.6 (1991), p. 715.
- [148] Hervé Tabuteau et al. “Propagation of a brittle fracture in a viscoelastic fluid”. In: *Soft Matter* 7.19 (2011), pp. 9474–9483.
- [149] David Gonzalez-Rodriguez et al. “Detachment and fracture of cellular aggregates”. In: *Soft Matter* 9.7 (2013), pp. 2282–2290.

## REFERENCES

---

- [150] A. M. VanDijk et al. “Mechanics of resting isolated single vascular smooth muscle cells from bovine coronary artery”. In: *American Journal of Physiology-Cell Physiology* 246.3 Pt 1 (1984), pp. C277–87. ISSN: 0002-9513 (Print) 0002-9513. DOI: [10.1152/ajpcell.1984.246.3.C277](https://doi.org/10.1152/ajpcell.1984.246.3.C277). URL: <https://journals.physiology.org/doi/pdf/10.1152/ajpcell.1984.246.3.C277>.
- [151] Karine Guevorkian et al. “Aspiration of biological viscoelastic drops”. In: *Physical review letters* 104.21 (2010), p. 218101.
- [152] David R Hathaway et al. “Vascular smooth muscle. A review of the molecular basis of contractility.” In: *Circulation* 83.2 (1991), pp. 382–390.
- [153] Jeffrey A Beamish et al. “Molecular regulation of contractile smooth muscle cell phenotype: implications for vascular tissue engineering”. In: *Tissue Engineering Part B: Reviews* 16.5 (2010), pp. 467–491.
- [154] Albert K Harris, Patricia Wild, and David Stopak. “Silicone rubber substrata: a new wrinkle in the study of cell locomotion”. In: *Science* 208.4440 (1980), pp. 177–179.
- [155] Kevin Burton and D Lansing Taylor. “Traction forces of cytokinesis measured with optically modified elastic substrata”. In: *Nature* 385.6615 (1997), pp. 450–454.
- [156] Micah Dembo and Yu-Li Wang. “Stresses at the cell-to-substrate interface during locomotion of fibroblasts”. In: *Biophysical journal* 76.4 (1999), pp. 2307–2316.
- [157] Benedikt Sabass et al. “High resolution traction force microscopy based on experimental and computational advances”. In: *Biophysical journal* 94.1 (2008), pp. 207–220.
- [158] Stacey A Maskarinec et al. “Quantifying cellular traction forces in three dimensions”. In: *Proceedings of the National Academy of Sciences* 106.52 (2009), pp. 22108–22113.
- [159] Qingzong Tseng et al. “A new micropatterning method of soft substrates reveals that different tumorigenic signals can promote or reduce cell contraction levels”. In: *Lab on a chip* 11.13 (2011), pp. 2231–2240.
- [160] Venkat Maruthamuthu et al. “Cell-ECM traction force modulates endogenous tension at cell–cell contacts”. In: *Proceedings of the National Academy of Sciences* 108.12 (2011), pp. 4708–4713.
- [161] Kenneth E White, Daniel L Koller, and Tim Corbin. “Skeletal Genetics: From Gene Identification to Murine Models of Disease”. In: *Basic and Applied Bone Biology*. Elsevier, 2014, pp. 149–171.
- [162] Paul A Fleming et al. “Fusion of uniluminal vascular spheroids: a model for assembly of blood vessels”. In: *Developmental Dynamics* 239.2 (2010), pp. 398–406.

- [163] Ashish Misra et al. “Integrin beta3 regulates clonality and fate of smooth muscle-derived atherosclerotic plaque cells”. In: *Nature communications* 9.1 (2018), pp. 1–13.
- [164] James F May et al. “The induction of atherosclerotic plaque-like mounds in cultures of aortic smooth muscle cells”. In: *Virchows Archiv B* 18.1 (1975), p. 205.
- [165] David H Anderson. *Compartmental modeling and tracer kinetics*. Vol. 50. Springer Science & Business Media, 2013.

# Chapter 6

## Appendix

### 6.1 Experimental protocols

#### Balloon protocol

Pre-experiment for one artery: cells: Two T25 flask of BVEC Materials: 12 mg/ml collagen (bubbles removed), 2 x T-25 BAEC, BAEC medium with 25mM HEPES, Harvard pump, autoclaved packs: 3.0 mm pin/sleeves/spatula pack, continuous flow pack, peristaltic pack with sensor and 3-way cap, non-autoclaved continuous flow linkage

Day 1

1. 8:45 AM Sterilization
  - (a) Ethanol and UV 20 min
    - i. 1 frame
    - ii. 1 × 60mm FEP
    - iii. 3 ways valve
    - iv. continuous flow linkage pack
  - (b) Add to PSM: autoclave packs, 2 x 50 ml syringes, 1 ml syringe, 16G needle, large Petri, 50 ml conical tube
  - (c) Start water bath with EC media
2. 9:10 AM Plasma treatment of FEP tube(45s)
3. 9:20 AM Prepare FEP (Tips: merge pins in PBS first)

- (a) 9:20 10 min immerse in 1% PEI
  - i. meanwhile prepare collagen kit - step 4
  - ii. remove FEP with tweezers, aspirate liquid
- (b) 9:30 20 min immerse in 0.1% GTA
  - i. meanwhile Label BVEC –step 5
  - ii. remove FEP with tweezers, aspirate liquid, dry on Kimwipe, place in frames
4. Hydrogel: 1 x 2 ml @ 6/8.4/37 in 50 ml tube (Tips: put the collagen kit on ice)
  - (a) 200  $\mu$ L 10  $\times$  DMEM
  - (b) 43.5  $\mu$ L 1N NaOH
  - (c) 756  $\mu$ L 1 $\times$  DMEM
  - (d) 1 ml collagen in 1 ml syringe with 16g needle
5. Label cells (EC P8)
  - (a) EC label: 10 ul Vybrant DiO in 2 ml EC media (for 2 flasks)
  - (b) rinse flasks with PBS
  - (c) vortex stains, add to each flask, incubate 20 min
  - (d) rinse flasks with PBS
  - (e) incubate in appropriate media until needed
  - (f) Meanwhile place 150 ml DMEM+ / + media in 250 ml bottle in incubator to equilibrate CO<sub>2</sub>
6. 10:00 AM Prepare channel
  - (a) Immerse pin in PBS
  - (b) Suspend SMC pellet in neutralization solution
  - (c) Add collagen, mix with spatula
  - (d) Add to FEP using 1 ml pipette (2x per channel), avoid bubbles, holding opposite end closed
  - (e) Insert first sleeve and add more collagen to open end of FEP to completely fill sleeve
  - (f) Insert pin into sleeve enough to ensure no air is introduced
  - (g) Add second sleeve and insert pin through
  - (h) Incubate 20 min
7. 10:10 AM Prepare three 800,000 EC pellets from first flask, centrifuge

## 6.1. EXPERIMENTAL PROTOCOLS

---

- (a) Remove pin from channel
  - (b) Suspend first pellet in 450 ul media
    - i. Inject into channel, place upside-down in incubator
    - ii. Incubate 20 min , meanwhile prepare the flow. –step8
  - (c) Suspend second pellet in 450 ul media
    - i. Inject into channel, place on side in incubator
    - ii. Incubate 10 min per side (total 20 min)
    - iii. Meanwhile prepare 800,000 EC pellet from second flask
  - (d) Suspend third pellet in 450 ul media
    - i. Inject into channel, place right-side-up in incubator, incubate 10 mins
    - ii. Turn left-side-up, incubate 10 mins
8. 10:30 AM MEANWHILE Prepare flow
- (a) Fill each 50 ml syringe with  $\sim 45$  ml media (need  $>80$  ml total): Pour media into 50 ml conical tube. Remove plunger, block outlet with gloved finger, pour media into syringe, insert plunger just enough to prevent leaks, invert syringe, release outlet, block spray with Kimwipe, insert plunger further for proper function
  - (b) Connect short peristaltic tubing to A-A ports of continuous flow linkage
  - (c) Connect box inlet and outlet to continuous flow linkage and link temporarily with male-male luer fitting
  - (d) Connect syringes to peristaltic tubing and then to continuous flow linkage
  - (e) Prime all sections of linkage by transferring media between syringes until all air is trapped in the syringes only
  - (f) Close valves closest to each syringe, remove syringes, remove air, reconnect, and reopen valves
  - (g) Place linkage in incubator and use tape to attach tubing to incubator walls as needed to prevent overlap/kinks
  - (h) Attach first syringe to left side of syringe pump, leaving adjustment knob loose
  - (i) Attach second syringe to right side of pump, adjusting central block as needed and locking adjustment knob when all syringe components are fixed
  - (j) Move central knob to 30/30 ml split between syringes
  - (k) Set method "EEATEST"
9. Start flow

- (a) Remove male-male lure connector from linkage and connect inlet and outlet tubing to channel

START FLOW at 12 PM on DAY 0

Day4: 12 PM

1. Place PBS for water bath in bain-marie
2. Prepare bain-marie and peristaltic pump
  - (a) Clean bain-marie and start at 38°C
  - (b) Set pump for at 42 ml/min, L/S 16
3. TURN ON room AC to 22C
4. Start up microscope and set up software
  - (a) Calibrate objective
  - (b) Camera ROI: 1800×1800
  - (c) Image background correction
  - (d) Pause/lamp switching for timelapse
  - (e) ph1 for brightfield imaging

Day4 12:45 PM

1. In PSM:
  - (a) assemble flow loop including media bottle, pressure sensor, three-way valve, and pinch valves
    - i. Working on Kimwipe, seal/grease coverslip to frame on side with sleeve overhang
    - ii. Seal/grease cover, using a 25G needle to release air and excess water.
    - iii. Triple check this seal
    - iv. Insert microchannel in flow loop
2. Transfer system to microscope
3. Seal imaging box to microscope stage plate, weight down
4. Collect zero-flow pressure trace

## 6.1. EXPERIMENTAL PROTOCOLS

---

5. Start flow and check seals 42 ml/min
6. Weight media bottle in water bath, add plastic wrap to minimize evaporation
7. Connect to CO<sub>2</sub> tank and open to start flow
8. Collect pressure trace and save to new text file - adjust valves for positive pressure only
9. Take test images to test parameters, start 1 h tangent+centerline series
10. Check imaging and focus regularly

### **SMC cluster culture**

Prepare PDMS wells:

1. Digging holes (diameter = 7mm) on 15×40×10mm PDMS block
2. Plasma treatment of digged PDMS block and 24×50mm coverslip for 45s.
3. Assemble the PDMS block and coverslip
4. Ethanol sterilization for 2 hours.
5. The PDMS well should be used within 48 hours.

Cell seeding:

1. Fibronectin coating for 30mins
2. Seed SMC at 320,000 cell/cm<sup>2</sup>
3. Change the medium twice a day for three days

### Western blot

#### Protocol for 10 wells *Cell lysis to extract protein*

Protein can be extracted from different kind of samples, such as tissue or cells. Below is the protocol to extract proteins from adherent cells. Adherent cells:

0. Prepare the centrifuge at 4°C; Prepare 2mL RIPA buffer with 40μL(1:500) inhibitor protease
1. Wash cells in the tissue culture flask or dish with phosphate buffered saline (PBS) and rocking gently. Discard PBS. (Tip: Keep tissue culture dish on ice throughout).
2. Add 100μLL RIPA buffer in each well and used a cell scraper to dislodge the cells. Pipette the mixture into microcentrifuge tubes.
3. Waiting 10 mins, meanwhile, prepare the 15mL solution for spectrophotometer (3mL dye in 12mL H2O)
4. Centrifuge at 13000 RPM for 10 minutes and discard the supernatant.
5. Pipette 3μL of samples in each tube of solution for spectrophotometer.
6. Measure the concentration of protein using a spectrophotometer.

#### *Sample preparation*

0. Prepare protein loading solution (4× solution 510vμLv(34); 10× 225 μL (15))
1. Using, concentration mass volume = mass/volume, determine the volume of protein extract to ensure the same amount in each well.
2. Make sure every sample has 50 μL in volume, samples have less volume compensate with RIPA buffer
3. Add 50μL loading solution in each 50μL sample, so the volume come to 100μL
4. Heat the samples with dry plate for 10 minutes at 70°C.
5. Centrifuge 10s

#### *Electrophoresis*

1. Pour the running buffer into the electrophorator (! Be careful of the running buffer, it should correspond to the gel you use)

2. Tear off the sticker on the bottom and place gel inside the electrophorator and connect to a power supply.
3. Make sure buffer covers the gel completely and remove the comb carefully.
4. Load marker (2-5 $\mu$ L, depend on size of the well of gel), Load samples (15-30 $\mu$ L, depend on the size)
5. Run the gel with voltage 100-140 V
6. This will take 60mins, or until the dye front runs off to the bottom of the gel

### ***Electrotransfer***

0. Prepare sponge (6 pieces for one gel) and filter paper (6 pieces for one gel) and one polyvinylidene fluoride (PDVF) to fit the size of the gel; Prepare 200mL transfer buffer: 160mL H<sub>2</sub>O, 10mL Transfer buffer (20x), and 30mL Methanol
1. Wet the sponge, filter paper and PDVF membrane in transfer buffer.
2. Separate glass plates and retrieve the gel.
3. Overlay sponge, filter paper, membrane and gel in orders as follows:  
3 Sponges 3 Filter papers PVDF membrane Gel 3 Filter papers 3 Sponges (Ensuring there is no bubble between each layer)
4. Rendering the sandwich to the transfer apparatus, which should put ice on the forward and backward of the sandwich. (Be careful, don't drop ice in the sandwich). Make sure transfer buffer cover the sandwich.
5. Place electrodes on top of the sandwich, ensuring that the PVDF membrane is between the gel and a positive electrode.
6. Run the gel with voltage  $\sim$  40–55 V
7. Transfer for  $\sim$  60 mins

### ***Blocking and antibody incubation***

1. Color rendering with ponceau S staining, then wash with water for 3 times (Tips: avoid pouring water right on the membrane)
2. Cut the membrane according to the protein stripes
3. Block the membrane with 5% milk in TBST (2.5g milk powder in 50mL TBST) for 60 mins on a shaker

## 6.1. EXPERIMENTAL PROTOCOLS

---

4. Wash with TBST 3 times
5. Incubate the membrane in primary antibody in 4°C on a shaker
6. Wash the primary carefully with TBST 3 times for 5 mins
7. Incubate the membrane in secondary antibody in room temperature for 1h.
8. Wash the secondary antibody with TBST 3 times for 5 mins
9. Prepare ECL mixture (following the proportion of solution A and B as 1:1), the total volume should be able to cover the area of membrane
10. Visualize the results with the machine, regulate the exposure time to ensure the best quality of images.

**TFM gel preparation***Coverslip activation*

1. Coverslips ( $\phi$  25 mm) are cleaned and sterilized with ethanol washes Plasma treatment for 10 minuts: coverslip held in Teflon holder
2. In chemical fume hood, dilute full strength 3-aminopropyltrimethoxysilane in isopropanol for a final concentration of 2% (1ml silane /49 ml isopropanol) in a glass container
3. Fully immerse coverslips from plasma treatment into this solution for 10 min while gently stirring on a stir plate in the fume hood
4. Wash coverslips by immersing in ddH<sub>2</sub>O (4 exchanges of water). Allow 10 min soaking time for the final exchange, with stirring. Amino-silane containing solutions should be disposed as hazardous waste.
5. In the fume hood, immerse coverslips in 2% glutaraldehyde solution in ddH<sub>2</sub>O (1ml glutaraldehyde /49 ml water)in a glass square dish on stir plate for 30 minutes
6. Wash by 3 exchanges of ddH<sub>2</sub>O for 10 minutes per exchange, with stirring. Dispose of glutaraldehyde as hazardous waste.
7. Dry coverslips with air pressure and keep till use up to 2 months

*Preparation of polyacrylamide(PPA) gel*

1. Glass slide (24x50mm) are cleaned and sterilized with ethanol washes
2. Coating fibronectin (25  $\mu$ m/mL) with parafilm on top of the glass slide for 1 hour
3. Once the coverslips and glass slides are all ready, prepare the PPA gel: 1mL stock solution for desired stiffness (here 10 kPa), 0.8 $\mu$ L beads (ultrasonic breakage before used), 10 uL TEMED and 1 $\mu$ L APS. In total, the volume is 190 $\mu$ L. Make sure for each overslip, 30uL PPA gel is needed.
4. Apply 30  $\mu$ L of the acrylamide solution to hydrophobic microscope slide (prepared in previous step2) and place activated 22x40mm coverslip on top of the droplet. Gel solution should coat entire coverslip. Smooth out any bubbles that may appear within the solution. Allow the gel solution to polymerize at room temperature for  $\sim$  10 min.
5. Once the gel solution is ready, quickly drop 30  $\mu$ LL on the glass slide and cover the coverslip on top of the gel droplet.

## 6.1. EXPERIMENTAL PROTOCOLS

---

6. Separate the coverslip from the glass slide. Using the fine tip of a pair of tweezers or a razor blade edge, carefully remove coverslip, with gel attached, from microscope slide surface and immerse gel in ddH<sub>2</sub>O, to maintain hydration.
7. Wash several times with PBS before stockage for use. Before cell seeding, the TFM gel coverslip should be merged in the cell culture medium for at least 30 mins.

### **Abdominal artery injury in rat**

1. Operation on Rat
  - (a) Anesthesia
  - (b) Exposure of abdominal artery
  - (c) Vascular ligation for different duration
  - (d) Suturing the muscle layer and skin
2. One month post-operative recovery
3. Dissection for blood vessels
  - (a) Anesthesia
  - (b) Exposure of abdominal artery
  - (c) Cut off the artery (the original ligated part) and collect the sample

### SEM sample preparation

1. Primary fixation with aldehydes (proteins)

Glutaraldehyde and formaldehyde are crosslinked by proteins to stabilize the ultrastructure prior to further processing.

2. Secondary fixation with osmium tetroxide (lipids)

Use a fixative, glutaraldehyde maintain the structural details of the sample. Note that if a fixative uses a phosphate based buffer for its preparation, salt deposits may interfere with the sample's image quality.

3. Dehydration series with solvent (ethanol or acetone)

For dehydration, use a graded series of alcohol ( 30%, 40%, 50%, 60%, 70%, 80%, 90%) and finish off the final dehydration step with 100% alcohol or acetone.

4. Drying

Hexamethyldisilazane (HMDS) or liquid CO<sub>2</sub> can be used in cell preparations and after 3 minute incubation it is removed and excess is left to evaporate.

5. Mounting on a stub

Using a sticky carbon disc, the specimen is placed on a metal stub, which increases conductivity. For even more conductivity, silver-containing glue may likewise be added.

6. Sputter coating with conductive material

The surface of sample should be coated with conductive material to prevent charge. The metal is applied in a controlled manner in a sputter coater to control the thickness is at around 10nm.

## 6.2 Matlab Codes

### Balloon intensity analysis code

```

1 %% Read image
2 clear all; close all
3
4 imcrop_saved=1;
5 path = ...
    'G:\Balloon\Step2_exported_files\PDMS\PDMS_translation_20201026_2';
6 filter = '*.tif';
7 button_type_movement = menu('Type of balloon movement?', 'Scratch', ...
    'Expansion', 'Translation', 'Rotation', 'Default');
8 thresholdValue = 125;
9 if button_type_movement == 1
10     Name3 = 'Scratch';
11 elseif button_type_movement == 2
12     Name3 = 'Expansion';
13 elseif button_type_movement == 3
14     Name3 = 'Translation';
15 elseif button_type_movement == 4
16     Name3 = 'Rotation';
17 else
18     Name3 = 'Default';
19 end
20 Name_results_folder = ['results_',Name3];
21
22 workspace; % Make sure the workspace panel is showing.
23 format long g;
24 format compact;
25 fontSize = 25;
26 linewidth = 3;
27 %% If you have saved the cropped image, run code directly from here
28 if imcrop_saved==1
29     I_ad_crop_before=imread('G:\Balloon\Step2_exported_files\PDMS\PDMS_translation_20201026_2\resul
30     I_ad_crop_after= ...
        imread('G:\Balloon\Step2_exported_files\PDMS\PDMS_translation_20201026_2\resul
31     path_results = [path,'\ ',Name_results_folder];
32 end
33 %% If you need to crop image first
34 if imcrop_saved==0
35
36 message_before = sprintf('Choose a photo "before"');
37 uiwait(msgbox(message_before));
38 Selectedfile_before = uigetfile(fullfile(path , filter));
39 message_after = sprintf('Choose a photo "after"');
40 uiwait(msgbox(message_after));
41 Selectedfile_after = uigetfile(fullfile(path , filter));
42 I_before=imread(fullfile(path,Selectedfile_before));

```

## 6.2. MATLAB CODES

---

```
43 I_after=imread(fullfile(path, Selectedfile_after));
44 % imshow(I);
45 I_adjust_after = imadjust(I_after);
46 I_adjust_before = imadjust(I_before);
47
48 figure %% cropped photos
49 subplot(2,1,1);imshow(I_adjust_before)
50 title('Original Artery')
51 subplot(2,1,2);imshow(I_adjust_after)
52 title('Wounded Artery')
53 %% Crop wounded artery
54 figure
55 imshow(I_adjust_after)
56 message1 = sprintf('Artery Lumen ROI After');
57 uiwait(msgbox(message1));
58 Artery_Lumen_ROI_before=getrect;
59
60 I_ad_crop_after = imcrop(I_adjust_after,Artery_Lumen_ROI_before);
61 imshow(I_ad_crop_after);
62
63
64 %% Crop original artery
65
66 button_crop=questdlg('Do you want to crop again the original ...
        artery?', 'Crop_before Request', 'Yes', 'No', 'default');
67
68 if ~isempty(strfind(button_crop, 'Yes'))
69     imshow(I_adjust_before)
70     message2 = sprintf('Click the upper left corner of the cropping ...
        box');
71     uiwait(msgbox(message2));
72     [x, y] = ginput(1); % Ask user to click the upper left corner.
73     I_ad_crop_before = imcrop(I_adjust_before, [x, y, ...
        Artery_Lumen_ROI_before(1,3), Artery_Lumen_ROI_before(1,4)]);
74 end
75 if ~isempty(strfind(button_crop, 'No'))
76     imshow(I_adjust_before)
77     I_ad_crop_before = imcrop(I_adjust_before, ...
        Artery_Lumen_ROI_before);
78 end
79
80 %% Save the cropped images
81 underlineLocations = find(Selectedfile_after == '_');
82 length_underline = length(underlineLocations);
83 Name1 = Selectedfile_after(1:underlineLocations(1)-1);
84 Name2 = ...
        Selectedfile_after(underlineLocations(1)+1:underlineLocations(2)-1);
85 % Name3 = input('Type of balloon movement','s');
86 % Choose the balloon movement by user
87
88 % Create a folder
89 if ~exist(Name_results_folder, 'dir')
```

```

90     mkdir(path,Name_results_folder);
91 end
92
93 % Save the wounded_crop_image
94 path_results = [path,'\ ',Name_results_folder];
95 Name_crop_wounded_image = [ ...
    Name3, '_',Name2, '_',Name1, 'crop_wounded_image.tif'];
96 imwrite(I_ad_crop_after, ...
    strcat(path_results,'\ ',Name_crop_wounded_image));
97 %Same the original_crop_image
98 Name_crop_original_image = [ ...
    Name3, '_',Name2, '_',Name1, 'crop_original_image.tif'];
99 imwrite(I_ad_crop_before, ...
    strcat(path_results,'\ ',Name_crop_original_image));
100
101 end
102
103
104 %% Calculate the intensity of the figure
105
106 [height_0,width_0] = size(I_ad_crop_after);
107 intensity_image_after=zeros(1,height_0);
108 intensity_image_before=zeros(1,height_0);
109 y_axe =zeros(1,height_0);
110 %Reverse of the height postion, in order to show the intensity and ...
    the image side-by-side
111 for i= 1:height_0
112     intensity_image_after(1,height_0+1-i)=sum(I_ad_crop_after(i,:)); ..
        %intensity of line
113     intensity_image_before(1,height_0+1-i)=sum(I_ad_crop_before(i,:));
114     y_axe(1,height_0+1-i)=height_0+1-i;
115 end
116
117 % figure
118 % plot(intensity_image_after,y_axe,'r',intensity_image_before, ...
    y_axe,'g'),title('')
119
120
121 figure;
122 subplot(2,3,1);imshow(I_ad_crop_before),title('Original Artery');
123 subplot(2,3,2);plot(intensity_image_before, ...
    y_axe,'g'),title('Original Artery Fluorescent Signal');
124 % xlim([0,8e8]) ...
    ...
    %the LIMITATION commandes need to be modified
125 xlabel('Intensity of each line')
126 ylabel('Y position')
127 subplot(2,3,3);histogram(I_ad_crop_before),title('Histogram of ...
    Original Artery');
128 % ylim([0,2e6])
129 xlabel('Tonal value')
130 ylabel('Number of pixels')

```

## 6.2. MATLAB CODES

---

```
131
132 subplot(2,3,4);imshow(I_ad_crop_after),title('Wounded Artery');
133 subplot(2,3,5);plot(intensity_image_after, ...
    y_axe, 'r'),title('Wounded Artery Fluorescent Signal');
134 % xlim([0,8e8])
135 xlabel('Intensity of each line')
136 ylabel('Y position')
137 subplot(2,3,6);histogram(I_ad_crop_after),title('Histogram of ...
    Wounded Artery');
138 % ylim([0,2e6])
139 xlabel('Tonal value')
140 ylabel('Number of pixels')
141
142 %% linkaxes didn't work : Error using ...
    matlab.graphics.axis.Axes/horzcat Conversion to ...
    matlab.graphics.axis.Axes from char is not possible.
143 % linkaxes([fig_intensity_before,fig_intensity_after,'xy'])
144 % linkaxes([fig_his_before,fig_his_after,'xy'])
145
146
147 %% Cut off the black boundary and alignment
148 threshold_bb = 5e7;
149 [I_artery_before,intensity_artery_before, y_artery_before]= ...
    cut_artery_align(I_ad_crop_before, intensity_image_before, ...
    y_axe, threshold_bb);
150
151 [I_artery_after,intensity_artery_after, y_artery_after]= ...
    cut_artery_align(I_ad_crop_after, intensity_image_after, y_axe, ...
    threshold_bb);
152
153 [h_before,-]=size(I_artery_before);
154 [h_after,-]=size(I_artery_after);
155
156 % Cut the bottom
157 if h_before-h_after>0
158     d=h_before-h_after;
159     I_artery_before((end+1-d):end,:)=[];
160 end
161 if h_before-h_after<0
162     d=h_after-h_before;
163     I_artery_after((end+1-d):end,:)=[];
164 end
165
166 % Cut the top
167 % if h_before-h_after>0
168 %     d=h_before-h_after;
169 %     I_artery_before(1:d,:)=[];
170 % end
171 % if h_before-h_after<0
172 %     d=h_after-h_before;
173 %     I_artery_after(1:d,:)=[];
174 % end
```

```

175
176 %% Recalculate the intensity
177 [height,width] = size(I_artery_before);
178 intensity_f_after=zeros(1,height);
179 intensity_f_before=zeros(1,height);
180 y_f =zeros(1,height);
181 %Reverse of the height postion, in order to show the intensity and ...
    the image side-by-side
182 for i= 1:height
183     intensity_f_after(1,height+1-i)=sum(I_artery_after(i,:)); ...
        %intensity of line
184     intensity_f_before(1,height+1-i)=sum(I_artery_before(i,:));
185     y_f(1,height+1-i)=height+1-i;
186 end
187 histogram_before=histogram(I_artery_before);
188 histogram_after=histogram(I_artery_after);
189
190 figure
191 plot(intensity_f_before, y_f,'g',intensity_f_after,y_f,'r')
192 %% Figures!!!!!!!!!!!!!!
193 % figure(1)
194 % subplot(2,1,1);imshow(I_artery_before);
195 % caption1_1 = sprintf('Original Artery');
196 % title(caption1_1, 'FontSize', fontSize, 'Interpreter', 'None');
197 % % Enlarge figure to full screen.
198 % set(gcf, 'Units', 'Normalized', 'OuterPosition', [0 0 1 1]);
199 % % Give a name to the figure
200 % % caption_totall = sprintf('Cropped images');
201 % % set(gcf, 'Name', caption_totall, 'NumberTitle', 'Off')
202 %
203 % subplot(2,1,2);imshow(I_artery_after);
204 % caption1_2 = sprintf('Wounded Artery');
205 % title(caption1_2, 'FontSize', fontSize, 'Interpreter', 'None');
206 % % Enlarge figure to full screen.
207 % set(gcf, 'Units', 'Normalized', 'OuterPosition', [0 0 1 1]);
208 %
209 % figure(2) %%intensity comparison
210 % plot(intensity_f_before, y_f,'g',intensity_f_after,y_f,'r');
211 % % set(gca, 'XTick', 1:num)
212 % set(findall(gca, 'Type', 'Line'),'LineWidth',linewidth);
213 % % Enlarge figure to full screen.
214 % set(gcf, 'Units', 'Normalized', 'OuterPosition', [0 0 1 1]);
215 % % Add title and axis labels
216 % caption2 = sprintf('Intensity of fluorescent endothelial cells');
217 % title(caption2, 'FontSize', fontSize, 'Interpreter', 'None');
218 % xlabel('Average Intensity over Length')
219 % ylabel('Y position')
220 % legend('Intensity of original artery','Intensity of artery ...
    wounded by balloon')
221 %
222 % figure(3) %%4 subplots
223 % subplot(2,3,1);imshow(I_artery_before);

```

## 6.2. MATLAB CODES

---

```
224 % title(caption1_1, 'FontSize', fontSize, 'Interpreter', 'None');
225 % subplot(2,3,2);plot(intensity_f_before, y_f,'g');
226 % % set(gca, 'XTick', 1:num)
227 % set(findall(gca, 'Type', 'Line'),'LineWidth',linewidth);
228 % % Enlarge figure to full screen.
229 % set(gcf, 'Units', 'Normalized', 'OuterPosition', [0 0 1 1]);
230 % % Add title and axis labels
231 % caption3_2 = sprintf('Intensity of fluorescent endothelial cells');
232 % title(caption3_2, 'FontSize', fontSize, 'Interpreter', 'None');
233 % xlabel('Average Intensity over Length')
234 % ylabel('Y position')
235 % % xlim([0,8e8]) ...
                                     ...
                                     %the LIMITATION commandes need to be modified
236 %
237 % subplot(2,3,3);histogram(I_artery_before);
238 % % Enlarge figure to full screen.
239 % set(gcf, 'Units', 'Normalized', 'OuterPosition', [0 0 1 1]);
240 % % Add title and axis labels
241 % caption3_3 = sprintf('Histogram of Original Artery');
242 % title(caption3_3, 'FontSize', fontSize, 'Interpreter', 'None');
243 % % ylim([0,2e6])
244 % xlabel('Tonal value')
245 % ylabel('Number of pixels')
246 %
247 % subplot(2,3,4);imshow(I_artery_after);
248 % title(caption1_2, 'FontSize', fontSize, 'Interpreter', 'None');
249 % subplot(2,3,5);plot(intensity_f_after, y_f,'r'),title('Wounded ...
    Artery Fluorescent Signal');
250 % % set(gca, 'XTick', 1:num)
251 % set(findall(gca, 'Type', 'Line'),'LineWidth',linewidth);
252 % % Enlarge figure to full screen.
253 % set(gcf, 'Units', 'Normalized', 'OuterPosition', [0 0 1 1]);
254 % % Add title and axis labels
255 % caption3_4 = sprintf('Intensity of fluorescent endothelial cells');
256 % title(caption3_4, 'FontSize', fontSize, 'Interpreter', 'None');
257 % xlabel('Average Intensity over Length')
258 % ylabel('Y position')
259 % % xlim([0,8e8])
260 %
261 % subplot(2,3,6);histogram(I_artery_after);
262 % % ylim([0,2e6])
263 % % Enlarge figure to full screen.
264 % set(gcf, 'Units', 'Normalized', 'OuterPosition', [0 0 1 1]);
265 % % Add title and axis labels
266 % caption3_6 = sprintf('Histogram of Wounded Artery');
267 % title(caption3_6, 'FontSize', fontSize, 'Interpreter', 'None');
268 % % ylim([0,2e6])
269 % xlabel('Tonal value')
270 % ylabel('Number of pixels')
271
272
```

```

273 %% Normalization of wounded artery
274 button_nor=questdlg('Do you want to normalize the wounded ...
    artery?', 'Normalization Request', 'Yes', 'No', 'default');
275
276 if ~isempty(strfind(button_nor, 'Yes'))
277
278     %Calculate the coeff_normalization
279
280     %Squeeze the inflated wounded artery by squeeze the y_f
281     coeff_normalizaion = 19/20;
282     y_f_nor_inter = coeff_normalizaion*y_f;
283
284     %Find the interpolated points to prepare later calcualtions
285     length_normalized = round(y_f_nor_inter(end));
286     y_f_nor = 1:1:length_normalized;
287
288     intensity_f_after_nor = ...
        interp1(y_f_nor_inter, intensity_f_after, y_f_nor, 'spline');
289
290     % Redress two images to same size
291     [w, h_before]=size(intensity_f_before);
292     [w, h_after]=size(intensity_f_after_nor);
293
294     % Cut the bottom
295     %     if h_before-h_after>0
296     %         d=h_before-h_after;
297     %         I_artery_before(1:d,:)=[];
298     %     end
299     %     if h_before-h_after<0
300     %         d=h_after-h_before;
301     %         I_artery_after(1:d,:)=[];
302     %     end
303     % Cut the top
304     if h_before-h_after>0
305         d=h_before-h_after;
306         I_artery_before(1:d,:)=[];
307     end
308     if h_before-h_after<0
309         d=h_after-h_before;
310         I_artery_after(1:d,:)=[];
311     end
312
313     figure %check if the interpolation method is correct
314     subplot(2,1,1);plot(intensity_f_before, y_f, 'g', ...
        intensity_f_after, y_f_nor_inter, 'r');
315     title('Intensity of fluorescent endothelial cells - Squeezed')
316     xlabel('Average Intensity over Length')
317     ylabel('Y position')
318     legend('Intensity of original artery', 'Intensity of artery ...
        wounded by balloon')
319     subplot(2,1,2);plot(intensity_f_before, ...
        y_f, 'g', intensity_f_after_nor, y_f_nor, 'r');

```

## 6.2. MATLAB CODES

---

```
320     title('Intensity of fluorescent endothelial cells - Normalized')
321     xlabel('Average Intensity over Length')
322     ylabel('Y position')
323     legend('Intensity of original artery','Intensity of artery ...
           wounded by balloon')
324
325     % Cut the original artery to a same size
326     intensity_f_before_cut = intensity_f_before(1:length_normalized);
327     figure
328     plot(intensity_f_before_cut, ...
           y_f_nor, 'g', intensity_f_after_nor, y_f_nor, 'r');
329     title('Intensity of fluorescent endothelial cells - Normalized ...
           & Cut')
330     xlabel('Average Intensity over Length')
331     ylabel('Y position')
332     legend('Intensity of original artery','Intensity of artery ...
           wounded by balloon')
333
334 end
335
336 %%
337 %% Redress the images to the same size
338 %%this part need to be skipped after normalization
339 if ~isempty(strfind(button_nor, 'No'))
340     [h_before, ~]=size(intensity_f_before);
341     [h_after, ~]=size(I_artery_after);
342
343     % Cut the bottom
344     if h_before-h_after>0
345         d=h_before-h_after;
346         I_artery_before((end+1-d):end, :)=[];
347     end
348     if h_before-h_after<0
349         d=h_after-h_before;
350         I_artery_after((end+1-d):end, :)=[];
351     end
352 end
353
354 % Cut the top
355 % if h_before-h_after>0
356 %     d=h_before-h_after;
357 %     I_artery_before(1:d, :)=[];
358 % end
359 % if h_before-h_after<0
360 %     d=h_after-h_before;
361 %     I_artery_after(1:d, :)=[];
362 % end
363 %
364 % end
365 %% Calculate the damaged ratio
366 % Project the area to the topology
367 if ~isempty(strfind(button_nor, 'No'))
```

```

368     r=1.5;
369     height = 1;
370     % unit_length = 2*r/height; %length of a pixel in mm
371     cur_length=zeros(height,1);
372     theta=zeros(height,1);
373     length_pixel=zeros(height,1);
374     % Give the unite value of length for the half of the topology
375     for i=1:round(height/2)
376         theta(i,1)= acos((height/2-i)/(height/2));
377         cur_length(i,1)=theta(i,1)*r;           % Length_curve = angle*R
378     end
379     % calculate the real height of each pixel for the quarter of a ...
        circle
380     length_pixel(1,1)= cur_length(1,1);
381     for i=2:round(height/2)
382         length_pixel(i,1)=cur_length(i,1)-cur_length(i-1,1);
383     end
384
385
386     % mirror value for the rest of half topology
387     t=1;
388     % if height is odd number
389     if rem(height,2)
390         for i=height:(-1):(round(height/2)+1)
391             length_pixel(i,1)=length_pixel(t,1);
392             t=t+1;
393         end
394     else
395         t=1;
396         % if height is even number
397         for i=height:(-1):(height/2+1)
398             length_pixel(i,1)=length_pixel(t,1);
399             t=t+1;
400         end
401     end
402 end
403 %% Sum up of the total area of white pixel in mm2
404 if ~isempty(strfind(button_nor,'No'))
405     % Area of each line (mm)
406     area_line=r/height*width*length_pixel;
407
408     area=zeros(height,1);
409     intensity_damage=intensity_f_before-intensity_f_after;
410     ratio_damage=intensity_damage./intensity_f_before;
411     ratio_glo = mean2(ratio_damage);
412
413 else if ~isempty(strfind(button_nor,'Yes'))
414     %%Damage ratio after normalized
415     intensity_damage_nor= ...
        intensity_f_before_cut-intensity_f_after_nor;
416     ratio_damage_nor=intensity_damage_nor./intensity_f_before_cut;
417     ratio_glo_nor = mean2(ratio_damage_nor);

```

## 6.2. MATLAB CODES

```
418     end
419 end
420
421 figure(4) %%Damage intensity vs. original intensity
422 if ~isempty(strfind(button_nor, 'No'))
423     plot(intensity_f_before, ...
424          y_f, 'g', intensity_f_after, y_f, 'r', intensity_damage, y_f, 'b')
425 else if ~isempty(strfind(button_nor, 'Yes'))
426     plot(intensity_f_before_cut, ...
427          y_f_nor, 'g', intensity_f_after_nor, y_f_nor, 'r', intensity_damage_nor, y_f_nor)
428     end
429 end
430
431 % set(gca, 'XTick', 1:num)
432 set(findall(gca, 'Type', 'Line'), 'LineWidth', linewidth);
433 % Enlarge figure to full screen.
434 set(gcf, 'Units', 'Normalized', 'OuterPosition', [0 0 1 1]);
435 % Add title and axis labels
436 caption4 = sprintf('Intensity of fluorescent endothelial cells');
437 title(caption4, 'FontSize', fontSize, 'Interpreter', 'None');
438 xlabel('Average Intensity over Length')
439 ylabel('Y position')
440 legend('Intensity of original artery', 'Intensity of wounded ...
441        artery', 'Intensity of damaged cells')
442
443 figure(5) %%Damage ratio
444 if ~isempty(strfind(button_nor, 'No'))
445     plot(ratio_damage, y_f, 'b')
446
447 else if ~isempty(strfind(button_nor, 'Yes'))
448     plot(ratio_damage_nor, y_f_nor, 'b')
449     end
450 end
451
452 % set(gca, 'XTick', 1:num)
453 set(findall(gca, 'Type', 'Line'), 'LineWidth', linewidth);
454 % Enlarge figure to full screen.
455 set(gcf, 'Units', 'Normalized', 'OuterPosition', [0 0 1 1]);
456 % Add title and axis labels
457 caption5 = sprintf('damaged ratio of each line');
458 title(caption5, 'FontSize', fontSize, 'Interpreter', 'None');
459 xlabel('Ratio of damage of each line')
460 ylabel('Y position')
461 xlim([-inf ,1])
462
463 figure(6) %%histogram of damage ratio
464 % nbin_damage = 50;
465 if ~isempty(strfind(button_nor, 'No'))
466     histogram(ratio_damage, nbin_damage);
467
468 else if ~isempty(strfind(button_nor, 'Yes'))
469     histogram(ratio_damage_nor, nbin_damage);
```

```
467         end
468     end
469     % set(gca, 'XTick', 1:num)
470     set(findall(gca, 'Type', 'Line'), 'LineWidth', linewidth);
471     % Enlarge figure to full screen.
472     set(gcf, 'Units', 'Normalized', 'OuterPosition', [0 0 1 1]);
473     % Add title and axis labels
474     caption6 = sprintf('Histogram of Artery Damage Ratio');
475     title(caption6, 'FontSize', fontSize, 'Interpreter', 'None');
476     xlabel('Damage Ratio')
477     ylabel('Number of pixels')
478     xlim([-1,1])
479
480
481     %% Save figures
482     saveas(figure(1), [path_results '\\' 'figure1_cropped_images.fig']);
483     saveas(figure(2), [path_results '\\' ...
484         'figure2_original_intensity_comparison.fig']);
485     saveas(figure(3), [path_results '\\' 'figure3_4_components.fig']);
486     saveas(figure(4), [path_results '\\' ...
487         'figure4_3_intensity_comparison.fig']);
488     saveas(figure(5), [path_results '\\' 'figure5_Damage_ratio.fig']);
489     saveas(figure(6), [path_results '\\' ...
490         'figure6_Histogram_damage_ratio.fig']);
491
492     %% Excel wirte
493     filename = 'global_damage_ratio.xlsx';
494     fullFileName = fullfile(path_results, filename);
495     xlswrite(fullFileName, ratio_glo, 'global_damage_ratio');
```

## SMC general code

```

1  %%%%%%%%%%%%%%%%%%%%%%%%%%%%%%%%%%%%%%%%%%%%%%%%%%%%%%%%%%%%%%%%%%%%%%%%%%
2  %           Code description and functionality                               %
3  %%%%%%%%%%%%%%%%%%%%%%%%%%%%%%%%%%%%%%%%%%%%%%%%%%%%%%%%%%%%%%%%%%%%%%%%%%
4  % This a code used to treat images and SMC cluster formation
5
6
7  clc; clear all; close all; %cleaning commands :)
8  %%%%%%%%%%%%%%%%%%%%%%%%%%%%%%%%%%%%%%%%%%%%%%%%%%%%%%%%%%%%%%%%%%%%%%%%%%
9  %           Parameters
10 %%%%%%%%%%%%%%%%%%%%%%%%%%%%%%%%%%%%%%%%%%%%%%%%%%%%%%%%%%%%%%%%%%%%%%%%%%
11
12 scale=0.65; % image resolution, in microns/pixel for Hamamatsu ...
    camera 10X
13 internal = 1200; %5mins(300);20mins(1200)
14 direc_code = 'I:\SMC\code';
15 cd(direc_code);
16 % macro_nd2_to_tif = ...
    'F:\SMC\matlab_imageJ\macro_nd2_to_tif.ijm';%location of ...
    associated imageJ macro
17 macro_ImageTransform='I:\SMC\code\macroImageTransform.ijm';
18 macro_ClusterTrack = 'macroClusterTrack_30k_inf.ijm'; %black ...
    cluster white background ...
    ==>'macroClusterTrack_30k_inf.ijm';black background white ...
    boundary ==>'macroClusterTrack_30k_inf_v2.ijm'
19 macro_MuskTransform='macroMuskTransform.ijm';%
20 macro_ClusterRead='macroClusterRead.ijm';
21 %Input for functions
22 % direc_in_NIS = ...
    'F:\Xiuyu_W\SMC_results\Step1_NIS_results\20180731_DIA_20X_sample20180726\post_tra
    % the location of the file, this folder will also be used to ...
    store the results of the experiment
23
24 imageJfolder = 'D:\Fiji.app\ImageJ-win64.exe'; % location of ...
    ImageJ program
25 direc_in_step3 = 'I:\SMC\Step3_TransformedImage\';
26 direc_output='I:\SMC\Step4_DataAnalysis\';
27 direc_step5='I:\SMC\Step5_DynamicAnalysis\';
28
29 %Folder to change for every new analysis
30 direc_in_image_tif = ...
    'I:\SMC\Step2_Exported_tif\20190423\day9\pos08\';%x1
31 a = dir([direc_in_image_tif '*.tif']);
32 num_images = size(a,1); % how many images do you want to treat
33
34 % filename information ==> needed check every new simulation
35 filename = ...
    '20190423_day9_pos08t\xy1c1';%'20181001_day2_loop2_2t\xy03';% x4
36 name_exp = '20190423_day9';

```

```

37 name_loop = 'day9';
38 name_pos = 'pos08';
39
40 fl = strsplit(filename, '/');
41 file_name1 = fl{1,1};
42 file_name2 = fl{1,2};
43
44 % modules you want to be run:
45
46 %%%%%%%%%%%%%%%%%%%%%%%%%%%%%%%%%%%%%%%%%%%%%%%%%%%%%%%%%%%%%%%%%%%%%%%%%
47 %           Analysis switch panel
48 %%%%%%%%%%%%%%%%%%%%%%%%%%%%%%%%%%%%%%%%%%%%%%%%%%%%%%%%%%%%%%%%%%%%%%%%%
49 imtransform=1;
50 clustertrack=1;
51 musktransform=1;
52 clusterread=1;
53 contourtreatment=1; %1 if you want to track the contour of cluster ...
    and smooth it
54 % contouranalysis=0; % Step after contour treatment; 1 if you want ...
    to analysis the clusters' area & radium
55 excelwriting=1;
56 makevideo=1;
57 dynamicanalysis=1;
58 sizeevaluation=1;
59 shapein=1;
60 roleframerate=0;
61 % clustermigration=0; %1 calculate the centroid velocity and plot ...
    the migration trajectory
62
63 %%
64 %%%%%%%%%%%%%%%%%%%%%%%%%%%%%%%%%%%%%%%%%%%%%%%%%%%%%%%%%%%%%%%%%%%%%%%%%
65 %           Program body
66 %%%%%%%%%%%%%%%%%%%%%%%%%%%%%%%%%%%%%%%%%%%%%%%%%%%%%%%%%%%%%%%%%%%%%%%%%
67 %Image Transfer
68 if (imtransform ==1)
69     %Creat output directory
70     direc_output_ImTrans=[direc_in_step3, ...
        name_exp, '\ImTrans\', name_loop, '\', name_pos, '\'];
71     if exist(direc_output_ImTrans, 'file')≠7
72         mkdir(direc_output_ImTrans); ...
        %creat new folder,
73     end
74     %call fuction
75     ImageTransform(imageJfolder, macro_ImageTransform, ...
        direc_in_image_tif, ...
        direc_output_ImTrans, filename, num_images);
76 end
77
78 %Wait for Fiji to finish
79 LastFileName_Imtrans = ...
    [direc_output_ImTrans, file_name1, num2str(num_images), file_name2, '.tif'];
80 pause on

```

## 6.2. MATLAB CODES

```
81 while exist(LastFileName_Imtrans)≠2
82     pause(0.1)
83 end
84 pause off
85
86 %% Convert to Musk
87 if (musktransform ==1)
88     %Creat output directory
89     direc_output_Musk=[direc_in_step3, ...
90         name_exp, '\ImageJ_Contour\' ,name_loop, '\', name_pos, '\'];
91     if exist(direc_output_Musk, 'file')≠7
92         mkdir(direc_output_Musk); ...
93                                     %creat new folder,
94     end
95     %call fuction
96     dir_in_musk = direc_output_ImTrans;
97     ClusterTrack(imageJfolder,macro_MuskTransform,dir_in_musk,direc_output_Musk,filena
98 end
99 % Wait for Fiji to finish
100 LastFileName_Musk = ...
101     [direc_output_Musk, 'Musk_', file_name1, num2str(num_images), file_name2, '.tif'];
102 pause on
103 while exist(LastFileName_Musk)≠2
104     pause(0.1)
105 end
106 pause off
107 %% Musk to contour
108 if (clusterread ==1)
109     %Creat output directory
110     direc_output_Contour=[direc_in_step3, ...
111         name_exp, '\ImageJ_Contour\' ,name_loop, '\', name_pos, '\'];
112     if exist(direc_output_Contour, 'file')≠7
113         mkdir(direc_output_Contour); ...
114                                     %creat new folder,
115     end
116     %call fuction
117     dir_in_clusterread = direc_output_Musk;
118     ClusterTrack(imageJfolder,macro_ClusterRead,dir_in_clusterread,direc_output_Contour
119 end
120 % Wait for Fiji to finish
121 LastFileName_Contour = ...
122     [direc_output_Contour, 'Drawing_', file_name1, num2str(num_images), file_name2, '.tif']
123 pause on
124 while exist(LastFileName_Contour)≠2
125     pause(0.1)
126 end
127 pause off
128 %% Contour Treatment
```

```

127 % cd 'F:\SMC\code'
128
129 % direc_in_image = ...
    'F:\SMC\Step3_TransformedImage\pre_20180722_DIA_10x\loop1\';%x1
130 % direc_in_contour = ...
    'F:\SMC\Step4_DataAnalysis\post_20180722_DIA_10x\ImageJ_contour_20180912\loop1\';%
131 % direc_output= ...
    'F:\SMC\Step4_DataAnalysis\post_20180722_DIA_10x\MatlabAnalysis_20180912\';%x3
132 % filename = '20180722_10x_loop1txy08c1';% x4
133 % num_images = 3;
134 % t = 37; % x5
135 if (contourtreatment ==1)
136     direct_output_contourtreatment=[direc_output, ...
        'post_',name_exp,'\ContourTreatment\',name_loop,'\ ',name_pos,'\ '];
137     if exist(direct_output_contourtreatment, 'file')≠7
138         mkdir(direct_output_contourtreatment); ...
                                                    %creat new folder,
139
140     end
141     %call the function ContourTreatment
142     for i = 1:num_images
143         % file_name = insertAfter(filename, ...
144             't',num2str(sprintf('%02d',i)));
145         file_name = strrep(filename,'/',num2str(sprintf('%02d',i)));
146         dir_in_image = direc_output_ImTrans;
147         dir_in_contour = direc_output_Contour;
148         I_bw_cluster = ...
149             ContourTreatment(dir_in_image,direc_output_Contour,direct_output_contourtr
150                 without .tif
151                 if i==1
152                     % Mat_cluster_contours = cluster_contours;
153                     Mat_I_bw_cluster = I_bw_cluster;
154                 else
155                     % Mat_cluster_contours = cat(3, Mat_cluster_contours, ...
156                         cluster_contours); %% save all contours as a multilayer of cell ...
157                         (in a same variable)
158                     Mat_I_bw_cluster = cat(3, ...
159                         Mat_I_bw_cluster,I_bw_cluster); %% save all ...
160                         I_bw_cluster image as a multilayer of matrix (in a ...
161                         same variable)
162                 end
163             end
164         end
165     end
166
167 % Save the matrix of "Mat_I_bw_cluster"
168 foldername_mat = [direc_output, ...
169     'post_',name_exp,'\MatVariable_',name_loop,'_',name_pos,'\ '];
170 if exist(foldername_mat, 'file')≠7
171     mkdir(foldername_mat);
172     %creat new folder,
173
174 end
175 filename = [foldername_mat,'Mat_I_bw_cluster.mat'];

```

## 6.2. MATLAB CODES

```
164 save(filename)
165
166 %% Excel writing
167 close all;
168 if (excelwriting==1)
169     foldername_output_clusteranalysis=[direc_output, ...
170         'post_',name_exp, ...
171         '\ClusterAnalysis\',name_loop,'\ ',name_pos,'\ ');
172     if exist(foldername_output_clusteranalysis, 'file')≠7
173         mkdir(foldername_output_clusteranalysis); ...
174             %creat new folder,
175     end
176 end
177
178 if (excelwriting ==1)
179     ExcelWriting(Mat_I_bw_cluster,foldername_output_clusteranalysis,scale,name_loop,n
180 end
181 nameExcel = ['Master_',name_loop,'_',name_pos];
182 adressExcel = [foldername_output_clusteranalysis,nameExcel,'.xlsx'];
183 %% Make Video
184 FrameRate=7;
185 cd(direc_code);
186 if (makevideo == 1)
187     foldername_output_video=[direc_step5, 'video'];
188     direc_output_ImTrans=[direc_in_step3, ...
189         name_exp,'\ImTrans\',name_loop,'\ ',name_pos,'\ ');
190 %
191     ...
192     direc_output_ImTrans='I:\SMC\Step2_Exported_tif\20181215_Day5_DIA_10X\loop123\pos2
193     if exist(foldername_output_video, 'file')≠7
194         mkdir(foldername_output_video); ...
195             %creat new folder,
196     end
197 end
198 if (makevideo ==1)
199     MakeVideo(direc_output_ImTrans,name_exp,name_loop,name_pos,direc_step5,FrameRate)
200 end
201
202 %% Create folder of step5
203 cd(direc_code);
204 if (dynamicanalysis||sizeevaluation||shapein==1)
205     foldername_output_excelanalysis=[direc_step5, ...
206         'GLASS\',name_exp, '_',name_pos,'\ ');
207     if exist(foldername_output_excelanalysis, 'file')≠7
208         mkdir(foldername_output_excelanalysis); ...
209             %creat new folder,
210     end
211 end
212 %% Dynamic Analysis
213 cd(direc_code);
214 % if (dynamicanalysis==1)
215 %     foldername_output_excelanalysis=[direc_step5, ...
216 %         'GLASS\',name_exp, '_',name_pos,'\ ');
```

```
207 %     if exist(foldername_output_excelanalysis, 'file')≠7
208 %         mkdir(foldername_output_excelanalysis); ...
                %creat new folder,
209 %     end
210 % end
211 movefile(adressExcel, foldername_output_excelanalysis);
212 FolderInfo = dir(direc_output_ImTrans);
213 ImageName = FolderInfo(3).name;
214 if (dynamicanalysis ==1)
215     DynamicAnalysis(foldername_output_excelanalysis, nameExcel, internal, scale, direc_out
216 end
217 %% Size Evaluation
218 close all
219 cd(direc_code);
220 if (sizeevaluation ==1)
221     SizeEvaluation(foldername_output_excelanalysis, nameExcel, internal);
222 end
223 %% Shape In(epsilon)
224 close all
225 cd(direc_code);
226 if (shapein ==1)
227     ShapeIn(foldername_output_excelanalysis, nameExcel, internal);
228 end
229 %% Role of Frame Rate
230 close all
231 cd(direc_code);
232 if (roleframerate ==1)
233     RoleFrameRate(foldername_output_excelanalysis, nameExcel, internal, scale);
234 end
```

## Image format transformation

```

1  %%%%%%%%%%%%%%%%%%%%%%%%%%%%%%%%%%%%%%%%%%%%%%%%%%%%%%%%%%%%%%%%%%%%%%%%%%
2  %%%%%%%%%%                               Image Transform
3  %%%%%%%%%%%%%%%%%%%%%%%%%%%%%%%%%%%%%%%%%%%%%%%%%%%%%%%%%%%%%%%%%%%%%%%%%%
4
5  function ImageTransform(x1,x2,x3,x4,x5,x6)
6  %User Input
7  imageJfolder=x1;
8  macro_ImageTransform=x2;
9  dir_in=x3;
10 dir_out=x4;
11 filename=x5;
12 num_images=x6;
13
14 fl = strsplit(filename, '/');
15 file_name1 = fl{1,1};
16 file_name2 = fl{1,2};
17 parseKey      = '#';
18
19 % imageJfolder = 'D:\Fiji.app\ImageJ-win64.exe';
20 % macro_ImageTransform = 'F:\SMC\code\macroImageTransform.ijm';
21 % dir_in = 'I:\SMC\Step2_Exported_tif\20190423\day3\pos07\';
22 % dir_out= ...
23 %       'I:\SMC\Step3_TransformedImage\20190423_day3\ImTrans\day3\pos07\';
24 % %file_name = '20180722_10x_loopt1t01xy08c1';
25 % file_name1 = '20190423_day3_pos07t';
26 % file_name2 = 'xylc1';
27 %
28 % a = dir([dir_in '*.tif']);
29 % num_images = size(a,1);
30 % parseKey      = '#';
31
32 input = ...
33     [char(fullfile(dir_in)),parseKey,char(file_name1),parseKey,char(file_name2),parseKey,
34     num2str(num_images), parseKey, fullfile(dir_out))];
35 % part1 = datafolder(dir_in); part2=datafilename(file_name); part3 ...
36     = number
37 % of image(num_image); part4 = savefolder(dir_out)
38 system([imageJfolder, ' -macro ',macro_ImageTransform, ' ',input, '&']);
39
40 % i=1;
41 % while ...
42     exist('Z:/Xiuyu_W/SMC_results/Step1_NIS_results/20180731_DIA_20X_sample20180726/po
43 %     pause(0.1)
44 % end
45 % pause(20)
46
47 end

```

## Cluster tracking

```

1  %%%%%%%%%%%%%%%%%%%%%%%%%%%%%%%%%%%%%%%%%%%%%%%%%%%%%%%%%%%%%%%%%%%%%%%%%%%
2  %%%%%%%%%%                track SMC cluster
3  %%%%%%%%%%%%%%%%%%%%%%%%%%%%%%%%%%%%%%%%%%%%%%%%%%%%%%%%%%%%%%%%%%%%%%%%%%%
4
5  function ClusterTrack(x1,x2,x3,x4,x5,x6)
6  %User Input
7  imageJfolder=x1;
8  macro_ClusterTrack=x2;
9  dir_in=x3;
10 dir_out=x4;
11 filename=x5;
12 num_images=x6;
13
14 fl = strsplit(filename, '/');
15 file_name1 = fl{1,1};
16 file_name2 = fl{1,2};
17 parseKey   = '#';
18
19 % imageJfolder = 'D:\Fiji.app\ImageJ-win64.exe';
20 % macro_ClusterTrack = 'F:\SMC\code\macroClusterTrack_20180912.ijm';
21 % dir_in = 'F:\SMC\Step3_TransformedImage\pre_20180722_DIA_10x\loop1\';
22 % dir_out= ...
    'F:\SMC\Step4_DataAnalysis\post_20180722_DIA_10x\ImageJ_contour_20180912\loop1\';
23 % %file_name = '20180722_10x_loop1t01xy08c1';
24 % file_name1 = '20180722_10x_loop1t';
25 % file_name2 = 'xy08c1';
26
27 % a = dir([dir_in '*.tif']);
28 % num_images = size(a,1);
29 % parseKey   = '#';
30
31
32 %input = [char(fullfile(dir_in)),parseKey,char(file_name),parseKey, ...
    num2str(num_images), parseKey, fullfile(dir_out)];
33
34 input = ...
    [char(fullfile(dir_in)),parseKey,char(file_name1),parseKey,char(file_name2),parseK
    num2str(num_images), parseKey, fullfile(dir_out)];
35 % part1 = datafolder(dir_in); part2=datafilename(file_name); part3 ...
    = number
36 % of image(num_image); part4 = savefolder(dir_out)
37 %input = [dir_in,parseKey,exp_name,parseKey, num2str(num_images), ...
    parseKey,dir_out];
38 system([imageJfolder, ' -macro ',macro_ClusterTrack, ' ',input, '&']);
39
40 for i = 1:num_images
41     fileName_Musk = [dir_out,'Musk_',file_name1,i,file_name2,'.tif'];

```

## 6.2. MATLAB CODES

---

```
42     fileName_Drawing = ...
        [dir_out, 'Drawing_', file_name1, i, file_name2, '.tif'];
43
44     %     while exist(fileName_Musk)-2
45     %         pause(0.1)
46     %     end
47     %     pause(2)
48     %
49     %     while exist(fileName_Drawing)-2
50     %         pause(0.1)
51     %     end
52     %     pause(2)
53 end
54
55 end
```

## Cluster contour analysis

```

1  %%%%%%%%%%%%%%%%%%%%%%%%%%%%%%%%%%%%%%%%%%%%%%%%%%%%%%%%%%%%%%%%%%%%%%%%%%
2  %%%%%%%%%%                               Contour Size Analysis
3  %%%%%%%%%%%%%%%%%%%%%%%%%%%%%%%%%%%%%%%%%%%%%%%%%%%%%%%%%%%%%%%%%%%%%%%%%%
4
5  function ContourAnalysis(x1,x2,x3,x4,x5)
6  %%
7  % User input
8  % cluster_contours=x1;
9  Mat_I_bw_cluster=x1;
10 dir_out=x2;
11 scale=x3;
12 loop=x4;
13 pos=x5;
14 %%
15 %Format
16 format long g;
17 format compact;
18 fontSize = 25;
19 linewidth = 3;
20
21
22
23 [m,n,num]=size(Mat_I_bw_cluster);
24 time1=1;
25 time2=num;
26 % Prepare variables for figures
27 num_ob_max = 4; %Maximum number of cluster ...
    happened in all time scales
28 x = 1:1:num; %X-axis of bar chart
29 x_timescale = x*20; %time-scale of X-axis of bar ...
    chart
30 y_num_ob = zeros(1,num); %define the size of 'Number ...
    of Cluster Y-axis' of bar chart
31 y_area = zeros(num_ob_max,num); %define the size of 'Area ...
    Y-axis' of bar chart
32 y_perimeter = zeros(num_ob_max,num); %define the size of ...
    'Perimeter Y-axis' of bar chart
33 y_eccentricity = zeros(num_ob_max,num); %define the size of ...
    'Eccentricity Y-axis' of bar chart
34 x_centroid = zeros(num_ob_max,num); %define the position-x of ...
    centroid
35 y_centroid = zeros(num_ob_max,num); %define the position-y of ...
    centroid
36 %%
37 for i = 1:num
38 T = num2str(i); % 't'
39
40     %% read objects in bwimage

```

## 6.2. MATLAB CODES

```
41 I_bw_cluster = Mat_I_bw_cluster(:, :, i);
42 [M,N] = size(I_bw_cluster);
43 Min_size = 500;
44 Max_size = M*N/2;
45 I_bw_cluster = bwareafilt(I_bw_cluster, [Min_size Max_size]);
46 CC = bwconncomp(I_bw_cluster);
47 labeled = labelmatrix(CC);
48 RGB_label = label2rgb(labeled, @spring, 'c', 'shuffle');
49
50
51 stats = ...
    regionprops('table', CC, 'Area', 'Perimeter', 'Eccentricity', 'Orientation', 'Centroid',
52
53 stats_scale=stats;
    %stats (structure) is in unit of pixel; stats_scale is the ...
54 stats_scale.Area = stats.Area.*(scale^2);
55 stats_scale.Perimeter = stats.Perimeter.*scale;
56 stats_scale.MajorAxisLength = stats.MajorAxisLength.*scale;
57 stats_scale.MinorAxisLength = stats.MinorAxisLength.*scale;
58 %stats_scale.Eccentricity = stats.Eccentricity;
59 %stats_scale.Orientation = stats.Orientation;
60
61 % Reshaped matrix prepared for figures
62 area = stats_scale.Area;
63 area(num_ob_max)=0; %reshape ...
    the matrix size to prepare the matrix for bar chart
64 perimeter = stats_scale.Perimeter;
65 perimeter(num_ob_max)=0;
66 eccentricity = stats_scale.Eccentricity;
67 eccentricity(num_ob_max)=0;
68 centroids = cat(1, stats_scale.Centroid); %%X,Y
69 centroids(num_ob_max,1)=0;
70
71 % Y_variables for bar chart
72 y_num_ob(1,i) = length(stats_scale.Area); %number ...
    of clusters at each time scale
73 y_area(:,i) = area;
74 y_perimeter(:,i) = perimeter;
75 y_eccentricity(:,i) = eccentricity;
76 x_centroid(:,i) = centroids(:,1); %define the ...
    position-x of centroid
77 y_centroid(:,i) = centroids(:,2);
78
79 % for ii = 1:y_num_ob(i)
80 %     y_area(ii,i) = stats_scale.Area(ii);
81 %     y_perimeter = ;
82 %     y_eccentricity = zeros(10,num);
83 %
84 % end
85
86
87
```

```

88
89 % centroids = cat(1, stats_scale.Centroid); %%X,Y
90 % figure                                %%Figure of centroids
91 % imshow(RGB_label)
92 % hold on
93 % plot(centroids(:,1),centroids(:,2), 'b*')
94 % title('Centroid of each centroid');
95 % hold off
96
97
98 % Save and Output
99
100 excelname=[dir_out 'ClusterAnalysis_t',T, '.xlsx'];
101 writetable(stats_scale, excelname)
102 while exist(excelname)-2
103     pause(0.1)
104 end
105 pause(5)
106 end
107 %%
108 % Figure: number of clusters variation of all time scales
109 figure(1)
110 bar(x,y_num_ob)
111 set(gca, 'fontSize',20)
112 axis([0 num+1 0 num_ob_max])
113 set(gca, 'XTick', 1:(num+1))
114 % Add title and axis labels
115 caption1 = sprintf('Number of cluster');
116 title(caption1, 'FontSize', fontSize, 'Interpreter', 'None');
117 xlabel('Time scale (every 20 mins)')
118 ylabel('Number of cluster')
119 % Enlarge figure to full screen.
120 set(gcf, 'Units', 'Normalized', 'OuterPosition', [0 0 1 1]);
121 % Set the axis limits
122
123 %Figure: area of all time scale
124 figure(2)
125 bar(y_area.')
126 set(gca, 'fontSize',20)
127 xlim([0 num]);
128 set(gca, 'XTick', 1:num)
129 % Add title and axis labels
130 caption2 = sprintf('Evaluation of Cluster Area');
131 title(caption2, 'FontSize', fontSize, 'Interpreter', 'None');
132 xlabel('Time scale (every 20 mins)')
133 ylabel('Area (um^2)', 'Interpreter', 'none')
134 % Enlarge figure to full screen.
135 set(gcf, 'Units', 'Normalized', 'OuterPosition', [0 0 1 1]);
136 % Set the axis limits
137
138 %Figure: eccentricity of all time scale
139 figure(3)

```

## 6.2. MATLAB CODES

---

```
140 bar(y_eccentricity.')
141 set(gca,'fontsize',20)
142 axis([0 num 0 1])
143 set(gca, 'XTick', 1:num)
144 % Add title and axis labels
145 caption3 = sprintf('Evaluation of Cluster Eccentricity');
146 title(caption3, 'FontSize', fontSize, 'Interpreter', 'None');
147 xlabel('Time scale (every 20 mins)')
148 ylabel('Eccentricity')
149 % Enlarge figure to full screen.
150 set(gcf, 'Units', 'Normalized', 'OuterPosition', [0 0 1 1]);
151
152 %Trajectory of centroid of a chosen time scales
153 figure(4);imshow(Mat_I_bw_cluster(:,:,time1));hold on
154 for ii=1:num_ob_max
155     plot(x_centroid(ii,time1:time2),y_centroid(ii,time1:time2));
156     axis([0 m 0 n]);
157     % hold on
158 end
159 hold off
160 % Add title and axis labels
161 set(gcf, 'Units', 'Normalized', 'OuterPosition', [0 0 1 1]);
162 caption4 = sprintf('Centroid trajectory');
163 title(caption4, 'FontSize', fontSize, 'Interpreter', 'None');
164
165
166 %Bar chart: Cluster Area of a chosen time scales 9-18
167 % Set time you want to analyze
168
169 % Count how many cluster during this period(No number variation)
170 num_iii=nnz(y_area(:,time1));
171 name_legend = cell(num_iii,1);
172 %Plot curve for first cluster
173 figure(5)
174 set(gca,'fontsize',20)
175 hold on
176 %plot curves for the rest of clusters
177 for iii=1:num_iii
178     plot(time1:time2,y_area(iii,time1:time2))
179     name_legend(iii,1) = [{'Curve', num2str(iii,'%02d')}]};
180 end
181 hold off
182 set(gca, 'XTick', 1:num)
183 set(findall(gca, 'Type', 'Line'),'LineWidth',linewidth);
184 % Enlarge figure to full screen.
185 set(gcf, 'Units', 'Normalized', 'OuterPosition', [0 0 1 1]);
186 % Add title and axis labels
187 caption2 = sprintf('Evaluation of Cluster Area');
188 title(caption2, 'FontSize', fontSize, 'Interpreter', 'None');
189 xlabel('Time scale (every 20 mins)')
190 ylabel('Area (um^2)', 'Interpreter', 'none')
191 legend(name_legend{:});
```

```

192
193 %Bar chart: Cluster Eccentricity of a chosen time scales 9-18
194 figure(6)
195 set(gca, 'fontsize',20)
196 hold on
197 for iii=1:num_iii
198     plot(time1:time2,y_eccentricity(iii,time1:time2))
199     name_legend(iii,1) = [{'Curve', num2str(iii, '%02d')}]};
200 end
201 hold off
202 set(gca, 'XTick', 1:num)
203 set(findall(gca, 'Type', 'Line'), 'LineWidth', linewidth);
204 % Enlarge figure to full screen.
205 set(gcf, 'Units', 'Normalized', 'OuterPosition', [0 0 1 1]);
206 % Add title and axis labels
207 caption3 = sprintf('Evaluation of Cluster Eccentricity');
208 title(caption3, 'FontSize', fontSize, 'Interpreter', 'None');
209 xlabel('Time scale (every 20 mins)')
210 ylabel('Eccentricity')
211 legend(name_legend{:});
212
213 %% Save figures
214 match = [loop, '/', pos, '/'];
215 todelete = length(match);
216 dir_out_fig = dir_out(1:end-todelete)
217 seri = [pos, '_', loop];
218
219 %Figure Globle view
220 figure1name=[dir_out_fig 'Bar_NumberVariation_',seri, '.fig'];
221 saveas (figure(1),figure1name);% Name of the figure with time-scale
222 pause(0.1)
223 figure2name=[dir_out_fig 'Bar_AreaVariation_',seri, '.fig'];
224 saveas (figure(2),figure2name);% Name of the figure with time-scale
225 pause(0.1)
226 figure3name=[dir_out_fig 'Bar_EccentricityVariation_',seri, '.fig'];
227 saveas (figure(3),figure3name);
228 pause(0.1)
229 figure4name=[dir_out_fig 'Bar_CentroidTrajectory_',seri, '.fig'];
230 saveas (figure(4),figure4name);
231 pause(0.1)
232 % Figure single cluster analysis
233 figure5name=[dir_out_fig 'Curve_AreaVariation_',seri, '.fig'];
234 saveas (figure(5),figure5name);% Name of the figure with time-scale
235 pause(0.1)
236 figure6name=[dir_out_fig 'Curve_EccentricityVariation_',seri, '.fig'];
237 saveas (figure(6),figure6name);% Name of the figure with time-scale
238 pause(0.1)
239
240 %% Write all seperated excel to a Master one, in different sheets
241
242 outfile = [dir_out , 'Master.xlsx'];
243 % outfile = ['a', '1'];

```

## 6.2. MATLAB CODES

---

```
244 fileNames = dir(dir_out);
245 fileNames = {fileNames.name};
246 fileNames = fileNames(cellfun(...
247     @(f)~isempty(strfind(f, '.xls')),fileNames));
248 for f = 1:numel(fileNames)
249
250     fTable = readtable([dir_out,fileNames{f}]);
251     writetable(fTable,outfile,'Sheet',fileNames{f});
252 end
253 while exist(outfile)-2
254     pause(0.1)
255 end
256 pause(30)
257 end
```

## Cluster contour treatment

```

1  %%%%%%%%%%%%%%%%%%%%%%%%%%%%%%%%%%%%%%%%%%%%%%%%%%%%%%%%%%%%%%%%%%%%%%%%%%
2  %%%%%%%%%%                               Cluster contour tracking
3  %%%%%%%%%%%%%%%%%%%%%%%%%%%%%%%%%%%%%%%%%%%%%%%%%%%%%%%%%%%%%%%%%%%%%%%%%%
4
5  function I_bw_cluster = ContourTreatment(x1,x2,x3,x4,x5)
6  %User Input
7  dir_in_image = x1;
8  dir_in_contour = x2;
9  dir_out = x3;
10 file_name = x4;
11 t=x5;
12 %pre-work
13
14 workspace; % Make sure the workspace panel is showing.
15 format long g;
16 format compact;
17 fontSize = 25;
18 % dir_in_image = ...
19   'F:\SMC\Step3_TransformedImage\pre_20180722_DIA_10x\loop1\';%x1
20 % dir_in_contour = ...
21   'F:\SMC\Step4_DataAnalysis\post_20180722_DIA_10x\ImageJ_contour_20180912\loop1\';%
22 % dir_out= ...
23   'F:\SMC\Step4_DataAnalysis\post_20180722_DIA_10x\MatlabAnalysis_20180912\ContourTr
24 % file_name = '20180722_10x_loop1t01xy08c1';% x4
25 % t = 1; % x5
26
27 T = num2str(t); % 't'
28
29 sub_name = 'Drawing_';
30 ext_name = '.tif';
31 % file_name1 = '20180722_10x_loop1t';%x4
32 % t = '37'; %x5
33 % file_name2 = 'xy08c1';%x6
34
35 %num_images = 37; %When test
36 %a = dir([dir_in '*.tif']);
37 %num_images = size(a,1);
38
39 file_original = [file_name,ext_name];
40 file_contour = [sub_name,file_original];
41 fileNameOriginal = [dir_in_image,file_original];
42 fileNameContour = [dir_in_contour,file_contour];
43
44 %% Read the initial photo in gray
45 % Check if file exists.
46 %=====

```

## 6.2. MATLAB CODES

```
46 if ~exist(fileNameOriginal, 'file')
47     % File doesn't exist -- didn't find it there. Check the search ...
        path for it.
48     fileNameOriginalOnSearchPath = file_original; % No path this time.
49     if ~exist(fileNameOriginalOnSearchPath, 'file')
50         % Still didn't find it. Alert user.
51         errorMessage = sprintf('Error: %s does not exist in the ...
            search path folders.', fileNameOriginal);
52         uiwait(warndlg(errorMessage));
53         return;
54     end
55 end
56 grayImage = imread(fileNameOriginal);
57 % Get the dimensions of the image.
58 % numberOfColorBands should be = 1.
59 [rows, ~, numberOfColorBands] = size(grayImage);
60 if numberOfColorBands > 1
61     % It's not really gray scale like we expected - it's color.
62     % Convert it to gray scale by taking only the green channel.
63     grayImage = grayImage(:, :, 2); % Take green channel.
64 end
65 % Display the original gray scale image.
66 figure(1);subplot(2, 2, 1);
67 imshow(grayImage, []);
68 axis on;grid on;
69 caption1 = sprintf('Original Grayscale Image - t%d', t);
70 title(caption1, 'FontSize', fontSize, 'Interpreter', 'None');
71 % Enlarge figure to full screen.
72 set(gcf, 'Units', 'Normalized', 'OuterPosition', [0 0 1 1]);
73 % Give a name to the title bar.
74 caption_total1 = sprintf('Cluster Treatment - t%d',t);
75 set(gcf, 'Name', caption_total1, 'NumberTitle', 'Off')
76 %% Draw Histogram
77 % Let's compute and display the histogram.
78 % [pixelCount, grayLevels] = imhist(grayImage);
79 % subplot(2, 3, 2);
80 % bar(grayLevels, pixelCount); % Plot it as a bar chart.
81 % grid on;
82 % title('Histogram of original image', 'FontSize', fontSize, ...
        'Interpreter', 'None');
83 % xlabel('Gray Level', 'FontSize', fontSize);
84 % ylabel('Pixel Count', 'FontSize', fontSize);
85 % xlim([0 grayLevels(end)]); % Scale x axis manually.
86
87 %% Read the contour of cluster & Convert to mask
88 if ~exist(fileNameContour, 'file')
89     % File doesn't exist -- didn't find it there. Check the search ...
        path for it.
90     fileNameOriginalOnSearchPath = file_contour; % No path this time.
91     if ~exist(fileNameOriginalOnSearchPath, 'file')
92         % Still didn't find it. Alert user.
```

```

93     errorMessage = sprintf('Error: %s does not exist in the ...
          search path folders.', fileNameContour);
94     uiwait(warndlg(errorMessage));
95     return;
96 end
97 end
98 binaryImage = imread(fileNameContour);
99 % Get the dimensions of the image.
100 % numberOfColorBands should be = 1.
101 [rows, columns, numberOfColorBands] = size(binaryImage);
102
103 if numberOfColorBands > 1
104     % It's not really gray scale like we expected - it's color.
105     % Convert it to gray scale by taking only the green channel.
106     binaryImage = binaryImage(:, :, 2); % Take green channel.
107
108 end
109 % Display the original gray scale image.
110 subplot(2, 2, 2);
111 imshow(binaryImage, []);
112 axis on;grid on;
113 caption2 = sprintf('Contour ImageJ - t%d', t);
114 title(caption2, 'FontSize', fontSize, 'Interpreter', 'None');
115
116 binaryImage2 = imcomplement(binaryImage);
117 I_bw = imfill(binaryImage2, 'holes');
118
119 %% Get the boundarie
120 %First, display the original gray scale image.
121
122 subplot(2, 2, 3);
123 imshow(grayImage, []);
124 axis image; % Make sure image is not artificially stretched because ...
          of screen's aspect ratio.
125 hold on;
126 % Now get the boundaries.
127 boundaries = bwboundaries(I_bw);
128 numberOfBoundaries = size(boundaries, 1);
129 for k = 1 : numberOfBoundaries
130     thisBoundary = boundaries{k};
131     plot(thisBoundary(:,2), thisBoundary(:,1), 'g', 'LineWidth', 2);
132 end
133 hold off;
134 axis on;grid on;
135 caption3 = sprintf('%d Clusters - t%d', numberOfBoundaries,t);
136 title(caption3, 'FontSize', fontSize);
137
138 %% read objects in bwimage
139 CC = bwconncomp(I_bw);
140 NumObjects = CC.NumObjects;
141
142 %% smoothen the boundary

```

## 6.2. MATLAB CODES

---

```
143 windowWidth = 599;
144 polynomialOrder = 2;
145 smoothBoundary = cell(NumObjects,1);
146 %figure(3);
147 subplot(2, 2, 4);
148 imshow(grayImage, []);
149 axis image; % Make sure image is not artificially stretched because ...
    of screen's aspect ratio.
150 hold on;
151 for ob = 1:NumObjects
152 firstBoundary = boundaries{ob};
153 % Get the x and y coordinates.
154 x = firstBoundary(:, 2);
155 y = firstBoundary(:, 1);
156 % Now smooth with a Savitzky-Golay sliding polynomial filter
157 smoothX = sgolayfilt(x, polynomialOrder, windowWidth);
158 smoothY = sgolayfilt(y, polynomialOrder, windowWidth);
159 % First, display the original gray scale image.
160 plot(smoothX, smoothY, 'r-', 'LineWidth', 2);
161 smoothBoundary{ob,1} = [smoothX,smoothY];
162 end
163 hold off;
164 axis on;
165 grid on;
166
167 caption4 = sprintf('Smoothed Boundaries - t%d', t);
168 title(caption4, 'FontSize', fontSize);
169
170 %% Smoothed boundary back to bwimage
171 [size_m,size_n]=size(I_bw);
172
173 I_bw_smooth = poly2mask(smoothX,smoothY,size_m,size_n);
174 % figure;imshow(I_bw);
175
176 for ob = 1:(NumObjects-1)
177 %get the objects
178 object=smoothBoundary{ob,1};
179 ob_X = object(:,1);
180 ob_Y = object(:,2);
181 %Polygon back to mask
182 I_ob = poly2mask(ob_X,ob_Y,size_m,size_n);
183 % figure;imshow(I_ob)
184 %Merge two binary image to one
185 I_bw_smooth = I_ob|I_bw_smooth;
186 end
187
188 % figure;imshow(I_bw_smooth)
189 figure(2);imshowpair(I_bw,I_bw_smooth,'montage')
190 % axis on;grid on;
191 % Enlarge figure to full screen.
192 set(gcf, 'Units', 'Normalized', 'OuterPosition', [0 0 1 1]);
193 % Give a name to the title bar.
```

```
194 caption_total2 = sprintf('Cluster Masks Comparison - t%d',t);
195 set(gcf, 'Name', caption_total2, 'NumberTitle', 'Off')
196 title(caption_total2, 'FontSize', fontSize, 'Interpreter', 'None');
197
198 figure(3);imshow(I_bw_smooth);
199 % axis on;grid on;
200 caption_total3 = sprintf('Smoothened Cluster Masks - t%d',t);
201 set(gcf, 'Name', caption_total3, 'NumberTitle', 'Off')
202 %% Save & Output
203
204 % cluster_contours = smoothBoundary;
205 I_bw_cluster = I_bw_smooth;
206
207 figure1name=[dir_out 'ContourTreatment_t',T, '.fig'];
208 figure2name=[dir_out 'ComparisonContourMasks_t',T, '.fig'];
209 figure3name=[dir_out 'ContourMask_t',T, '.fig'];
210 saveas(figure(1),figure1name); %Name of the figure with time-scale
211 saveas(figure(2),figure2name); %Name of the figure with time-scale
212 saveas(figure(3),figure3name);
213 while exist(figure1name)-2
214     pause(0.1)
215 end
216 pause(15)
217 while exist(figure2name)-2
218     pause(0.1)
219 end
220 pause(5)
221 while exist(figure3name)-2
222     pause(0.1)
223 end
224 pause(5)
225 end
```

## Cluster shape analysis

```

1 function ShapeIn(x1,x2,x3)
2 %%%%%%%%%%%%%%%%%%%%%%%%%%%%%%%%%%%%%%%%%%%%%%%%%%%%%%%%%%%%%%%%%%%%%%%%%%
3 %
4 %           Shape evaluation ...
5 %
6 %%%%%%%%%%%%%%%%%%%%%%%%%%%%%%%%%%%%%%%%%%%%%%%%%%%%%%%%%%%%%%%%%%%%%%%%%%
7 %% Read MajorAxisLength(c), MinorAxisLength(a), time(t)
8 dir_in=x1;
9 ExcelName=x2;
10 internal=x3;
11
12 %Check these three lines for every run
13 dir_in = 'I:\SMC\Step5_DynamicAnalysis\GLASS\20190423_day9_pos08\';
14 ExcelName='Master_day9_pos08';
15 internal = 1200;
16 % dir_in = ...
17 %   'I:\SMC\Step5_DynamicAnalysis\GLASS\20181001_loop12_pos03_20min\';
18 % ExcelName='Master_loop_pos03';
19 % internal = 1200;
20
21 adressExcel = [dir_in,ExcelName, '.xlsx'];
22 [num,txt,row] = xlsread(adressExcel) ;
23
24 c = num(:,4);
25 a = num(:,5);
26 c = c(1:2:end);
27 a = a(1:2:end);
28
29 n=length(c);
30 n_interval = (0:n-1)';
31 t=n_interval*internal; %[s]
32 t_h = t/3600; %[h]
33 %% Calculation
34 %Shape ratio: sr= c/a           []
35 %Mean radius: r= (c+2*a)/3     [um]
36 %Shape factor: epsilon= (c-a)/(c+2*a) []
37 %           : t/mr             [s/um]
38 %In(epsilon/epsilon0):
39
40 % sr= c./a;
41 r= (c+2*a)/3;
42 epsilon= (c-a)./(c+2*a);
43 t_r = t./r;           %t/r
44 In = log10(epsilon./epsilon(1));
45 % aspect_ratio = a/c;
46 %% Save Shape Variables:t_h, r, epsilon, t_r, In

```

```

47 save([dir_in, ...
      ExcelName, '_Shape.mat'], 't_h', 'r', 'epsilon', 't_r', 'In', 'dir_in', 'ExcelName');
48 %% Gamme/eta Curve fitting
49 figure(1);
50 p_ep = polyfit(t_r, In, 1);
51 f_ep = polyval(p_ep, t_r);
52 plot(t_r, In, '*r', t_r, f_ep, '-k');
53
54 legend('\fontsize{15}data', '\fontsize{15}linear fit')
55 xlabel('\fontsize{22}t/r [s/um]')
56 ylabel('\fontsize{22}In (\epsilon/\epsilon_0)')
57 set(gca, 'FontSize', 22)
58 xlim([0 250])
59 % axes('Ylim', [-1, 0], 'YTick', -1:0.1:0, 'NextPlot', 'add');
60
61 xl = xlim;
62 yl = ylim;
63 xt = 0.05 * (xl(2)-xl(1)) + xl(1);
64 yt = 0.15 * (yl(2)-yl(1)) + yl(1);
65
66 % gamma/eta
67 gamma_eta = -p_ep(1)*56/15*10^(-6); % [m/s]
68
69 caption = sprintf('y = %.2e * x + %.2e \r\ngamma/eta= %.2e [m/s]', ...
      p_ep(1), p_ep(2), gamma_eta);
70 text(xt, yt, caption, 'FontSize', 15, 'Color', 'k', 'FontWeight', ...
      'bold');
71
72 %% plot r
73 figure(2);
74 plot(t_h, r, '-o', 'Color', [0.6350 0.0780 0.1840], 'MarkerSize', 3)
75
76 % Curve fitting
77 n_power = 2;
78 figure(2);
79 p_r = polyfit(t_h, r, n_power);
80 f_r = polyval(p_r, t_h);
81 plot_r = plot(t_h, r, '*', t_h, f_r, '-k');
82 plot_r(1).Color = [0.6350 0.0780 0.1840];
83
84 legend('\fontsize{15}data', '\fontsize{15}curve fit')
85 xlabel('\fontsize{22}t [h]')
86 ylabel('\fontsize{22}r [um]')
87 set(gca, 'FontSize', 22)
88 xlim([0 25])
89
90 xl = xlim;
91 yl = ylim;
92 xt = 0.03 * (xl(2)-xl(1)) + xl(1);
93 yt = 0.10 * (yl(2)-yl(1)) + yl(1);
94
95 % DA/dt

```

## 6.2. MATLAB CODES

```
96 if n_power==1
97     DA_dt = p_r(1);    %[m/s]
98     caption = sprintf('y = %.2e * x + %.2e \r\nDNP(t)/dt= %.2e ...
99         [s-1]', p_r(1), p_r(2), DA_dt);
100 else if n_power==2
101     caption = sprintf('y = %.2e*x^2 + %.2e*x + %.2e ', p_r(1), ...
102         p_r(2),p_r(3));
103 end
104 text(xt, yt, caption, 'FontSize', 15, 'Color', 'k', 'FontWeight', ...
105     'bold');
106 %% Plot Major Axis Length & Minor Axis Length
107
108 figure(3); % Major Axis
109 plot(t_h,c, '-o', 'Color', [0.4940 0.1840 0.5560], 'MarkerSize', 3);
110 xlabel('\fontsize{22}t [h]')
111 ylabel('\fontsize{22}Major Axis Length [um]')
112 set(gca, 'FontSize', 22)
113 xlim([0 25])
114 %
115 figure(4); % Minor Axis
116 plot(t_h,a, '-o', 'Color', [0.8 0.65 0.2], 'MarkerSize', 3);
117 xlabel('\fontsize{22}t [h]')
118 ylabel('\fontsize{22}Minor Axis Length [um]')
119 set(gca, 'FontSize', 22)
120 xlim([0 25])
121
122 %% Save figure
123 FigureName_In=[dir_in, 'In_', ExcelName, '.fig'];
124 saveas (figure(1), FigureName_In);
125 FigureName_r=[dir_in, 'r_', ExcelName, '.fig'];
126 saveas (figure(2), FigureName_r);
127 FigureName_Max=[dir_in, 'Max_', ExcelName, '.fig'];
128 saveas (figure(3), FigureName_Max);
129 FigureName_Min=[dir_in, 'Min_', ExcelName, '.fig'];
130 saveas (figure(4), FigureName_Min);
131 end
```

## Cluster contour dynamics analysis

```

1 function DynamicAnalysis(x1,x2,x3,x4,x5,x6)
2 %%%%%%%%%%%%%%%%%%%%%%%%%%%%%%%%%%%%%%%%%%%%%%%%%%%%%%%%%%%%%%%%%%%%%%%%%%
3 %
4 %           Dynamic analysis ...
5 %           %
6 %%%%%%%%%%%%%%%%%%%%%%%%%%%%%%%%%%%%%%%%%%%%%%%%%%%%%%%%%%%%%%%%%%%%%%%%%%
7 %% Read Centroid(x), Centroid(y), time(t)
8 % clear all;close all; clc
9 %Input
10 dir_in=x1;
11 ExcelName=x2;
12 internal=x3;
13 scale=x4;
14 dirTransImage=x5;
15 ImageName=x6;
16
17 %Check these three lines for every run
18 dir_in = 'I:\SMC\Step5_DynamicAnalysis\GLASS\20190423_day9_pos08\';
19 ExcelName='Master_day9_pos08';
20 internal = 1200;
21 scale = 0.65; %um/pixel
22 dirTransImage = ...
    'I:\SMC\Step3_TransformedImage\20181001_day2_loop2_1\ImTrans\loop2_1\pos03\';
23 ImageName = '20181001_day2_loop2_1t01xy03.tif';
24
25 addressExcel = [dir_in,ExcelName, '.xlsx'];
26 [num,txt,row] = xlsread(addressExcel) ;
27
28 c_x = num(:,2);
29 c_y = num(:,3);
30 % c_xb = num(:,2);
31 % c_yb = num(:,3);
32 % c_x = c_xb(1:2:end);
33 % c_y = c_yb(1:2:end);
34
35 n=length(c_x);
36 n_interval = (0:n-1)';
37 t=n_interval*internal;
38 t_h = t/3600;
39 interval_h = 3600;
40 %% Calculation log(MSD)-log(t)
41 MSD=zeros(n,1);
42 MSD_Sum=zeros(n,1);
43 log_t=zeros(n-1,1);
44 log_MSD=zeros(n-1,1);
45 for i=2:n
46     MSD(i) = ((c_x(i)-c_x(1))*scale)^2+((c_y(i)-c_y(1))*scale)^2;

```

## 6.2. MATLAB CODES

```
47 %     MSD_Sum(i)=MSD(i); %MSD_Sum(i-1)+MSD(i);
48     log_t(i-1)=log10(t(i));
49     log_MSD(i-1) = log10(MSD(i));
50 end
51
52 % Curve fitting
53 n_power = 1;
54 figure(1);
55 p_MSD = polyfit(log_t,log_MSD,n_power);
56 f_MSD = polyval(p_MSD,log_t);
57 plot_r = plot(log_t,log_MSD,'*',log_t,f_MSD,'-k');
58 plot_r(1).Color = [0.6350 0.0780 0.1840];
59
60 legend('\fontsize{15}data', '\fontsize{15}linear fit', ...
        'Location','southeast')
61 xlabel('\fontsize{22}log(t)')
62 ylabel('\fontsize{22}log<MSD>')
63 set(gca,'FontSize',22)
64 xlim([0 5]);ylim([0 6])
65
66 xl = xlim;
67 yl = ylim;
68 xt = 0.05 * (xl(2)-xl(1)) + xl(1);
69 yt = 0.90 * (yl(2)-yl(1)) + yl(1);
70
71 % DA/dt
72 alpha = p_MSD(1);      % [m/s]
73 caption = sprintf('y = %.2e * x + %.2e \r\nalpha= %.2e ', p_MSD(1), ...
        p_MSD(2), alpha);
74
75 text(xt, yt, caption, 'FontSize', 15, 'Color', 'k', 'FontWeight', ...
        'bold');
76
77 %% MSD(t)
78 figure(2);
79 plot_MSD = plot(t_h,MSD,'*b')
80 p_MSD = polyfit(t_h,MSD,2);
81 f_MSD = polyval(p_MSD,t_h);
82 plot_MSD = plot(t_h,MSD,'*b',t_h,f_MSD,'-k');
83 xlabel('\fontsize{22}t [h]')
84 ylabel('\fontsize{22}<MSD> [um^2]')
85 legend('data','Curve fit', 'Location','southeast')
86 set(gca,'FontSize',22)
87 xlim([0 25])
88
89 xl = xlim;
90 yl = ylim;
91 xt = 0.05 * (xl(2)-xl(1)) + xl(1);
92 yt = 0.90 * (yl(2)-yl(1)) + yl(1);
93
94 % alpha
95 a = p_MSD(1);      % [m/s]
```

```

96 caption = sprintf('y = %.2e * x + %.2e \r\nalpha= %.2e [s-1]', ...
    p_MSD(1), p_MSD(2), a);
97 text(xt, yt, caption, 'FontSize', 10, 'Color', 'k', 'FontWeight', ...
    'bold');
98
99 %% Draw trajectory
100 NameImage = [dirTransImage, ImageName];
101 figure(3)                                %%Figure of centroids
102 imshow(NameImage)
103 hold on
104 plot(c_x, c_y, '-', 'LineWidth', 3)
105 % title('Trajectory of centroid');
106 hold off
107 %% Calculate curvilinear velocity
108 Delta_x = zeros(n,1);
109 Delta_y = zeros(n,1);
110 V_x = zeros(n,1);
111 V_y = zeros(n,1);
112 V_curvilinear = zeros(n,1);
113 for i=2:n
114     Delta_x(i) = (c_x(i)-c_x(i-1))*scale;
115
116     V_x(i) = (c_x(i)-c_x(i-1))*scale/internal; %Deat_X*scale/t_h
117     V_y(i) = (c_y(i)-c_y(i-1))*scale/internal; %Deat_Y*scale/t_h
118     V_curvilinear(i) = sqrt(V_x(i)^2+V_y(i)^2)*10^(-6);
119 end
120
121 figure(4);
122 plot(t_h, V_curvilinear, 'r-')
123 hold on
124 scatter(t_h, V_curvilinear, 'ro', 'filled')
125 hold off
126 xlabel('\fontsize{22}t [h]')
127 ylabel('\fontsize{22}Curvilinear Velocity(m/s)')
128 legend('dt = 20min')
129 xlim([0 25])
130 set(gca, 'FontSize', 22)
131 %% Save
132 save([dir_in, ...
    ExcelName, '_Dynamics.mat'], 't', 't_h', 'log_t', 'V_curvilinear', 'MSD', 'log_MSD', 'dir_
133 %% Save figure
134 MSDlogFigureName=[dir_in, 'MSD_log_', ExcelName, '.fig'];
135 saveas (figure(1), MSDlogFigureName);
136 MSDFigureName=[dir_in, 'MSD_', ExcelName, '.fig'];
137 saveas (figure(2), MSDFigureName);
138 TrajectoryFigureName=[dir_in, 'Trajectory_', ExcelName, '.fig'];
139 saveas (figure(3), TrajectoryFigureName);
140 CurviVelocityFigureName=[dir_in, 'Curvilinear_Velocity_', ExcelName, '.fig'];
141 saveas (figure(4), CurviVelocityFigureName);
142
143 end

```

## Microinjection analysis

```

1  %y(1): c1
2  %y(2): c2
3
4  [t,y] = ode45(@vdp1,[0 111],[10; 6]);%[y1;y2];[0; -0.1]
5  % y_interp = interp1(t,y(:,1),time);
6  % coeff_nor = 12;
7  figure
8  plot(t,y(:,1)*coeff_nor,'-o',t,y(:,2)*coeff_nor,'-o')
9
10
11 legend('Cluster 1','Cluster 2')
12 set(gca,'FontSize',18)
13 pbaspect([1.5,1,1])
14 xlim([0,120])
15 % set(gca, 'XTick', [0 50 100 200])
16 % ylim([-20,200])
17 % set(gca, 'YTick', [-20 0 50 100 200])
18 xlabel('Time (s)', 'FontSize',22);
19 ylabel('Intensity', 'FontSize',22);
20 %Legend
21 lgd=legend('Cluster center 1','Cluster center ...
           2', 'Location', 'northeast');%legend('Layer 1','Layer 2', 'Layer 3');
22 legend boxoff
23 lgd.FontSize=18
24
25 %%
26
27 function dydt = vdp1(t,y)
28 c=-0.03; %interface diffusion: decide ratio = amp1/amp2. c ...
           decrease, ratio decrease
29 ksi1=0.03; %self dissipation for c1
30 ksi2=ksi1/0.9; %self dissipation for c2; 0.3 decide delay of top 2 ...
           and amp2
31 omega=13; %injection speed
32 tfin=33; %end of injection time
33 tmid=16.5;
34 input_r1 = (t<tmid)*t/tmid;% /
35 input_r2 = (t<tfin)*(t>tmid);% -
36 input_r3 = ((t>tmid)*(tfin-t))/tmid;% \
37 dydt = [c*(y(1)-y(2))-ksi1*y(1)+input_r1*omega+input_r2*omega; ...
           c*(y(2)-y(1))-ksi2*y(2)];
38 end

```

**Titre:** Transitions morphologiques induites par la contractilité dans les cellules musculaires lisses : des feuilles cellulaires multicouches aux amas tridimensionnels

**Mots clés:** Athérosclérose, Dommages endothéliaux, Cellules musculaires lisses, Sphéroïde, Clusteur, Transition morphologique

**Résumé:** Les crises cardiaques et les accidents vasculaires cérébraux sont la principale cause de mortalité dans le monde. La resténose et la thrombose sont parmi les complications les plus fréquentes du traitement de l'athérosclérose. Une étude montre que l'étendue des dommages induits par les dispositifs endovasculaires est sensiblement plus élevée pour une paroi artérielle rigide que pour une paroi souple. Les études sur

les cellules musculaires lisses montrent que lorsqu'elles atteignent une densité critique, ces cellules peuvent passer spontanément de feuilles cellulaires plates à des amas tridimensionnels de type sphéroïde. La description des mécanismes physiques régissant l'émergence spontanée de ces intrigants amas tridimensionnels permet de mieux comprendre les troubles liés aux cellules musculaires lisses.

**Title:** Contractility-induced morphological transitions in smooth muscle cells: from multilayered cell sheets to three-dimensional clusters

**Keywords:** Atherosclerosis, Endothelial damage, Smooth muscle cells, Spheroid, Cluster, Morphological transition

**Abstract:** Heart attacks and strokes are the leading cause of mortality worldwide. Restenosis and thrombosis are among the most common complications of atherosclerosis treatment. Study shows that the extent of damage induced by endovascular devices is significantly higher for a rigid arterial wall than for a soft wall. The smooth

muscle cell investigations demonstrate that upon reaching a critical density, these cells can spontaneously transition from flat cell sheets to three-dimensional spheroid-like clusters. The description of the physical mechanisms governing the spontaneous emergence of these intriguing 3-D clusters offers insight into smooth muscle cell-related disorders.